
**U.S. DEPARTMENT OF THE INTERIOR**
**U.S. GEOLOGICAL SURVEY**

# PRELIMINARY MINERALOGICAL CHARACTERIZATION OF WEATHERED AND LESS-WEATHERED STRATA OF THE MEADE PEAK PHOSPHATIC SHALE MEMBER OF THE PERMIAN PHOSPHORIA FORMATION: MEASURED SECTIONS A AND B, CENTRAL PART OF RASMUSSEN RIDGE, CARIBOU COUNTY, IDAHO

By Andrew C. Knudsen[1], Mickey E. Gunter[1], and James R. Herring[2]
Western U.S. Phosphate Project

Prepared in Collaboration With
Bureau of Land Management
Forest Service
Agrium U.S. Inc.
FMC Corporation
J.R. Simplot Company
Rhodia Inc.
and Solutia Inc.

**Open-File Report 00-116**



[1] University of Idaho, Department of Geological Sciences, Moscow ID 83844
[2] U.S. Geological Survey, DFC, Box25046, MS 973, Denver CO 80225

## Contents



### Figures



### Tables

## ABSTRACT

The Permian Phosphoria Formation of southeastern Idaho is one of the largest phosphate producing deposits in the world. Despite the economic significance of this Formation, the fine-grained nature of this phosphorite deposit has discouraged detailed mineralogical characterization and quantification studies. Recently, the issue of naturally occurring Se and other potentially hazardous trace elements from mine wastes has drawn increased attention to this Formation, and motivated more extensive study. Part of this effort has focused on conducting a more detailed geological, including a mineralogical, characterization of the area.

Past research has identified the presence of major minerals in the formation, including carbonate-fluorapatite, quartz, and dolomite, along with a variety of sheet silicates and feldspar phases. Minor phases such as pyrite and sphalerite have also been identified in the deposit and have been suggested as possible sites for Se residence.

This study used powder X-ray diffraction (XRD), with Rietveld quantification software, to characterize the 67 samples collected from two stratigraphic sections measured by the U.S. Geological Survey at the Enoch Valley mine in the Meade Peak Member of the Phosphoria Formation. This analysis shows extensive variability of carbonate substitution into the fluorapatite structure, determined by measurements of the apatite a-cell dimension. The analysis produced quantitative mineralogical results for the 67 samples, showing some patterns of correlation between mineralogy and the stratigraphy.

# INTRODUCTION

## Location and Background

The U. S. Geological Survey (USGS) has studied the Permian Phosphoria Formation and related rock units in southeastern Idaho and the entire Western Phosphate Field through much of the twentieth century. The Phosphoria Formation hosts one of the worlds most economically significant phosphate deposits; however, it is also enriched in Se and other environmentally sensitive trace elements, including As, Cd, Cr, Mo, Ni, V, and Zn. Elevated concentrations of these trace elements and the possible environmental impact they pose have increased interest in the geology of the area. In response to a request by the Bureau of Land Management (BLM), a new series of resource, geological, and geoenvironmental studies was undertaken by the USGS in 1998. To carry out these studies, the USGS has formed collaborative research relationships with two federal agencies, the BLM and the U.S. Forest Service (FS), tasked with land management and resource conservation on public lands, and with five companies currently leasing or developing phosphate resources in southeast Idaho. The five companies are Agrium U.S. Inc. (Rasmussen Ridge mine), FMC Corporation (Dry Valley mine), J. R. Simplot Company (Smokey Canyon mine), Rhodia Inc. (Wooley Valley mine – inactive), and Solutia Inc. (Enoch Valley mine).

Present studies consist of integrated, multidisciplinary research directed toward (1) resource and reserve estimation of phosphate in selected 7.5-minute quadrangles; (2) elemental residence, mineralogical, and petrochemical characteristics; (3) mobilization and reaction pathways, transport, and fate of potentially toxic elements associated with the occurrence, development, and societal use of phosphate; (4) geophysical signatures;

and (5) improved understanding of depositional origin. Because raw data acquired during the project will require time to interpret, the data are released in open-file reports for prompt availability to other workers. Open-file reports associated with this series of resource and geoenvironmental studies are submitted to each of the Federal and industry cooperators for technical review; however, the USGS is solely responsible for the data contained in the reports. This report summarizes the results of mineralogical studies conducted on samples collected from two measured stratigraphic sections at an operating mine in the central part of Rasmussen Ridge (figure 1).

**Previous Studies**

Historic mineralogical analyses of the Phosphoria Formation produced qualitative characterizations of the distribution of major and minor mineral phases in the deposit. Petrographic analyses, particularly Mabie and Hess (1963) combined with XRD studies supported by chemical analyses (Lehman, 1966) identified many of the minerals found in the area. The most significant attempt to quantify the mineralogy of the region was made by Medrano and Piper (1992). This study used normalizing techniques to arrive at the mineralogy of the Phosphoria Formation. Along with the more common minerals considered in these studies, Gulbrandson (1974) identified the presence of the ammonium feldspar buddingtonite in the Phosphoria Formation. These studies, along with current work on the mineral chemistry (Desborough and others, 1999), constitute the foundation of background literature for the mineralogical investigation.

## METHODS

Materials analyzed for the mineralogical study were splits from samples collected by the USGS from two measured stratigraphic sections across the Meade Peak Phosphatic Shale Member of the Phosphoria Formation exposed on the central part of Rasmussen Ridge, Caribou County, Idaho. Lithologic descriptions of the measured stratigraphic sections are reported in Tysdal and others (1999), and chemical analyses of samples are presented in Herring and others (1999). The two measured sections include one from a shallow (less that 10 m), more weathered exposure (A) and the other from a deeper, less-weathered exposure (B) at an active mine. Data sets for this study include XRD and Inductively Coupled Plasma (ICP) analyses for each sample. XRD analyses were conducted with a 2-Theta scan from 2° - 62° over 28 minutes, using Cu radiation on a Siemens D5000 diffractometer operating at 40 kV and 30 mA. These relatively fast scans reveal the major phases in the samples; however, low peak to background ratios prevent accurate identification of minor phases (generally those less than 1%) in the samples. Once the phases in the scans are identified, the patterns are analyzed using the Siroquant program (Taylor 1991). Using Rietveld analysis, the program generates a scan with a known mineralogy, matching it to the collected scan, thus quantifying and characterizing the collected scan. Siroquant refines the shapes of the XRD peaks, accounts for shifts in cell parameters, and considers preferred orientation of minerals when necessary. Mineralogical characterization of the samples is also used to determine the extent of carbonate substitution into the fluorapatite structure. Measurement of the a-cell dimensions of the fluorapatite provides an estimate of the $CO_3^{2-}$ substitution for $PO_4^{3-}$ in the fluorapatite structure, as calculated by McClellan (1980). Finally, a calculated

chemistry is determined, based on the quantification results from the XRD, and then compared to the ICP data of Herring and others (1999).

## RESULTS

### Carbonate substitution

As well as quantifying the mineralogy of a sample, Rietveld analysis can be used to characterize individual mineral phases. This is particularly useful for the primary ore mineral in the Phosphoria Formation and other phosphorite deposits, carbonate-fluorapatite. In this mineral, varying amounts of planar $CO_3^{2-}$ groups substitute into the fluorapatite structure for $PO_4^{3-}$ tetrahedra. The resulting charge imbalance can be accounted for with an additional $F^-$ entering the structure. This relationship has been observed (McClellan and van Kauwenbergh, 1990) in numerous chemical analyses where substitution of $CO_3^{2-}$ for $PO_4^{3-}$ is coupled with $F^-$ to balance the charges. However, the charge can also be balanced with the addition of an $OH^-$ or with the substitution of a monovalent cation such as $Na^+$ for $Ca^{2+}$. McClellan (1980) devised a method with which to estimate the degree of substitution in a given carbonate-fluorapatite based on the change of the a-cell parameter, as can be measured using the Rietveld analysis. McClellan's formula yields the proportion of carbonate to phosphate in a sample based on the following equation:

$$CO_3^{2-} / PO_4^{3-} = Z / (6 - Z) = (9.369 - a_{obs}) / 0.185$$

McClellan also determined that substitution of Na and Mg could be estimated using the measured a-cell parameter:

$$\text{(Moles Na) } x = 7.173\ (9.369 - a_{obs})$$

$$\text{(Moles Mg) } y = 2.784\ (9.369 - a_{obs})$$

These substitutions are based on the assumption that the formula for carbonate-fluorapatite is $Ca_{10-x-y}\ Na_x\ Mg_y\ (PO_4)_{6-z}\ (CO_3)_z\ F_{0.4z}F_2$.

This method has been used for preliminary compositional estimates based on the a-cell parameters measured using the Siroquant software. For each sample, the calculated $CO_3^{2-}$, $Na^+$, and $Mg^{2+}$ content in the carbonate fluorapatite are produced (table 1, figure 2). However, the method does not take into account other substitutions such as $SO_4^{2-}$ for $PO_4^{2-}$ so the presented data can only be considered a preliminary estimate.

While table 1 lists the average amounts of substitution in the samples, the samples are not homogenous in their apatite composition. Splitting of the apatite peaks on the XRD pattern (figure 3) reveals that the degree of $CO_3^{2-}$ substitution varies not only between samples but within individual samples as well. Some of the peak splitting in the samples could be a result of slight mineralogical variation over the length of the sample trenches. However, this phenomenon has also been observed in grab samples collected from the same locality. This multi-apatite phase presence suggests that the apatite has recrystallized since deposition.

## Calculated mineralogy from ICP data

To establish a baseline for comparison, the normative mineralogy (table 2) of the samples (reported in weight percent) was determined using chemical data from Herring and others (1999). This method made many assumptions, oversimplifying the data to acquire estimates and establish limits for the mineral composition of the samples. This method was designed to arrive at semi-quantitative results for the mineralogy.

Fluorapatite quantities were calculated assuming that all of the P in each of the samples resides in fluorapatite, but it neglects to account for the significant presence of carbonate substitution for phosphate as discussed above. Likewise, values for maximum "quartz" are based on a calculation in which all of the silica in each sample is contained in quartz. This assumption is obviously inaccurate, as there are certainly other silicate phases present; however, it is useful in that it provides an upper limit on the total amount of silicate phases in each sample. Dolomite compositions are estimated twice: (1) based on the assignment of all Mg in the samples to dolomite; and (2) based on the carbonate content. Other phases present in the sample, such as feldspars and sheet silicates, cannot be easily estimated using the bulk chemistry due to their complex stoicheometry, so these are not included in this aspect of the study. A more complete normative-calculation to arrive at the mineral abundance was completed by Medrano and Piper (1992).

**Quantified mineralogy**

The Siroquant software package uses Rietveld analysis to quantify the mineralogical content in weight percent based on the XRD patterns. First, the phases in each sample must be identified, and then the program will match a calculated XRD pattern based on the known crystal structure of the mineral to the actual pattern to determine the quantities of each phase. Siroquant refines each identified phase, correcting for variable peak shape, preferred orientation, and shifts in cell parameters (figure 4). The quantity of each phase is reported along with an error value (table 3, figure 5). The overall quality of the match between the calculated and collected patterns

is shown in the $\chi^2$ value, where lower values are more accurate and any value under 3.0 is considered acceptable

Two main problems were encountered while quantifying these samples. First, not all of the phases were accounted for in some of the samples. Those samples marked with an (*) in table 3 have a significant crystalline phase that was not analyzed. In most of these, such a phase is believed to be the mineral rectorite, an interlayered illite-smectite clay. The database on the Siroquant program does not contain all minerals, and less common phases such as rectorite must be added. Analysis of this and other minor phases will be completed in a later study. Still, data for these samples displays the proportions of other phases to one another, so they are included. In addition, because the scans that were analyzed were short (28 minutes), each sample is currently being reanalyzed using an 8-hour scan, which should greatly improve the peak-background ratio. Improved resolution will enable better analysis of minor phases and more detailed mineralogical characterization, such as resolution between feldspars.

**Comparison of XRD and ICP data**

To compare the results from the ICP with those from the XRD, the quantified mineralogical data derived from XRD analysis were used to calculate a theoretical chemical composition and were then compared to the ICP data (table 4, figure 6). Weight percents for the major elements were calculated using ideal formulas for the identified mineral phases. These formulas include; apatite $Ca_5(PO_4)_3$, quartz $SiO_2$, muscovite-illite $KAl_2(AlSi_3)_{10}(OH)_2$, albite $NaAlSi_3O_8$, orthoclase $KAlSi_3O_8$, buddingtonite $(NH_4)AlSi_3O_8 \cdot 0.5H_2O$, $Al_2Si_2O_5(OH)_4$, dolomite $CaMg(CO_3)_2$, and calcite

$CaCO_3$. A slight adjustment factor was applied to the calculated chemical data to account for $NH_4^+$ and $OH^-$ because these were not measured on the ICP. These weight percents were then compared to the values gathered on the ICP. The ICP values were adjusted to exclude those elements that were not accounted for in the mineralogy (such as Fe, S, and the trace elements) in order to improve the comparability of the data sets. The quality of the correlation between the two data sets is variable. While many of the samples show nearly perfect matches for some elements, others reveal differences of more than 100% between them. These differences can be attributed to a combination of causes, a testament to the complexity of the mineral chemistry in the samples.

First, both data sets are subject to standard experimental error, which undoubtedly has some role in the discrepancies. Errors for the ICP data are listed in table 5, accounting for some of the discrepancies. In addition, the simplicity of the assumed stoicheometry in transferring mineralogical data to chemical data has likely skewed the results. By using the ideal chemical formulas, the presence of significant substitutions would not be taken into account. For instance, reported K values could be affected by this oversimplification. With sufficient $NH_4^+$ <-> $K^+$ substitution in orthoclase, the mineral buddingtonite is formed, as discussed by Gulbrandssen (1974). While orthoclase and buddingtonite are both analyzed, it is possible that a solid solution between $K^+$ and $NH_4^+$ exists in these phases, as well as in muscovite and other sheet silicates. The substitution of $NH_4^+$ <-> $K^+$ is only considered for the end-member compositions; consequently, failure to recognize the possibility of this and other solid solution series could play a major role in the discrepancies between the calculated and measured chemical compositions.

Another source of significant error is the potential failure to recognize phases in the XRD analysis. Quantification of both minor crystalline and amorphous phases has not yet been determined in many of the samples. For instance, sample WPSA062C shows an extremely large difference between the calculated chemistry and the measured chemistry. This sample is from a carbon seam, rich in noncrystalline organic matter that is not accounted for in this Siroquant quantification, thus falsely elevating the relative percents of the crystalline phases present. In addition, the presence of minor phases such as pyrite, which has been reported to be present in concentrations as high as 5%, will most certainly skew the calculated chemistry because it is based on the incomplete mineralogy.

## SUMMARY AND FURTHER WORK

These preliminary studies reveal an extremely complicated and highly variable mineralogy throughout the two sections measured and sampled across the Meade Peak Phosphatic Shale Member of the Phosphoria Formation. Major minerals observed thus far include carbonate-fluorapatite, quartz, dolomite, albite, orthoclase, buddingtonite, and muscovite. Numerous other minor phases can be seen in a number of the samples as well. Graphs of the major mineral phases, plotted in stratigraphic order, show evidence of a pattern (figure 5). The graphs include gaps to visually separate the middle waste shale from the upper and lower ore producing bodies. These plots show the strong presence of feldspars, particularly the ammonium feldspar buddingtonite, in the middle waste shale of both benches. Additionally, the presence of fluorapatite and quartz, both in the middle waste as well as in the ore bodies, is highly variable. As expected based on

the ICP data, the A-bench is very low in dolomite in comparison to the less-weathered B-bench. These are only preliminary observations, and many more comparisons will be made combining the mineralogical data and much of the other data that has been, and continues to be, produced as a part of the USGS Western U.S. Phosphate Project.

Along with the quantitative results, numerous other alternative observations were made. The $CO_3^{2-}$ substitution into fluorapatite is shown to be highly variable, both over the stratigraphic sections and within individual samples. Through the two measured sections, the degree of substitution is highly variable, with few obvious stratigraphic controls (figure 2). The B-bench does show a generally higher level of $CO_3^{2-}$ substitution than the A-bench. Because of the relatively unstable presence of the $CO_3^{2-}$ in the fluorapatite structure, the more weathered samples should contain less $CO_3^{2-}$ rich apatite, as is indeed seen with the more weathered A-bench having lower $CO_3^{2-}$ levels than the B-bench. The presence of multi-apatite phases in samples from the sections suggests that apatite has recrystallized since initial deposition. This suggests that the rocks have undergone weathering to remove $CO_3^{2-}$ and then a recrystallization period. While this change can be observed in the fluorapatite, it could also have affected other phases and elements.

Also of note in this study is the significant presence of the rare ammonium feldspar mineral buddingtonite, first reported to exist in the Phosphoria Formation by Gulbrandson (1974). Although relatively uncommon, this mineral was found at levels of over 30% in one sample and above 20% in many others. The large amount of buddingtonite suggests a significant presence of ammonium in the Formation. The

possibility of extensive solid solutions between buddingtonite and orthoclase, as well as between muscovite/illite and an ammonium sheet silicate must be considered as well.

Plans for additional studies include continuations of much of the work reported here. More detailed XRD scans should lead to a better resolution for understanding minor phases as well as more complicated phases such as the feldspars. Ultimately, these mineralogical studies will be integrated with the ongoing research of others associated with the project. These other studies, such as microprobe and scanning electron microscope analyses, could be combined with this and further mineralogical work, to establish a better understanding of the mineralogy and overall geology of the area.

## REFERENCES CITED


Desborough, George, DeWitt, Ed, Jones, Jeff, Meier, Alan, and Meeker, George, 1999, Preliminary mineralogical and chemical studies related to the potential mobility of selenium and associated elements in Phosphoria formation strata, southeastern Idaho: U.S. Geological Survey Open-File Report 99-129, 20 p.

Gulbrandsen, R.A., 1974, Buddingtonite, ammonium feldspar, in the Phosphoria Formation, southeastern Idaho: Journal of Research of the U.S. Geological Survey, v. 2, no. 6, p. 693-697.

Herring, J.R., Desborough, G.A., Wilson, S.A., Tysdal, R.G., Grauch, R.I., and Gunter, M.E., 1999, Chemical composition of weathered and unweathered strata of the Meade Peak phosphatic shale member of the Permian Phosphoria Formation: U.S. Geological Survey Open-File Report 99-147-A, 24 p.

Lehman, Norman E. 1966, Geology and mineralogy of the Fort Hall phosphate deposit, Idaho: MS Thesis, Univ. of Arizona.

Medrano, M.D., and Piper, D.Z., 1992, A normative-calculation procedure used to determine mineral abundances in rocks from the Montpelier Canyon section of the Phosphoria Formation, Idaho: a tool in deciphering the minor-element geochemistry of sedimentary rocks, *in* The Phosphoria Formation: Its geochemical and biological environment of deposition: U.S. Geological Survey Bulletin 2023A, A1-A23 p.

Mabie, C.P. and Hess, H.D., 1963, Petrographic study and classification of western phosphate ores: Industrial Paper, J.R. Simplot Company.

McClellan, G.H. 1980, Mineralogy of carbonate fluorapatites: Geological Society of London, v. 137, p. 675-681.

McClellan, G.H. and Van Kauwenbergh, S.J., 1990, Mineralogy of sedimentary apatites: Phosphorite Research and Development, Geological Society of America Special Publication no. 52, p. 23-31,

Taylor, J.C., 1991, Computer programs for standardless quantitative analysis of minerals using the full powder diffraction profile: Powder Diffraction, v. 6, p. 2-9.

Tysdal, R.R., Johnson, E.A., Herring, J.R., and Desborough, G.A., 1999, Stratigraphic sections and equivalent uranium (eU), Meade Peak Phosphatic Shale Member of Permian Phosphoria Formation, central part of Rasmussen Ridge, Caribou County, Idaho: U.S. Geological Survey Open-File Report 99-20, 1 plate.

## FIGURES AND TABLES

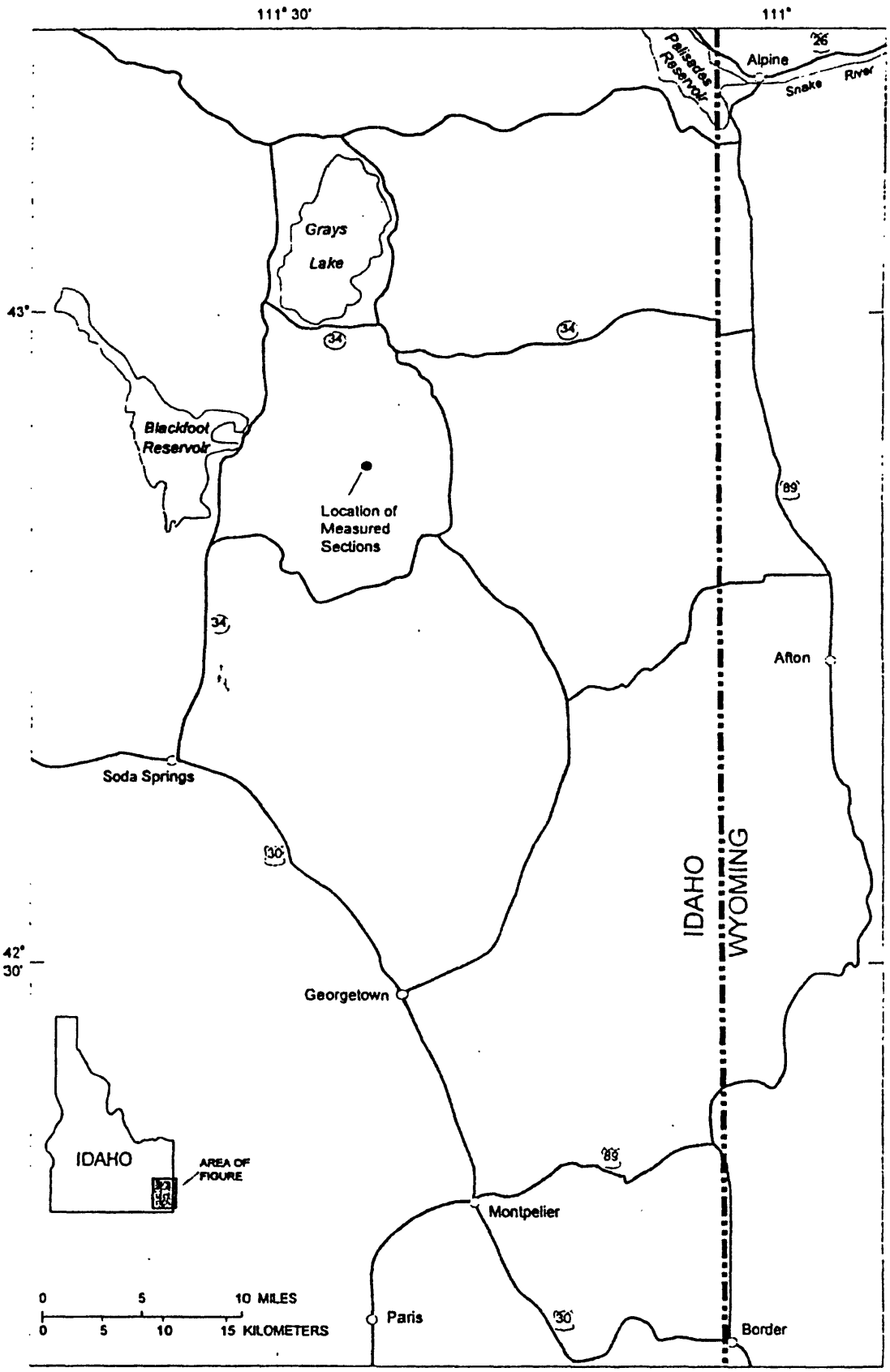


**Figure 1.** Index map of southeastern Idaho showing location of measured sections from which samples were collected.

**Table 1:** Composition of fluorapatite for each sample based a-cell dimensions. The concentrations of $CO_3^{2-}$, $Na^+$, and $Mg^{2+}$ in the fluorapatite are given in moles for the unit formula:

$$Ca_{10-x-y}\,Na_x\,Mg_y\,(PO_4)_{6-z}\,(CO_3)_z\,F_{0.4z}F_2,$$ ( McClellan 1980).

$CO_3^{2-}$ content is also given as percent molar substitution for $PO_4^{3-}$.

| Sample # | fluorapatite a-cell (Å) | $CO_3^{2-}$ content (Z) per unit formula | Percent $CO_3^{2-}$ substitution for $PO_4^{3-}$ | Na content (X) per unit formula | Mg content (Y) per unit formula |
|---|---|---|---|---|---|
| WPSA002C | 9.365 | 0.12 | 2% | 0.03 | 0.01 |
| WPSA006C | 9.360 | 0.28 | 5% | 0.06 | 0.03 |
| WPSA008C | 9.358 | 0.33 | 5% | 0.08 | 0.03 |
| WPSA015C | 9.361 | 0.26 | 4% | 0.06 | 0.02 |
| WPSA022C | 9.362 | 0.21 | 3% | 0.05 | 0.02 |
| WPSA024C | 9.362 | 0.21 | 3% | 0.05 | 0.02 |
| WPSA026C | 9.368 | 0.02 | 0% | 0.00 | 0.00 |
| WPSA030C | 9.362 | 0.21 | 3% | 0.05 | 0.02 |
| WPSA035C | 9.360 | 0.27 | 4% | 0.06 | 0.02 |
| WPSA040C | 9.362 | 0.23 | 4% | 0.05 | 0.02 |
| WPSA050C | 9.368 | 0.02 | 0% | 0.00 | 0.00 |
| WPSA057C | 9.359 | 0.30 | 5% | 0.07 | 0.03 |
| WPSA060C | 9.364 | 0.16 | 3% | 0.04 | 0.01 |
| WPSA062C | 9.362 | 0.21 | 3% | 0.05 | 0.02 |
| WPSA063C | 9.361 | 0.24 | 4% | 0.05 | 0.02 |
| WPSA070C | 9.363 | 0.18 | 3% | 0.04 | 0.02 |
| WPSA072C | 9.358 | 0.35 | 6% | 0.08 | 0.03 |
| WPSA080C | 9.362 | 0.21 | 3% | 0.05 | 0.02 |
| WPSA085C | 9.371 | -0.06* | -1% | -0.01 | 0.00 |
| WPSA087C | 9.357 | 0.38 | 6% | 0.09 | 0.03 |
| WPSA096C | 9.366 | 0.11 | 2% | 0.03 | 0.01 |
| WPSA100C | 9.365 | 0.14 | 2% | 0.03 | 0.01 |
| WPSA123C | 9.366 | 0.11 | 2% | 0.02 | 0.01 |
| WPSA124C | 9.373 | -0.14 | -2% | -0.03 | -0.01 |
| WPSA127C | 9.366 | 0.10 | 2% | 0.02 | 0.01 |
| WPSA129C | 9.368 | 0.02 | 0% | 0.00 | 0.00 |
| WPSA131C | 9.377 | -0.27 | -5% | -0.06 | -0.02 |
| WPSA133C | 9.364 | 0.17 | 3% | 0.04 | 0.02 |
| WPSA134C | 9.361 | 0.24 | 4% | 0.06 | 0.02 |
| WPSA138C | 9.362 | 0.23 | 4% | 0.05 | 0.02 |
| WPSA144C | 9.358 | 0.33 | 6% | 0.08 | 0.03 |
| WPSA147C | 9.358 | 0.35 | 6% | 0.08 | 0.03 |
| WPSA151C | 9.355 | 0.42 | 7% | 0.10 | 0.04 |
| WPSA153C | 9.360 | 0.28 | 5% | 0.06 | 0.03 |
| WPSA154C | 9.363 | 0.20 | 3% | 0.05 | 0.02 |
| WPSA156C | 9.361 | 0.24 | 4% | 0.06 | 0.02 |
| WPSA158C | 9.364 | 0.16 | 3% | 0.04 | 0.01 |
| WPSA163C | 9.364 | 0.16 | 3% | 0.04 | 0.01 |

* Negative values result from either inaccurate a-cell measurements or a weakness in the model.

**Figure 2:** Graphical view of the data presented in Table 1, showing variations in carbonate substitution in fluorapatite through the measured stratigraphic section. Gaps are inserted to separate the middle waste from the upper and lower ore producing bodies.

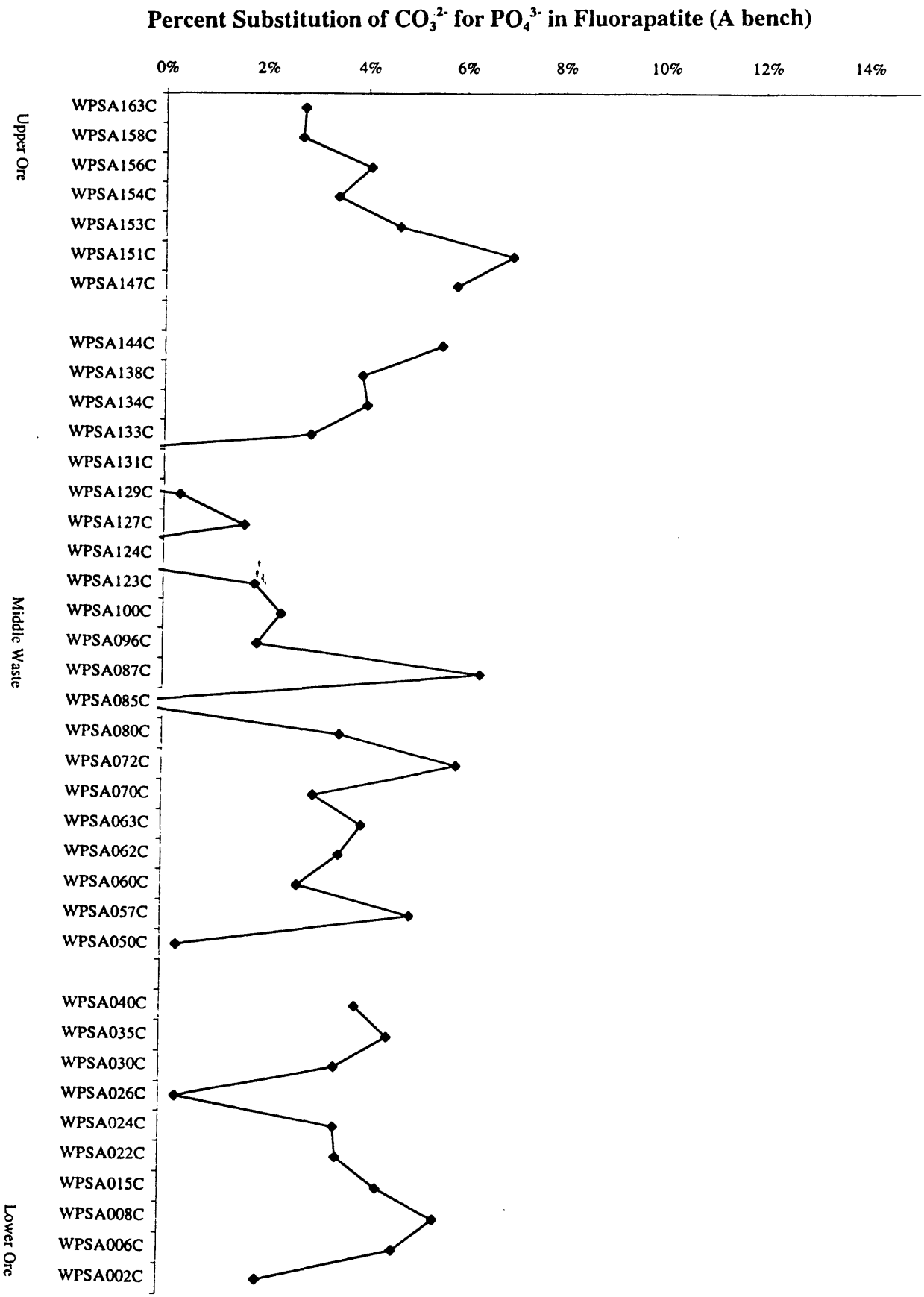

**Table 1:** Composition of fluorapatite for each sample based a-cell dimensions. The concentrations of $CO_3^{2-}$, $Na^+$, and $Mg^{2+}$ in the fluorapatite are given in moles for the unit formula:

$$Ca_{10-x-y}\,Na_x\,Mg_y\,(PO_4)_{6-z}\,(CO_3)_z\,F_{0.4z}F_2,$$ ( McClellan 1980).

$CO_3^{2-}$ content is also given as percent molar substitution for $PO_4^{3-}$.

| Sample # | fluorapatite a-cell (Å) | $CO_3^{2-}$ content (Z) per unit formula | Percent $CO_3^{2-}$ substitution for $PO_4^{3-}$ | Na content (X) per unit formula | Mg content (Y) per unit formula |
|---|---|---|---|---|---|
| WPSB003C | 9.369 | 0.01 | 0% | 0.00 | 0.00 |
| WPSB008C | 9.359 | 0.31 | 5% | 0.07 | 0.03 |
| WPSB018C | 9.356 | 0.39 | 7% | 0.09 | 0.04 |
| WPSB025C | 9.360 | 0.29 | 5% | 0.07 | 0.03 |
| WPSB026C | 9.354 | 0.46 | 8% | 0.11 | 0.04 |
| WPSB027C | 9.352 | 0.50 | 8% | 0.12 | 0.05 |
| WPSB033C | 9.366 | 0.11 | 2% | 0.02 | 0.01 |
| WPSB038C | 9.361 | 0.25 | 4% | 0.06 | 0.02 |
| WPSB047C | 9.362 | 0.23 | 4% | 0.05 | 0.02 |
| WPSB059C | 9.363 | 0.18 | 3% | 0.04 | 0.02 |
| WPSB065C | 9.371 | -0.07 | -1% | -0.01 | -0.01 |
| WPSB070C | 9.363 | 0.19 | 3% | 0.04 | 0.02 |
| WPSB080C | 9.363 | 0.19 | 3% | 0.04 | 0.02 |
| WPSB084C | 9.356 | 0.40 | 7% | 0.10 | 0.04 |
| WPSB087C | 9.364 | 0.16 | 3% | 0.04 | 0.01 |
| WPSB091C | 9.361 | 0.24 | 4% | 0.06 | 0.02 |
| WPSB095C | 9.362 | 0.22 | 4% | 0.05 | 0.02 |
| WPSB097C | 9.364 | 0.16 | 3% | 0.04 | 0.01 |
| WPSB100C | 9.359 | 0.30 | 5% | 0.07 | 0.03 |
| WPSB107C | 9.366 | 0.11 | 2% | 0.02 | 0.01 |
| WPSB117C | 9.360 | 0.27 | 5% | 0.06 | 0.02 |
| WPSB131C | 9.358 | 0.35 | 6% | 0.08 | 0.03 |
| WPSB133C | 9.357 | 0.36 | 6% | 0.09 | 0.03 |
| WPSB134C | 9.363 | 0.19 | 3% | 0.04 | 0.02 |
| WPSB136C | 9.360 | 0.28 | 5% | 0.07 | 0.03 |
| WPSB137C | 9.369 | 0.00 | 0% | 0.00 | 0.00 |
| WPSB139C | 9.355 | 0.41 | 7% | 0.10 | 0.04 |
| WPSB145C | 9.367 | 0.07 | 1% | 0.02 | 0.01 |
| WPSB157C | 9.366 | 0.08 | 1% | 0.02 | 0.01 |

**Figure 2:** Graphical view of the data presented in Table 1, showing variations in carbonate substitution in fluorapatite through the measured stratigraphic section. Gaps are inserted to separate the middle waste from the upper and lower ore producing bodies.

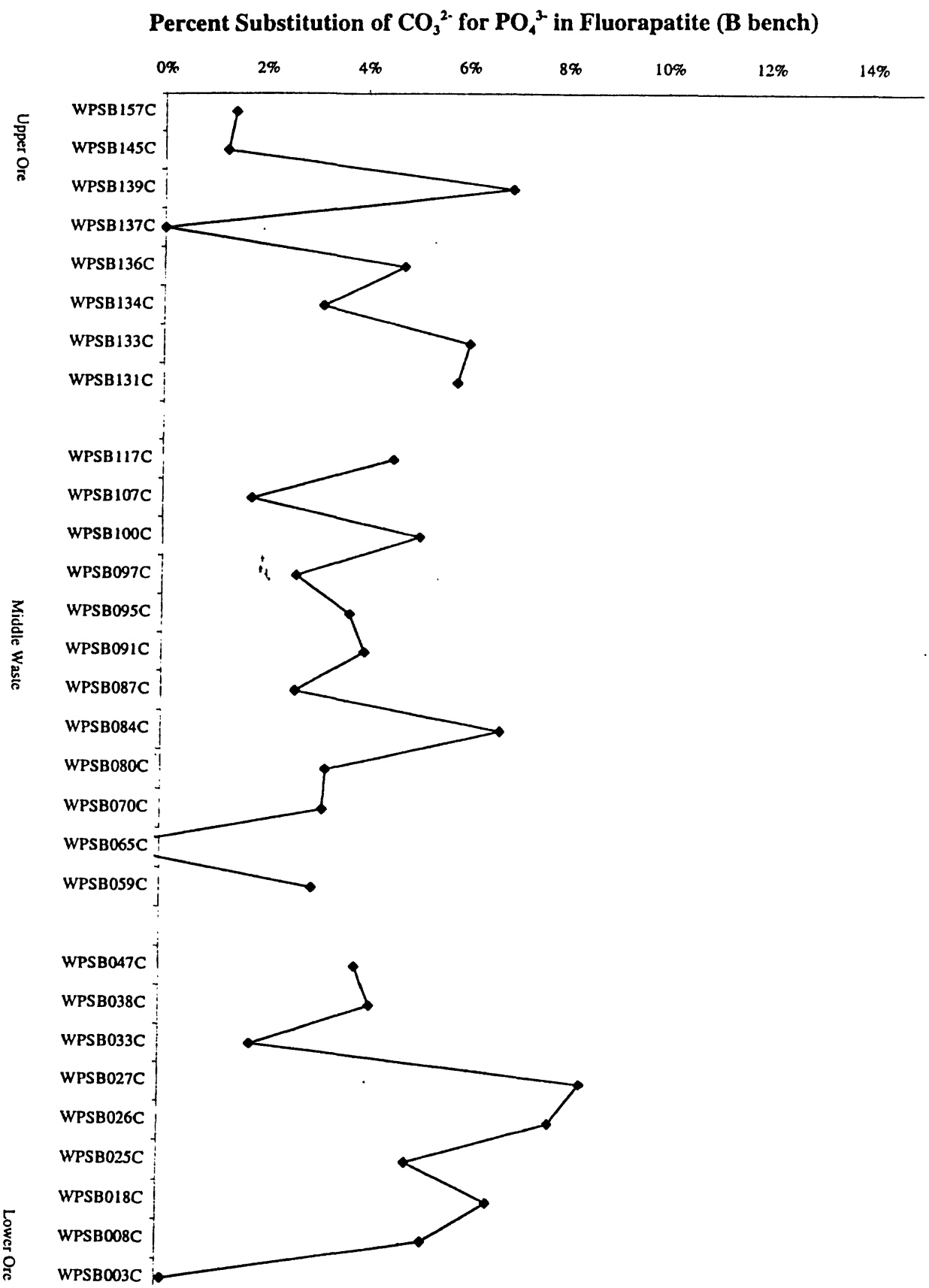

**Figure 3:** XRD pattern between 30° and 35° 2θ for a grab sample taken from near the measured section A. The splitting of the apatite (300) peak shows that multiple phases of fluorapatite with varying amounts of $CO_3$ substitution coexist.

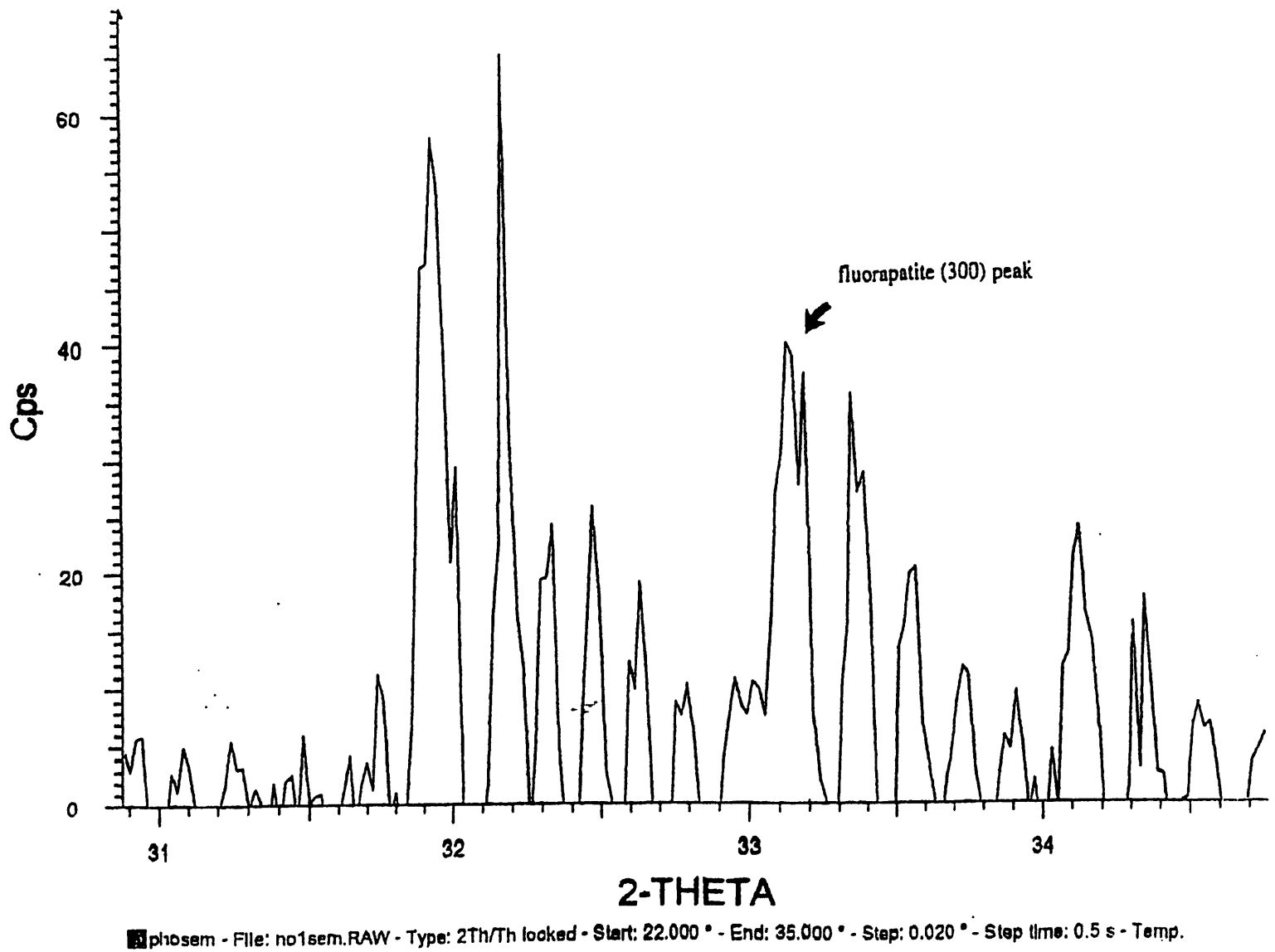

**Figure 4:** Printout from the Siroquant program for sample WPSA040C. The printout shows the collected pattern, the calculated pattern, and the difference. Data collected for this and other samples are given in table 3.

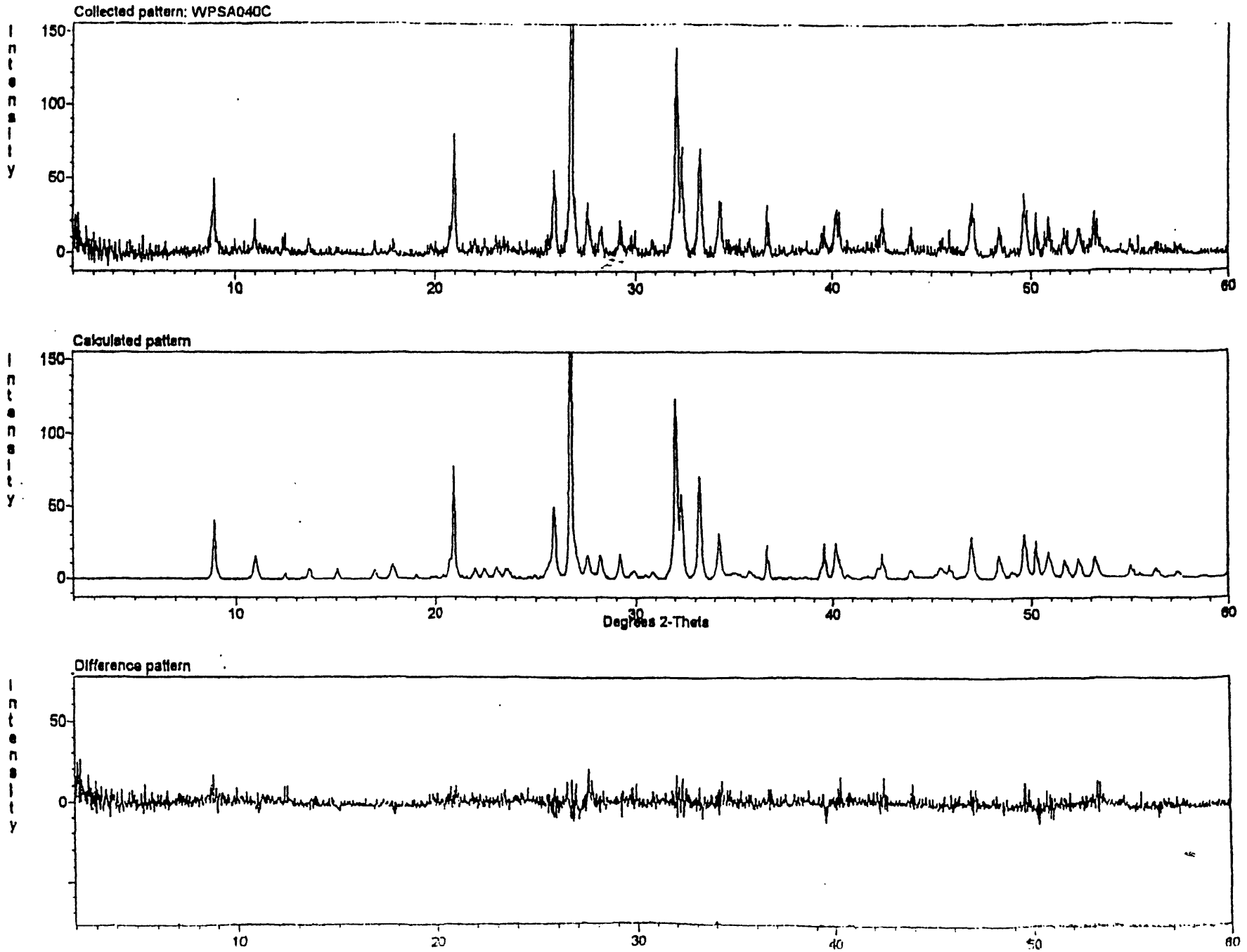

**Table 2:** Theoretical mineral quantities based on the ICP data. Quantities are maximum amounts of a given mineral that can occur in a sample assuming that all P is in apatite ($Ca_5(PO_4)_3F$), all $CO_3^{2-}$ and Mg are in dolomite ($CaMg(CO_3)_2$), and all Si is quartz ($SiO_2$). This neglects other silicate phases, so "quartz" is used here as a proxy for all silicate phases.

| Sample # | maximum % apatite (P) | maximum % dolomite (Mg) | maximum % dolomite ($CO_3^{2-}$) | maximum % "quartz" (Si) |
|---|---|---|---|---|
| WSPA002C | 9 | 3 | 1 | 60 |
| WSPA006C | 84 | 1 | 3 | 8 |
| WSPA008C | 57 | 1 | 2 | 27 |
| WSPA015C | 72 | 1 | 2 | 15 |
| WSPA022C | 20 | 1 | 1 | 55 |
| WSPA024C | 67 | 1 | 2 | 17 |
| WSPA026C | 23 | 1 | 1 | 47 |
| WSPA030C | 72 | 1 | 2 | 15 |
| WSPA035C | 55 | 1 | 2 | 26 |
| WSPA040C | 58 | 1 | 2 | 23 |
| WSPA050C | 34 | 2 | 1 | 39 |
| WSPA057C | 35 | 1 | 1 | 37 |
| WSPA060C | 28 | 3 | 1 | 33 |
| WSPA062C | 10 | 3 | 0 | 11 |
| WSPA063C | 37 | 2 | 1 | 29 |
| WSPA070C | 29 | 2 | 1 | 36 |
| WSPA072C | 18 | 1 | 1 | 48 |
| WSPA080C | 16 | 1 | 0 | 49 |
| WSPA085C | 7 | 2 | 0 | 54 |
| WSPA087C | 14 | 1 | 1 | 46 |
| WSPA096C | 70 | 1 | 1 | 17 |
| WSPA100C | 40 | 2 | 1 | 33 |
| WSPA123C | 27 | 2 | 1 | 48 |
| WSPA124C | 17 | 1 | 0 | 55 |
| WSPA127C | 24 | 1 | 0 | 53 |
| WSPA129C | 38 | 1 | 1 | 43 |
| WSPA131C | 8 | 0 | 0 | 61 |
| WSPA133C | 47 | 1 | 1 | 35 |
| WSPA134C | 71 | 1 | 2 | 18 |
| WSPA138C | 30 | 2 | 1 | 39 |
| WSPA144C | 11 | 3 | 0 | 53 |
| WSPA147C | 67 | 2 | 2 | 19 |
| WSPA151C | 92 | 1 | 3 | 6 |
| WSPA153C | 34 | 2 | 1 | 49 |
| WSPA154C | 79 | 1 | 2 | 15 |
| WSPA156C | 19 | 2 | 1 | 57 |
| WSPA158C | 87 | 1 | 3 | 5 |
| WSPA163C | 10 | 2 | 0 | 64 |

**Table 2:** Theoretical mineral quantities based on the ICP data. Quantities are maximum amounts of a given mineral that can occur in a sample assuming that all P is in apatite ($Ca_5(PO_4)_3F$), all $CO_3^{2-}$ and Mg are in dolomite ($CaMg(CO_3)_2$), and all Si is quartz ($SiO_2$). This neglects other silicate phases, so "quartz" is used here as a proxy for all silicate phases.

| Sample # | maximum % apatite (P) | maximum % dolomite (Mg) | maximum % dolomite ($CO_3^{2-}$) | maximum % "quartz" (Si) |
|---|---|---|---|---|
| WSPB003C | 1 | 28 | 29 | 48 |
| WSPB008C | 79 | 1 | 4 | 6 |
| WSPB018C | 82 | 1 | 4 | 6 |
| WSPB025C | 34 | 48 | 51 | 11 |
| WSPB026C | 72 | 4 | 6 | 12 |
| WSPB027C | 11 | 61 | 64 | 14 |
| WSPB033C | 79 | 2 | 4 | 11 |
| WSPB038C | 5 | 67 | 70 | 18 |
| WSPB047C | 55 | 7 | 8 | 20 |
| WSPB059C | 44 | 16 | 18 | 19 |
| WSPB065C | 2 | 65 | 73 | 17 |
| WSPB070C | 27 | 3 | 3 | 34 |
| WSPB080C | 17 | 1 | 0 | 51 |
| WSPB084C | 36 | 5 | 7 | 31 |
| WSPB087C | 41 | 3 | 2 | 28 |
| WSPB091C | 53 | 1 | 1 | 23 |
| WSPB095C | 15 | 8 | 7 | 49 |
| WSPB097C | 68 | 1 | 2 | 16 |
| WSPB100C | 20 | 1 | 1 | 51 |
| WSPB107C | 8 | 0 | 0 | 56 |
| WSPB117C | 22 | 7 | 7 | 40 |
| WSPB131C | 69 | 1 | 3 | 9 |
| WSPB133C | 83 | 1 | 3 | 12 |
| WSPB134C | 28 | 2 | 1 | 51 |
| WSPB136C | 82 | 1 | 3 | 10 |
| WSPB137C | 7 | 2 | 0 | 68 |
| WSPB139C | 89 | 1 | 3 | 4 |
| WSPB145C | 5 | 3 | 0 | 67 |

**Table 3:** Mineralogical composition calculated by the Rietveld method. The ($\chi^2$) value is a numerical statement of the quality of the fit between the calculated and collected XRD patterns, where any value less than 3 is considered acceptable, with smaller ($\chi^2$) inferring better results. Percents are listed with an accepted error in the last decimal place given in parentheses.

| Sample # | $\chi^2$ | % apatite | % quartz | % muscovite | % illite | % albite | % orthoclase | % buddingtonite | % kaolinite | % dolomite | % calcite |
|---|---|---|---|---|---|---|---|---|---|---|---|
| WPSA002C | 1.62 | 6.7 (6) | 76 (1) | 5.4 (5) | 5.5 (8) | 0.0 (0) | 0.0 (0) | 0.0 (0) | 5.8 (6) | | |
| WPSA006C | 1.33 | 90.1 (7) | 7.6 (3) | 1.2 (6) | 0.0 (0) | 0.0 (0) | 0.0 (0) | 0.0 (0) | 1.1 (5) | | |
| WPSA008C | 1.43 | 58 (1) | 26.6 (5) | 3 (1) | 0.1 (7) | 0.5 (5) | 4.7 (8) | 3.2 (6) | 2.8 (4) | | |
| WPSA015C | 1.48 | 73 (1) | 18.5 (4) | 2.8 (5) | 1.7 (8) | 0.1 (6) | 0.1 (9) | 2.0 (3) | 1.4 (5) | | |
| WPSA022C | 1.62 | 14.8 (6) | 40 (1) | 7 (1) | 0.1 (5) | 11.0 (6) | 14 (1) | 10 (1) | 2.2 (5) | | |
| WPSA024C | 1.48 | 60 (1) | 20.8 (4) | 6.4 (3) | 0.1 (8) | 4.4 (4) | 0 (1) | 7.7 (9) | 0.3 (5) | | |
| WPSA026C | 1.69 | 17.9 (6) | 50 (1) | 7.1 (9) | 0.1 (8) | 2.2 (6) | 14.5 (8) | 4.2 (7) | 3.7 (5) | | |
| WPSA030C | 1.35 | 76 (2) | 14.8 (4) | 2.2 (1) | 0.1 (8) | 0.1 (6) | 3.1 (6) | 2.9 (9) | 0.8 (6) | | |
| WPSA035C | 1.48 | 61 (2) | 17.9 (7) | 1 (2) | 0 (1) | 0 (2) | 5 (1) | 13 (1) | 0.9 (6) | | |
| WPSA040C | 1.48 | 55 (1) | 25.3 (5) | 6.7 (9) | 0.1 (7) | 0.1 (5) | 2.8 (7) | 9.1 (8) | 1.1 (4) | | |
| WPSA050C | 1.76 | 28.5 (6) | 25.1 (5) | 18 (1) | 0.1 (8) | 1.4 (1) | 4.9 (7) | 22.1 (8) | 0.4 (5) | | |
| WPSA057C | 1.57 | 37 (1) | 30 (1) | 1.6 (1) | 0.1 (9) | 3.7 (6) | 2.7 (7) | 19.2 (8) | 0.5 (5) | | |
| WPSA060C | 1.61 | 30.5 (8) | 20.7 (6) | 21 (1) | 0 (1) | 0.1 (7) | 1.2 (8) | 25 (9) | 1.3 (6) | | |
| WPSA062C | 1.54 | 34.4 (2) | 18 (1) | 20 (3) | 9 (2) | 0 (1) | 1.5 (1) | 2 (2) | 2.1 (2) | | |
| WPSA063C | 1.54 | 39.2 (7) | 23.5 (4) | 8.1 (4) | 0.1 (8) | 0.1 (6) | 3.7 (4) | 24.4 (7) | 1.0 (5) | | |
| WPSA070C | 1.68 | 30.5 (5) | 25.7 (3) | 10.2 (5) | 0.1 (0) | 0.1 (0) | 0.1 (0) | 33.3 (6) | 0.0 (0) | | |
| WPSA072C | 1.69 | 14.0 (5) | 41.7 (9) | 8.4 (8) | 0.1 (7) | 8.3 (6) | 2 (1) | 24.2 (9) | 0.5 (3) | | |
| WPSA080C | 1.64 | 12.8 (5) | 40 (9) | 12 (1) | 0.1 (8) | 7 (8) | 5.3 (5) | 21.4 (5) | 1.7 (5) | | |
| WPSA085C | 1.56 | 4.1 (4) | 45.2 (6) | 17 (3) | 0.1 (8) | 2.5 (1) | 4.1 (4) | 23.5 (6) | 3.6 (5) | | |
| WPSA087C | 1.72 | 10.9 (7) | 9.6 (5) | 19 (2) | 0 (1) | 0.1 (7) | 4.6 (8) | 53 (2) | 2.6 (6) | | |
| WPSA096C* | 1.40 | 75 (6) | 13 (1) | 2 (4) | 0 (3) | 0 (2) | 0 (3) | 9 (4) | 0 (2) | 0 (1) | 0 (1) |
| WPSA100C* | 1.50 | 38 (2) | 28 (1) | 15 (2) | 0 (1) | 0.1 (9) | 5 (1) | 11 (1) | 1.2 (7) | | |
| WPSA123C* | 1.50 | 18.1 (7) | 50 (1) | 11 (1) | 0.1 (9) | 3.8 (7) | 1 (1) | 15 (1) | 0.6 (6) | 0.1 (4) | |
| WPSA124C* | 3.10 | 8.4 (7) | 63 (1) | 0.1 (0) | 0.1 (9) | 11.1 (7) | 4.4 (9) | 12.5 (9) | 0.5 (7) | | |
| WPSA127C* | 1.57 | 18.9 (5) | 44 (9) | 13 (1) | 0.1 (6) | 8.5 (6) | 4.5 (5) | 10.2 (5) | 0.4 (4) | | |

* Samples that contain a high percentage of an unanalyzed phase with a prominent peak at about 23 Å, possibly the clay rectorite.

**Table 3:** Mineralogical composition calculated by the Rietveld method. The ($\chi^2$) value is a numerical statement of the quality of the fit between the calculated and collected XRD patterns, where any value less than 3 is considered acceptable, with smaller ($\chi^2$) inferring better results. Percents are listed with an accepted error in the last decimal place given in parentheses.

| Sample # | $\chi^2$ | % apatite | % quartz | % muscovite | % illite | % albite | % orthoclase | % buddingtonite | % kaolinite | % dolomite | % calcite |
|---|---|---|---|---|---|---|---|---|---|---|---|
| WPSA129C | 1.40 | 25 (1) | 49.2 (2) | 2 (3) | 0 (1) | 0.6 (1) | 18.8 (2) | 4 (1) | 0 (7) | | |
| WPSA131C | 1.67 | 0.9 (4) | 40.8 (8) | 4.5 (8) | 0.1 (8) | 26.3 (7) | 11.2 (8) | 16.2 (9) | 0.0 (5) | | |
| WPSA133C* | 1.43 | 29.7 (6) | 32.7 (6) | 10 (9) | 0.1 (8) | 11.9 (5) | 8.8 (7) | 0.62 (6) | 0.6 (5) | | |
| WPSA134C* | 1.22 | 78 (2) | 16.2 (5) | 2 (1) | 0 (1) | 1 (1) | 0.7 (6) | 0.7 (7) | | | |
| WPSA138C* | 1.57 | 27.6 (7) | 36.6 (8) | 13.6 (1) | 0.5 (8) | 8.4 (8) | 3.3 (5) | 8.9 (6) | 1.0 (5) | | |
| WPSA144C | 1.61 | 7.0 (8) | 40.5 (1) | 13 (2) | 3 (1) | 26.7 (1) | 2 (1) | 6.8 (9) | 0.1 (8) | | |
| WPSA147C | 1.39 | 58 (2) | 22.5 (8) | 4 (2) | 0.1 (9) | 0.1 (9) | 12.7 (1) | 2.5 (8) | | | |
| WPSA151C | 1.26 | 89 (2) | 5.9 (3) | 3 (1) | 0 (1) | 0.1 (7) | 0.1 (8) | 0.1 (8) | | | |
| WPSA153C | 1.41 | 24.8 (5) | 54.5 (7) | 9.3 (3) | 0.6 (8) | 4.9 (2) | 2.9 (6) | 1.5 (5) | 1.6 (5) | | |
| WPSA154C | 1.29 | 81 (2) | 15.3 (4) | 1 (1) | 0.2 (7) | 1.4 (7) | 0.4 (7) | 0.3 (6) | | | |
| WPSA156C | 1.62 | 10.1 (5) | 59 (1) | 8.6 (3) | 0 (1) | 5.7 (6) | 11.9 (6) | 0.4 (7) | 4.8 (4) | | |
| WPSA158C | 1.19 | 88 (2) | 3.5 (3) | 7.5 (1) | 0.2 (9) | 0.1 (7) | 0.1 (8) | 0.1 (7) | | | |
| WPSA163C | 1.54 | 6.2 (5) | 60 (1) | 13.7 (1) | 1.2 (8) | 8.3 (6) | 5 (1) | 4.5 (8) | | | |

**Figure 5:** Graphical view of the data presented in Table 3. Variations over the two measured stratigraphic sections are shown for each of the major mineral phases, including; apatite, quartz, muscovite, total feldspar (including albite, orthoclase, and buddingtonite), buddingtonite, and dolomite. Gaps are inserted in the graph to separate the middle waste from the upper and lower ore producing bodies.

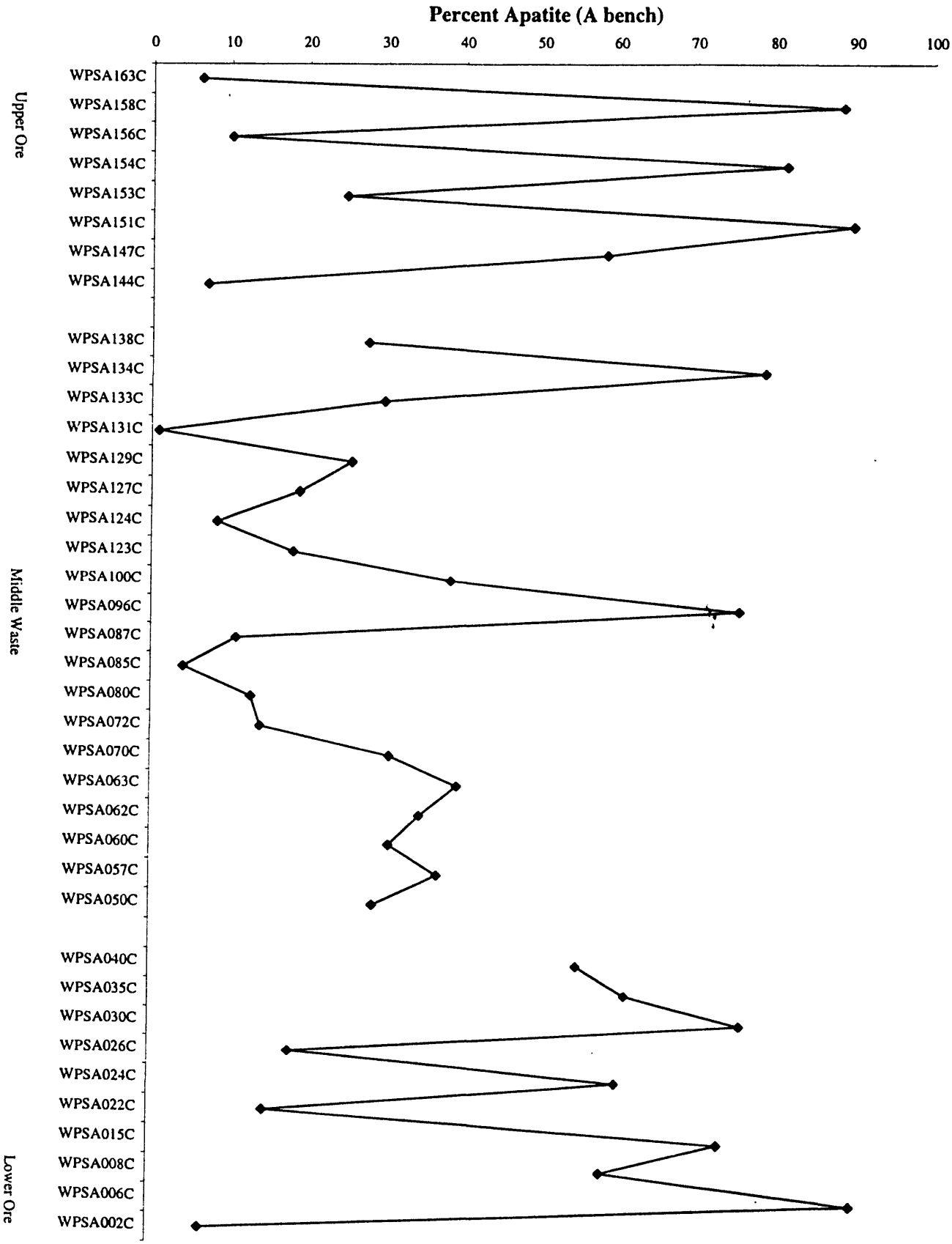

**Figure 5:** Graphical view of the data presented in Table 3. Variations over the two measured stratigraphic sections are shown for each of the major mineral phases, including; apatite, quartz, muscovite, total feldspar (including albite, orthoclase, and buddingtonite), buddingtonite, and dolomite. Gaps are inserted in the graph to separate the middle waste from the upper and lower ore producing bodies.

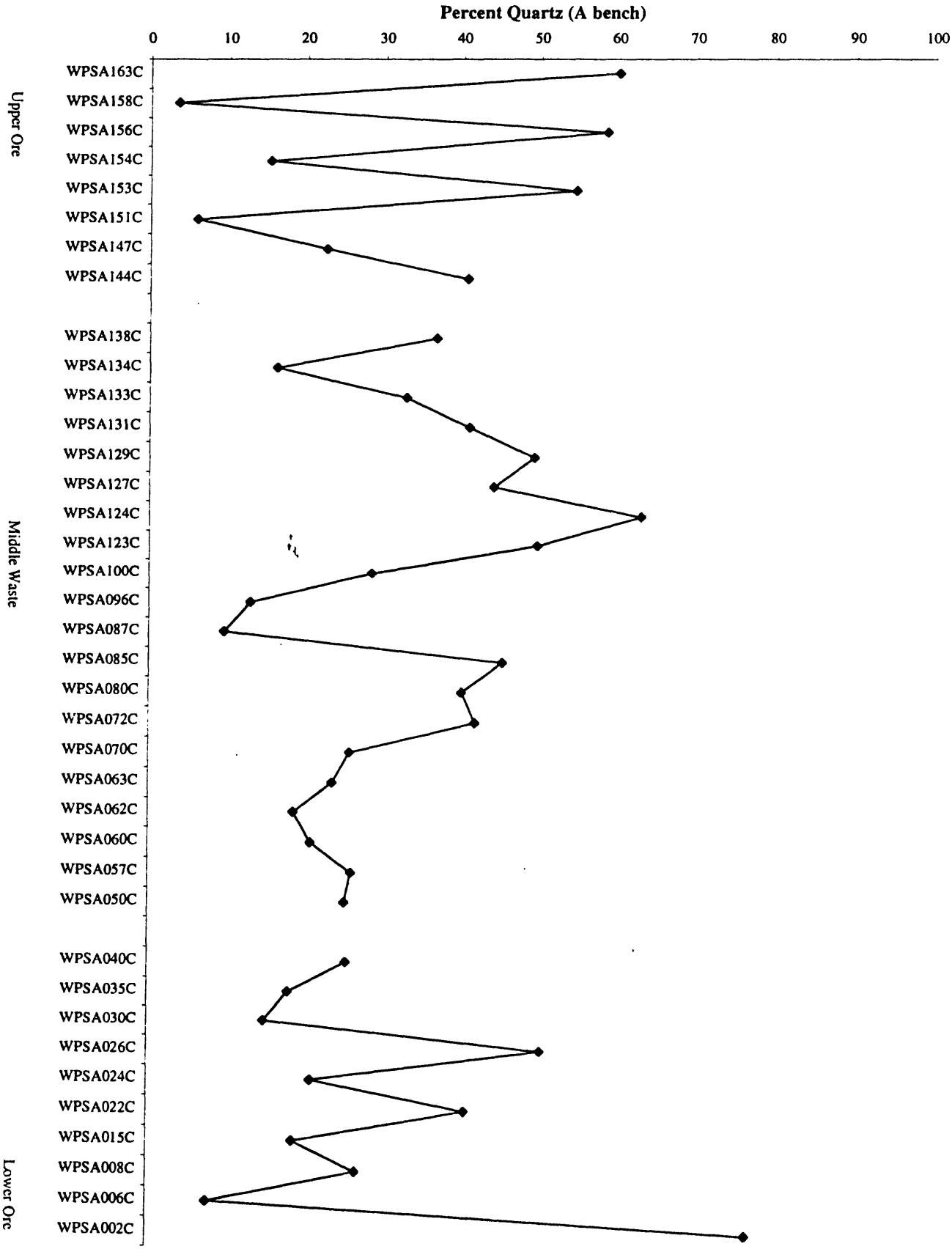

**Figure 5:** Graphical view of the data presented in Table 3. Variations over the two measured stratigraphic sections are shown for each of the major mineral phases, including; apatite, quartz, muscovite, total feldspar (including albite, orthoclase, and buddingtonite), buddingtonite, and dolomite. Gaps are inserted in the graph to separate the middle waste from the upper and lower ore producing bodies.

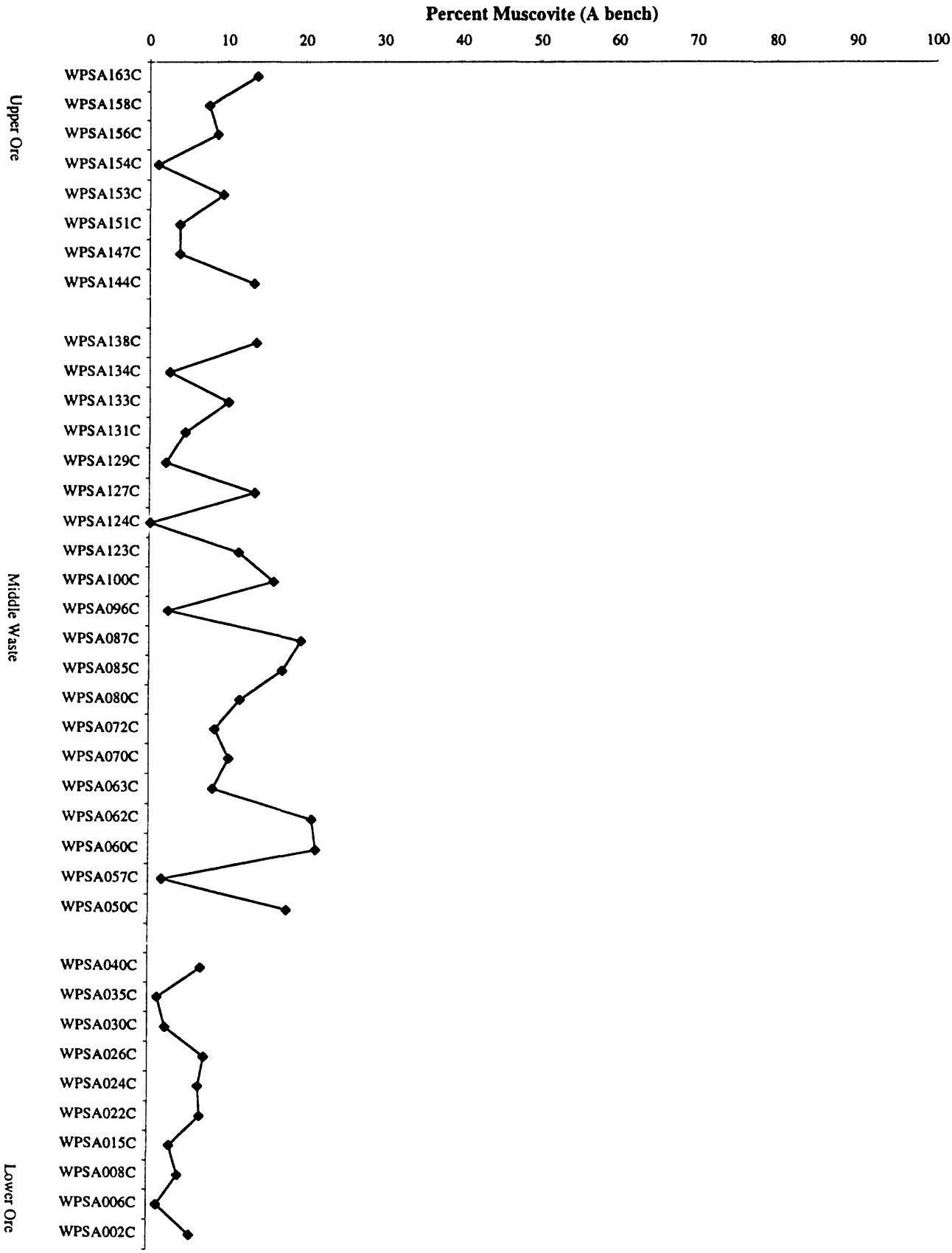

**Figure 5:** Graphical view of the data presented in Table 3. Variations over the two measured stratigraphic sections are shown for each of the major mineral phases, including; apatite, quartz, muscovite, total feldspar (including albite, orthoclase, and buddingtonite), buddingtonite, and dolomite. Gaps are inserted in the graph to separate the middle waste from the upper and lower ore producing bodies.

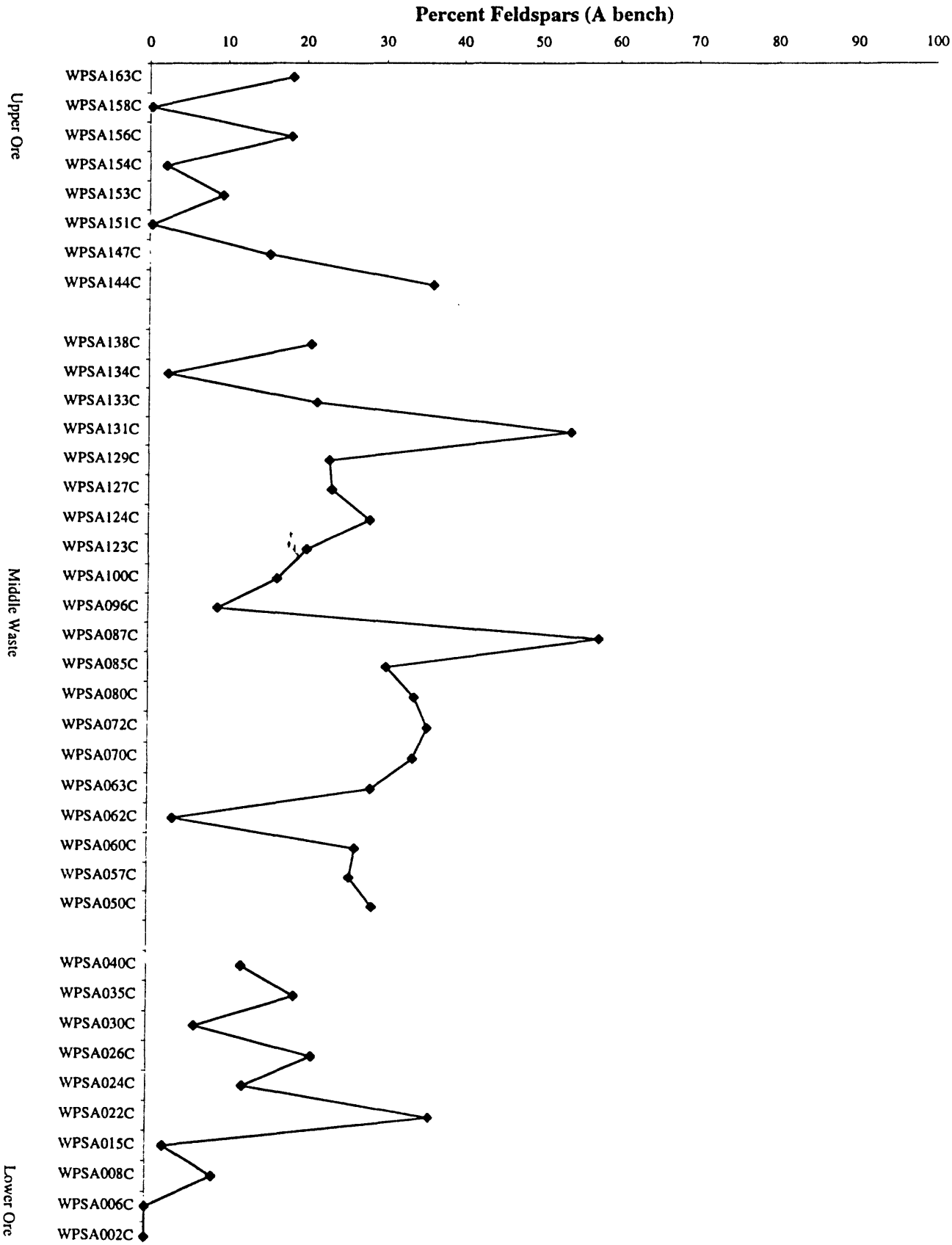

**Figure 5:** Graphical view of the data presented in Table 3. Variations over the two measured stratigraphic sections are shown for each of the major mineral phases, including; apatite, quartz, muscovite, total feldspar (including albite, orthoclase, and buddingtonite), buddingtonite, and dolomite. Gaps are inserted in the graph to separate the middle waste from the upper and lower ore producing bodies.

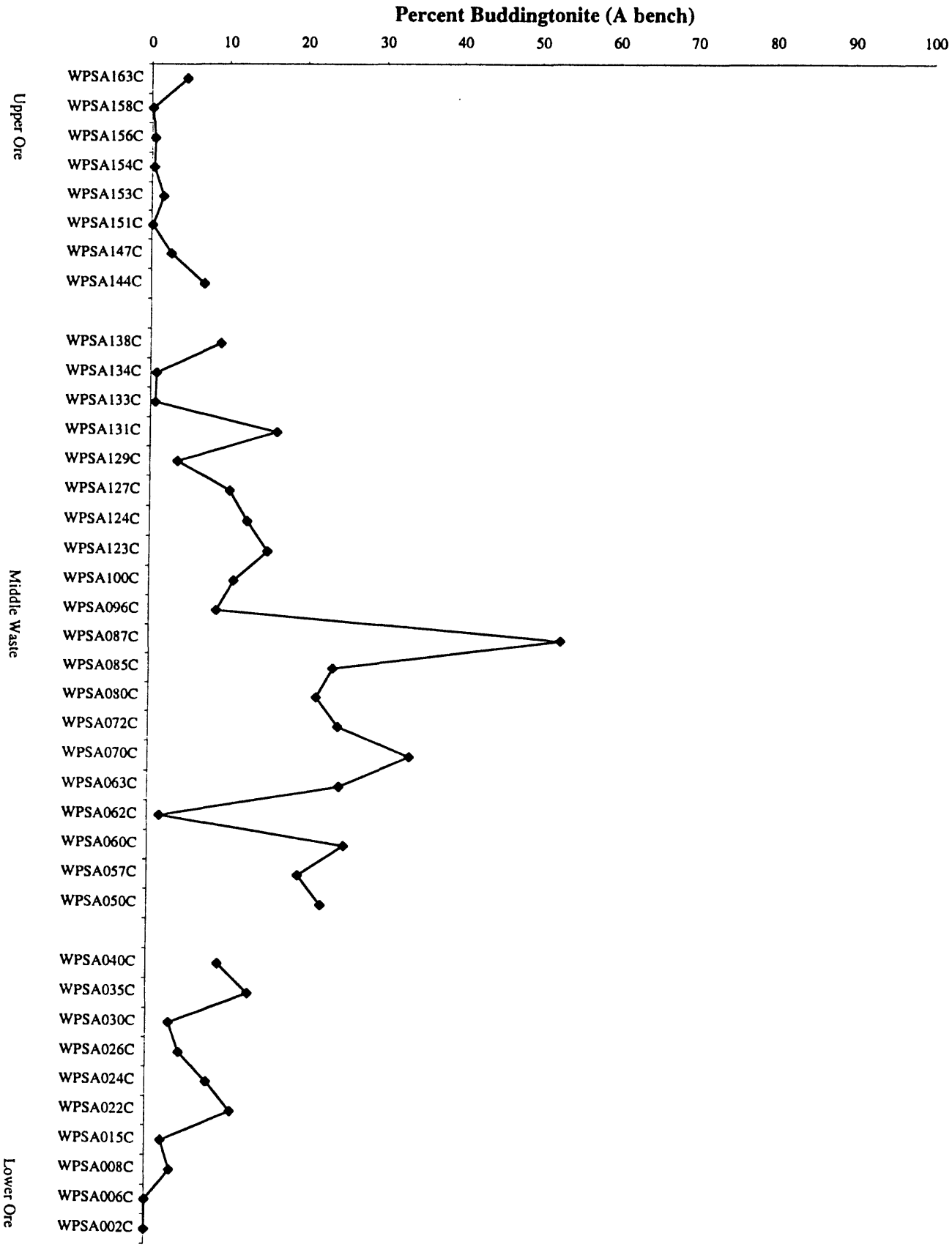

**Figure 5:** Graphical view of the data presented in Table 3. Variations over the two measured stratigraphic sections are shown for each of the major mineral phases, including; apatite, quartz, muscovite, total feldspar (including albite, orthoclase, and buddingtonite), buddingtonite, and dolomite. Gaps are inserted in the graph to separate the middle waste from the upper and lower ore producing bodies.

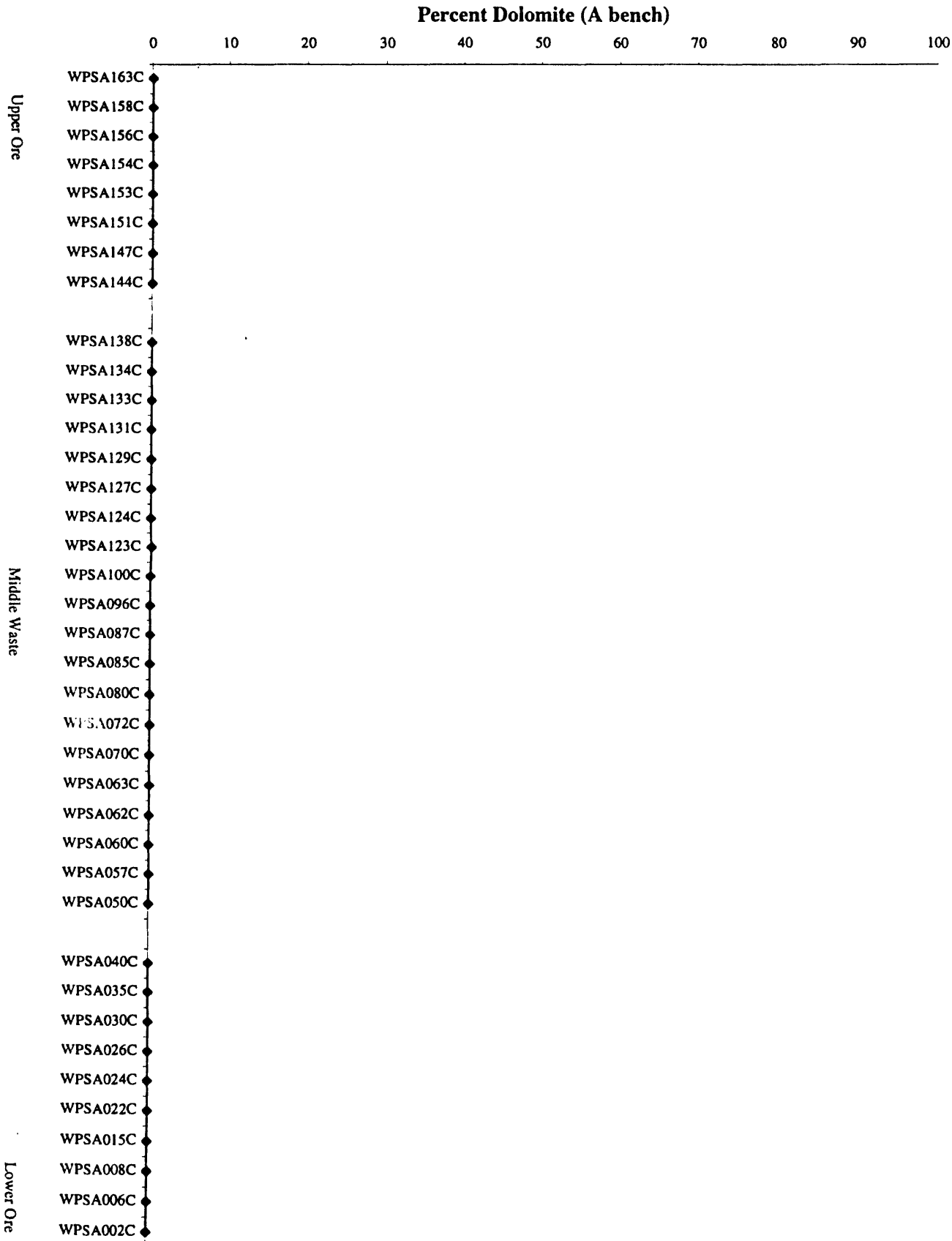

**Table 3:** Mineralogical composition calculated by the Rietveld method. The ($\chi^2$) value is a numerical statement of the quality of the fit between the calculated and collected XRD patterns, where any value less than 3 is considered acceptable, with smaller ($\chi^2$) inferring better results. Percents are listed with an accepted error in the last decimal place given in parentheses.

| Sample # | $\chi^2$ | % apatite | % quartz | % muscovite | % illite | % albite | % orthoclase | % buddingtonite | % kaolinite | % dolomite | % calcite |
|---|---|---|---|---|---|---|---|---|---|---|---|
| WPSB003C | 1.71 | 0.8 (5) | 51.0 (9) | 7.4 (3) | 1.8 (8) | 0.0 (0) | 2.8 (5) | 0.3 (7) | 1.6 (6) | 33.5 (6) | 0.3 (3) |
| WPSB008C | 1.42 | 88 (2) | 7.3 (3) | 2 (1) | 0.1 (8) | 0.1 (6) | 0.1 (7) | 0.8 (6) | 0.0 (0) | 0.4 (1) | 0.0 (0) |
| WPSB018C* | 1.23 | 91 (2) | 5.0 (3) | 2.1 (4) | 0.2 (9) | 0.1 (9) | 0.6 (8) | 0.1 (7) | 0.0 (0) | 0.0 (0) | 0.0 (0) |
| WPSB025C* | 1.42 | 11.6 (4) | 9.4 (2) | 3.2 (5) | 0.1 (7) | 0.1 (5) | 4.4 (4) | 2.6 (5) | 2.0 (4) | 66.7 (9) | 0.0 (0) |
| WPSB026C | 1.40 | 72 (2) | 17.3 (4) | 3 (2) | 0.1 (7) | 0.1 (7) | 1.5 (4) | 0.1 (6) | 0.6 (5) | 3.7 (6) | 0.0 (0) |
| WPSB027C | 1.39 | 9.9 (5) | 5.4 (2) | 4 (1) | 0.1 (8) | 0.0 (0) | 3.1 (5) | 0.5 (5) | 1.2 (4) | 75 (2) | 0.1 (2) |
| WPSB033C | 1.38 | 82 (2) | 9.8 (3) | 3 (1) | 0.1 (8) | 0.2 (6) | 2 (7) | 1.4 (5) | 0.3 (5) | 1.1 (3) | 0.0 (0) |
| WPSB038C | 1.30 | 4.4 (3) | 10.1 (2) | 0.1 (4) | 0.1 (5) | 3.4 (4) | 1.9 (3) | 1.0 (3) | 0.0 (3) | 79.0 (8) | 0.0 (0) |
| WPSB047C | 1.56 | 56 (1) | 22.3 (6) | 4 (1) | 0.1 (8) | 2.3 (9) | 1.6 (6) | 4 (1) | 0.5 (5) | 8.4 (3) | 0.0 (0) |
| WPSB059C | 1.47 | 50 (1) | 10.9 (3) | 5 (1) | 0.1 (8) | 0.6 (6) | 0.1 (6) | 9.2 (8) | 0.6 (5) | 21.7 (8) | 1.6 (2) |
| WPSB065C | 1.34 | 1.2 (3) | 6.7 (2) | 0.7 (5) | 0.1 (5) | 4.9 (4) | 1.3 (3) | 7.8 (5) | 0.2 (3) | 71.1 (9) | 6.0 (5) |
| WPSB070C | 1.56 | 37 (1) | 21.6 (6) | 9 (1) | 0 (1) | 0.4 (7) | 0.1 (5) | 27 (1) | 0.9 (7) | 1.4 (5) | 1.7 (3) |
| WPSB080C | 1.63 | 14.9 (5) | 34.3 (7) | 7.6 (8) | 0.1 (7) | 15.7 (5) | 5.5 (7) | 20.4 (8) | 1.2 (5) | 0.1 (3) | 0.0 (3) |
| WPSB084C | 1.55 | 34 (1) | 20.3 (6) | 13 (2) | 0.1 (8) | 6.2 (1) | 0.3 (4) | 21.2 (9) | 0.5 (5) | 3.3 (7) | 1.3 (3) |
| WPSB087C* | 1.58 | 43 (1) | 23.6 (8) | 14 (2) | 0 (1) | 3 (1) | 1.7 (5) | 12.9 (9) | 0.0 (6) | 2 (1) | 0.0 (4) |
| WPSB091C* | 1.50 | 58 (2) | 17.1 (5) | 11 (2) | 0.1(9) | 1.3 (7) | 1.0 (4) | 11 (1) | 0.0 (6) | 0.0 (4) | 0.0 (3) |
| WPSB095C | 1.55 | 10.9 (5) | 40.3 (8) | 9.7 (9) | 0.1 (7) | 10.3 (5) | 4.3 (6) | 17.0 (7) | 0.4 (5) | 8.7 (7) | 1.3 (3) |
| WPSB097C | 1.38 | 74 (1) | 15.3 (4) | 5 (1) | 0.1 (8) | 1.3 (6) | 0.3 (6) | 3.1 (7) | 0.0 (5) | 0.0 (3) | 0.0 (3) |
| WPSB100C | 1.54 | 22.1 (6) | 53 (1) | 1.6 (1) | 0.1 (7) | 5.5 (6) | 6.2 (7) | 10.1 (7) | 1.3 (5) | 0.0 (3) | 0.0 (3) |
| WPSB107C | 1.55 | 5.9 (4) | 41.3 (6) | 5.0 (6) | 0.1 (5) | 16.7 (5) | 7.2 (5) | 22.0 (6) | 1.7 (4) | 0.1 (2) | 0.0 (2) |
| WPSB117C | 1.61 | 21.7 (7) | 33.7 (7) | 11 (1) | 0.1 (8) | 8.4 (6) | 1.6 (5) | 10.9 (7) | 0.4 (5) | 6.6 (9) | 0.2 (3) |
| WPSB131C | 1.39 | 80 (2) | 8.3 (4) | 9 (2) | 2 (1) | 0.1 (7) | 0.1 (8) | 0.1 (7) | 0.0 (6) | 0.0 (4) | 0.0 (3) |
| WPSB133C | 1.37 | 83 (2) | 8.8 (3) | 6 (1) | 0.1 (8) | 0.1 (6) | 0.1 (6) | 1.7 (9) | 0.4 (5) | 0.1 (3) | 0.0 (3) |
| WPSB134C | 1.46 | 20.2 (5) | 49.1 (8) | 9.3 (7) | 1.9 (6) | 10.1 (5) | 4.9 (6) | 2.6 (5) | 1.7 (5) | 0.0 (3) | 0.1 (2) |
| WPSB136C | 1.39 | 88 (2) | 7.8 (3) | 3 (1) | 0.1 (8) | 0.2 (2) | 0.1 (7) | 0.1 (6) | 0.0 (5) | 0.0 (4) | 0.0 (3) |
| WPSB137C | 2.33 | 0 (1) | 44 (3) | 5.9 (6) | 2 (2) | 44 (3) | 2 (1) | 2 (1) | 0 (1) | 0 (7) | 0 (5) |
| WPSB139C | 1.28 | 93 (2) | 3.8 (2) | 2.4 (9) | 0.1 (7) | 0.1 (5) | 0.1 (6) | 0.1 (6) | 0.0 (5) | 0.0 (3) | 0.0 (3) |
| WPSB145C | 1.67 | 4.8 (5) | 61 (1) | 10.4 (9) | 1.9 (6) | 8.4 (5) | 9.6 (6) | 2.7 (5) | 0.6 (4) | 0.0 (3) | 0.0 (2) |
| WPSB157C | 1.58 | 10.2 (6) | 49 (1) | 17 (2) | 5.4 (8) | 4.7 (6) | 1.4 (7) | 2.5 (6) | 0.3 (1) | 2 (1) | 0.4 (4) |

This Page Intentionally Left Blank

**Figure 5:** Graphical view of the data presented in Table 3. Variations over the two measured stratigraphic sections are shown for each of the major mineral phases, including; apatite, quartz, muscovite, total feldspar (including albite, orthoclase, and buddingtonite), buddingtonite, and dolomite. Gaps are inserted in the graph to separate the middle waste from the upper and lower ore producing bodies.

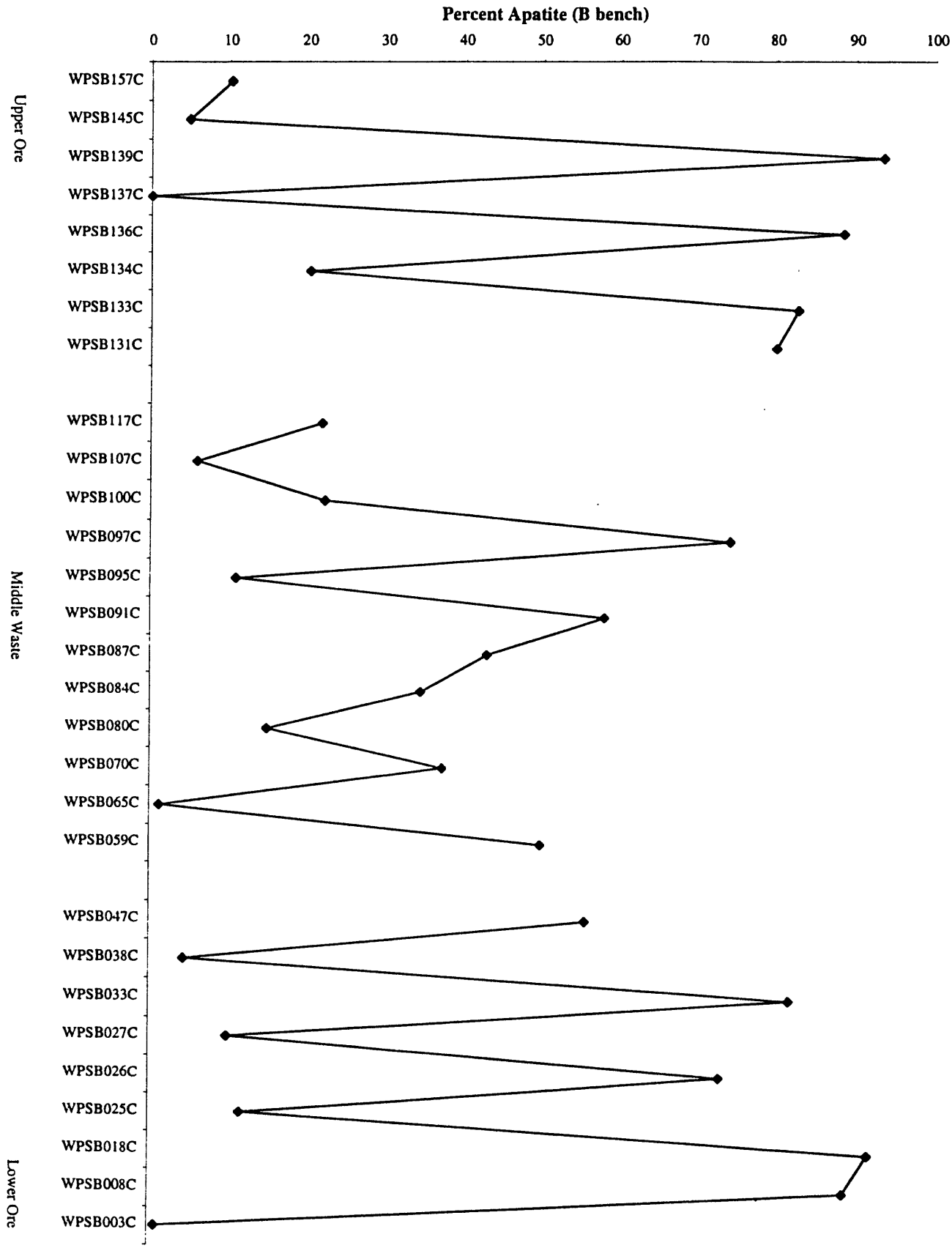

**Figure 5:** Graphical view of the data presented in Table 3. Variations over the two measured stratigraphic sections are shown for each of the major mineral phases, including; apatite, quartz, muscovite, total feldspar (including albite, orthoclase, and buddingtonite), buddingtonite, and dolomite. Gaps are inserted in the graph to separate the middle waste from the upper and lower ore producing bodies.

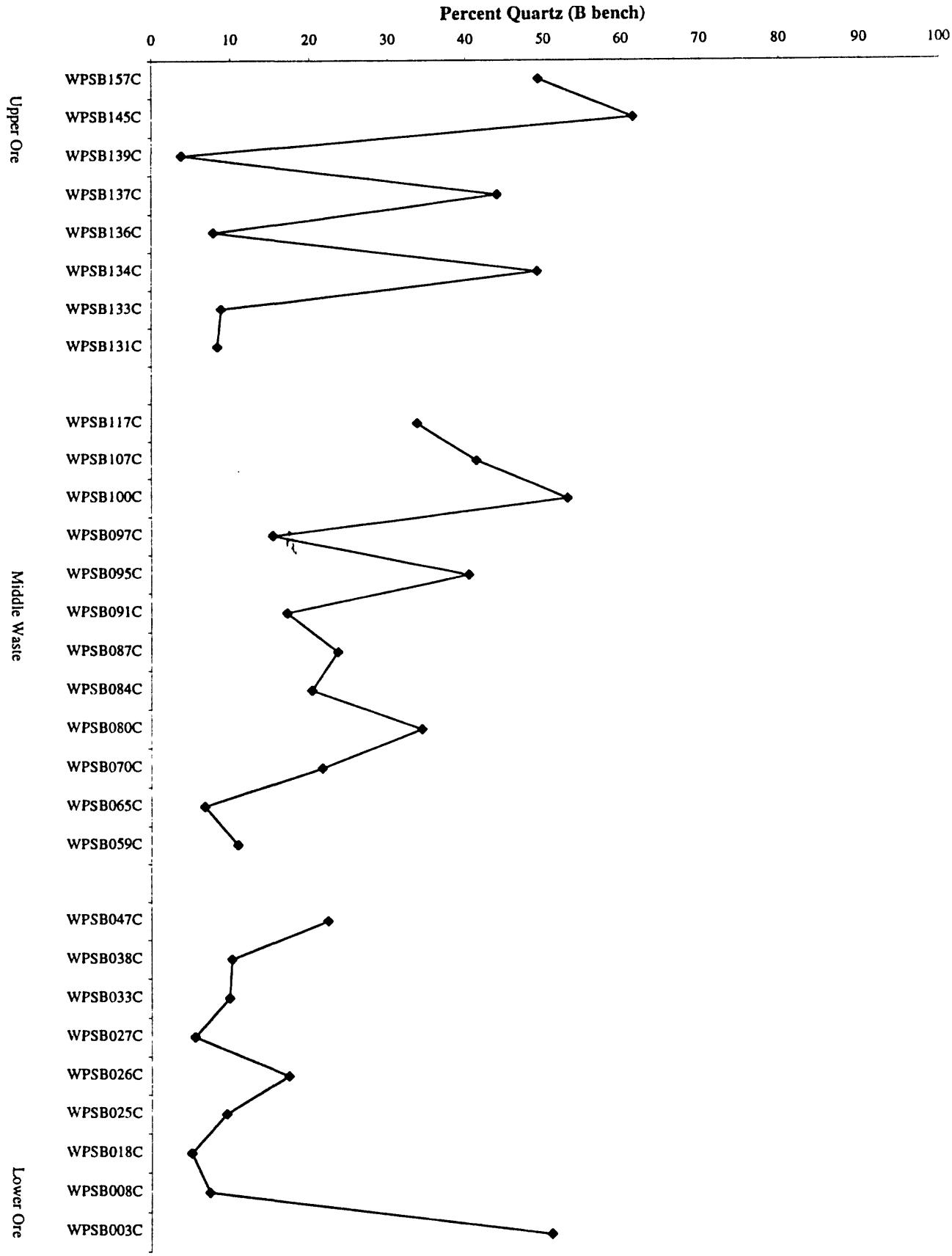

**Figure 5:** Graphical view of the data presented in Table 3. Variations over the two measured stratigraphic sections are shown for each of the major mineral phases, including; apatite, quartz, muscovite, total feldspar (including albite, orthoclase, and buddingtonite), buddingtonite, and dolomite. Gaps are inserted in the graph to separate the middle waste from the upper and lower ore producing bodies.

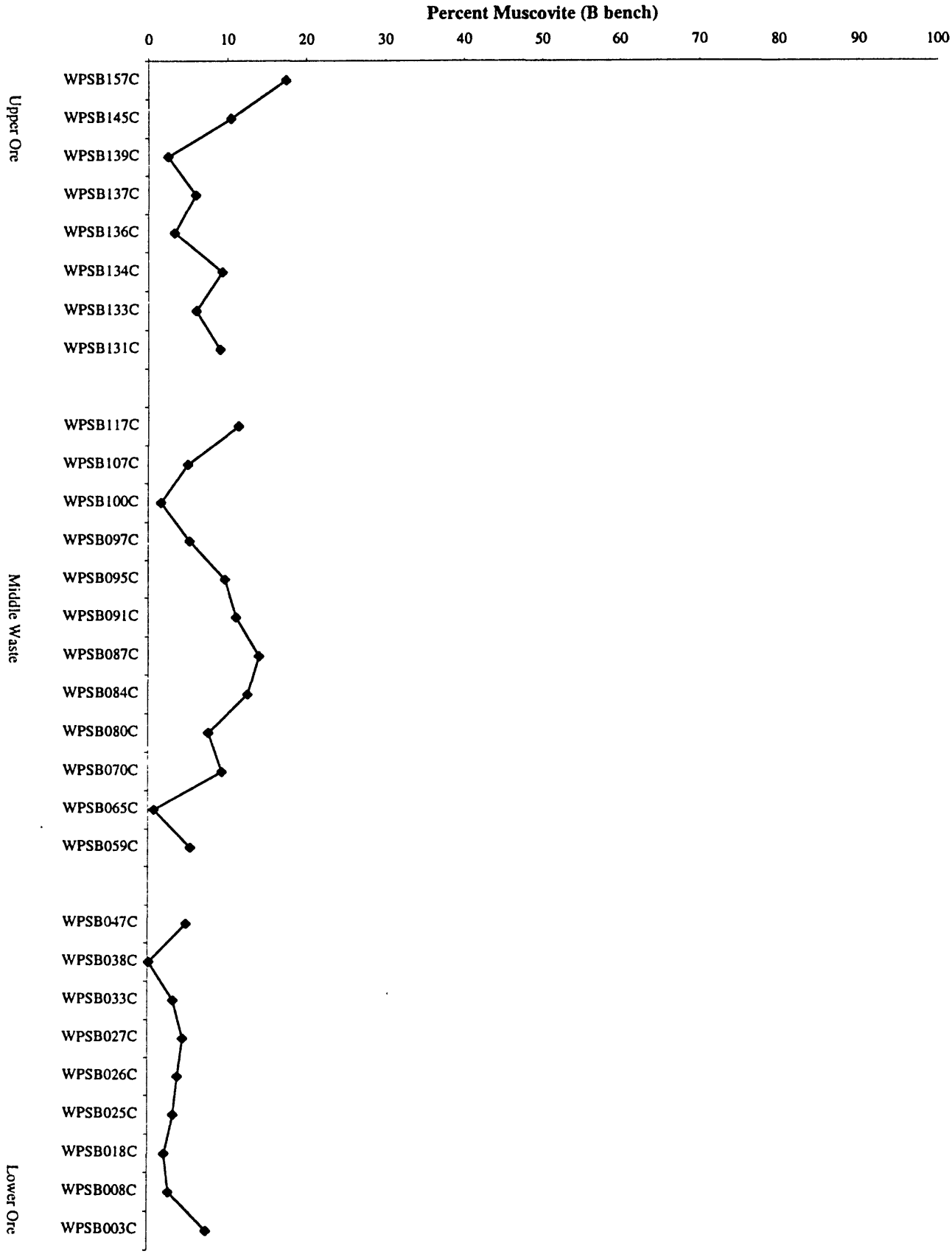

**Figure 5:** Graphical view of the data presented in Table 3. Variations over the two measured stratigraphic sections are shown for each of the major mineral phases, including; apatite, quartz, muscovite, total feldspar (including albite, orthoclase, and buddingtonite), buddingtonite, and dolomite. Gaps are inserted in the graph to separate the middle waste from the upper and lower ore producing bodies.

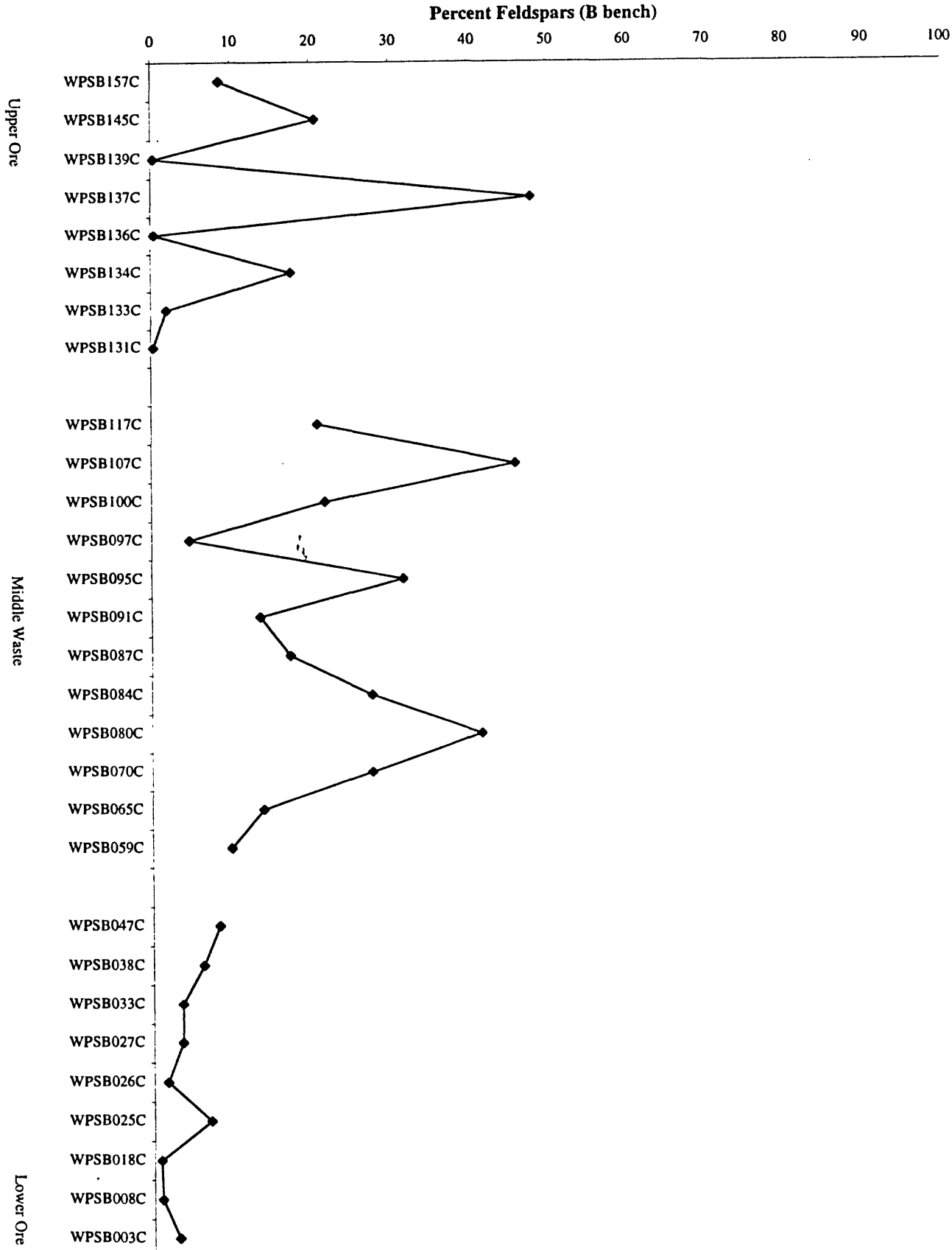

**Figure 5:** Graphical view of the data presented in Table 3. Variations over the two measured stratigraphic sections are shown for each of the major mineral phases, including; apatite, quartz, muscovite, total feldspar (including albite, orthoclase, and buddingtonite), buddingtonite, and dolomite. Gaps are inserted in the graph to separate the middle waste from the upper and lower ore producing bodies.

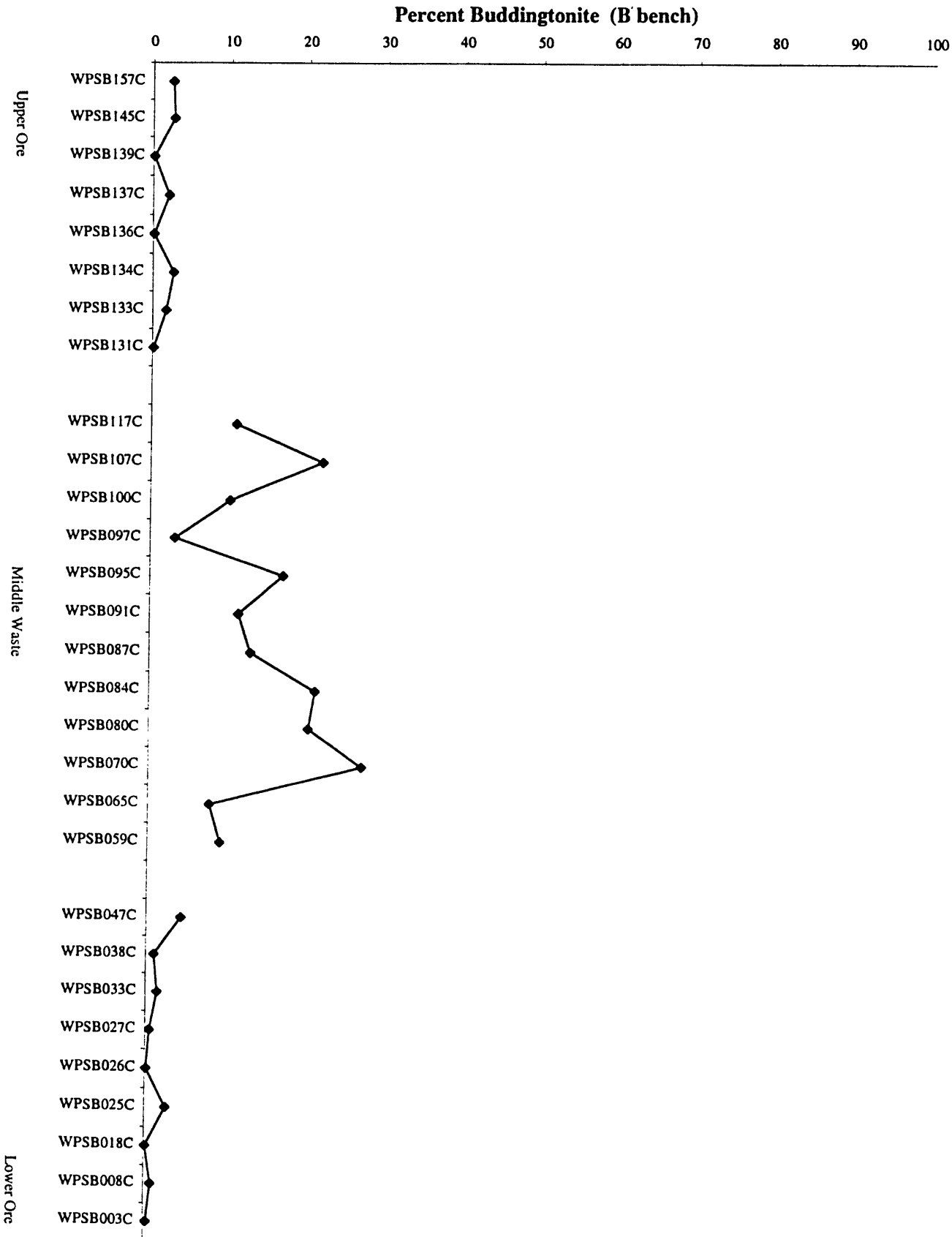

**Figure 5:** Graphical view of the data presented in Table 3. Variations over the two measured stratigraphic sections are shown for each of the major mineral phases, including; apatite, quartz, muscovite, total feldspar (including albite, orthoclase, and buddingtonite), buddingtonite, and dolomite. Gaps are inserted in the graph to separate the middle waste from the upper and lower ore producing bodies.

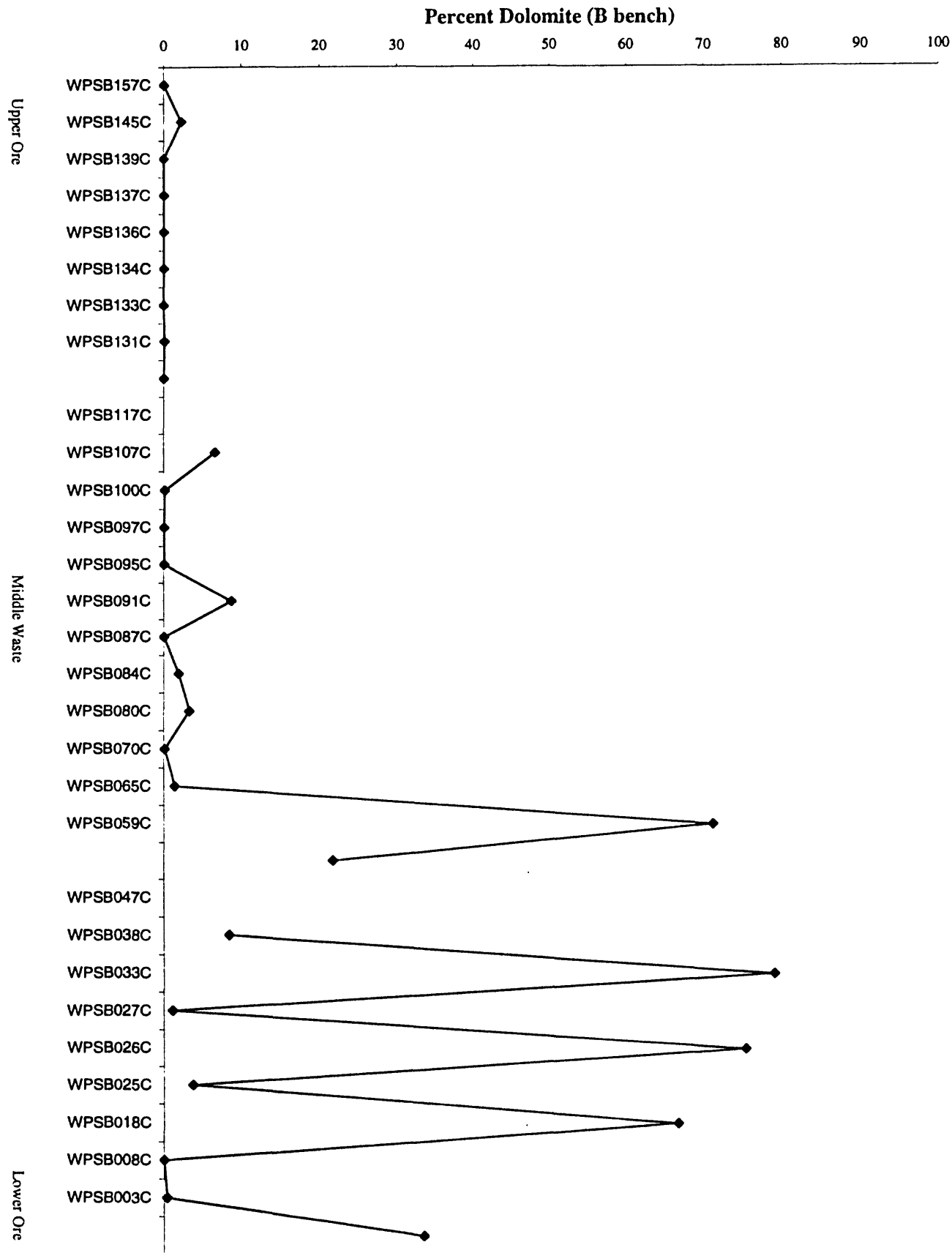

**Table 4:** Comparison of ICP data (Herring and others 1999) and calculated chemistry based on mineral compositions from Rietveld analysis. ICP data are normalized to include the elements that are calculated using the XRD data. The average difference shows whether the XRD data overstate ("-" values) or understate ("+" values) the ICP data. A weighted error is calculated by multiplying the error's absolute value by a weighting factor (measured / measured average). This value shows the comparability of the two data sets.

| Sample # | Measured % (ICP) | Normalized % (ICP) | Ca Calculated % (XRD) | Difference (Normalized - Calculated) | % Error (Difference / Normalized) | Weighted % error |
|---|---|---|---|---|---|---|
| WPSA002C | 3.4 | 3.9 | 2.7 | 1.2 | 30.9 | 7.0 |
| WPSA006C | 33.7 | 35.4 | 37.2 | -1.8 | -4.9 | 10.3 |
| WPSA008C | 23.0 | 24.8 | 23.8 | 1.1 | 4.3 | 6.3 |
| WPSA015C | 29.0 | 30.8 | 30.1 | 0.7 | 2.3 | 4.1 |
| WPSA022C | 7.6 | 8.1 | 6.0 | 2.2 | 26.7 | 12.8 |
| WPSA024C | 25.2 | 26.8 | 24.6 | 2.1 | 8.0 | 12.5 |
| WPSA026C | 9.0 | 9.9 | 7.2 | 2.7 | 27.2 | 15.8 |
| WPSA030C | 27.4 | 29.3 | 31.2 | -1.9 | -6.6 | 11.3 |
| WPSA035C | 22.1 | 23.5 | 25.2 | -1.7 | -7.3 | 10.1 |
| WPSA040C | 22.5 | 24.4 | 22.4 | 2.0 | 8.0 | 11.5 |
| WPSA050C | 12.1 | 14.0 | 11.6 | 2.4 | 17.0 | 14.0 |
| WPSA057C | 13.6 | 15.5 | 16.6 | -1.2 | -7.6 | 6.9 |
| WPSA060C | 9.7 | 12.9 | 12.5 | 0.4 | 3.0 | 2.2 |
| WPSA062C | 5.8 | 19.5 | 15.8 | 3.8 | 19.3 | 22.1 |
| WPSA063C | 13.6 | 17.4 | 16.1 | 1.3 | 7.3 | 7.5 |
| WPSA070C | 11.0 | 13.1 | 12.6 | 0.5 | 3.6 | 2.8 |
| WPSA072C | 6.8 | 7.7 | 5.7 | 2.0 | 25.9 | 11.7 |
| WPSA080C | 5.6 | 7.2 | 5.2 | 2.0 | 27.3 | 11.5 |
| WPSA085C | 2.3 | 2.7 | 1.7 | 1.0 | 38.0 | 6.0 |
| WPSA087C | 4.2 | 4.9 | 4.5 | 0.4 | 7.6 | 2.2 |
| WPSA096C | 24.4 | 27.2 | 31.2 | -4.0 | -14.7 | 23.6 |
| WPSA100C* | 14.3 | 16.3 | 15.5 | 0.8 | 5.0 | 4.8 |
| WPSA123C* | 9.4 | 10.7 | 7.4 | 3.4 | 31.5 | 19.9 |
| WPSA124C* | 4.2 | 4.5 | 3.4 | 1.1 | 25.0 | 6.6 |
| WPSA127C* | 8.5 | 9.6 | 7.6 | 2.0 | 20.6 | 11.6 |
| WPSA129C | 14.6 | 15.8 | 10.3 | 5.5 | 34.8 | 32.4 |
| WPSA131C | 1.6 | 1.8 | 0.4 | 1.4 | 79.8 | 8.4 |
| WPSA133C* | 17.8 | 19.5 | 12.7 | 6.8 | 35.1 | 40.3 |
| WPSA134C* | 27.5 | 29.4 | 32.3 | -2.9 | -9.9 | 17.2 |
| WPSA138C* | 11.2 | 13.5 | 11.2 | 2.3 | 16.9 | 13.4 |
| WPSA144C | 4.2 | 4.7 | 2.8 | 1.9 | 40.9 | 11.4 |
| WPSA147C | 26.9 | 29.1 | 23.8 | 5.3 | 18.3 | 31.3 |
| WPSA151C | 36.8 | 38.6 | 37.1 | 1.6 | 4.0 | 9.1 |
| WPSA153C | 12.8 | 13.7 | 10.0 | 3.8 | 27.4 | 22.1 |
| WPSA154C | 30.8 | 31.9 | 33.4 | -1.6 | -4.9 | 9.2 |
| WPSA156C | 7.3 | 7.9 | 4.0 | 3.9 | 49.2 | 23.0 |
| WPSA158C | 34.9 | 36.2 | 36.4 | -0.3 | -0.7 | 1.5 |
| WPSA163C | 4.0 | 4.3 | 2.5 | 1.8 | 41.4 | 10.4 |
| average | | 17.0 | | | 16.6 | 16.6 |

* Samples that contain a high percentage of an unanalyzed phase with a prominent peak at about 23 Å, possibly the clay rectorite.

**Figure 6:** Graphical view of the data presented in Table 4, showing the comparability of the ICP and XRD data sets over the measured stratigraphic sections. Gaps are inserted in the graph to separate the middle waste from the upper and lower ore producing bodies.

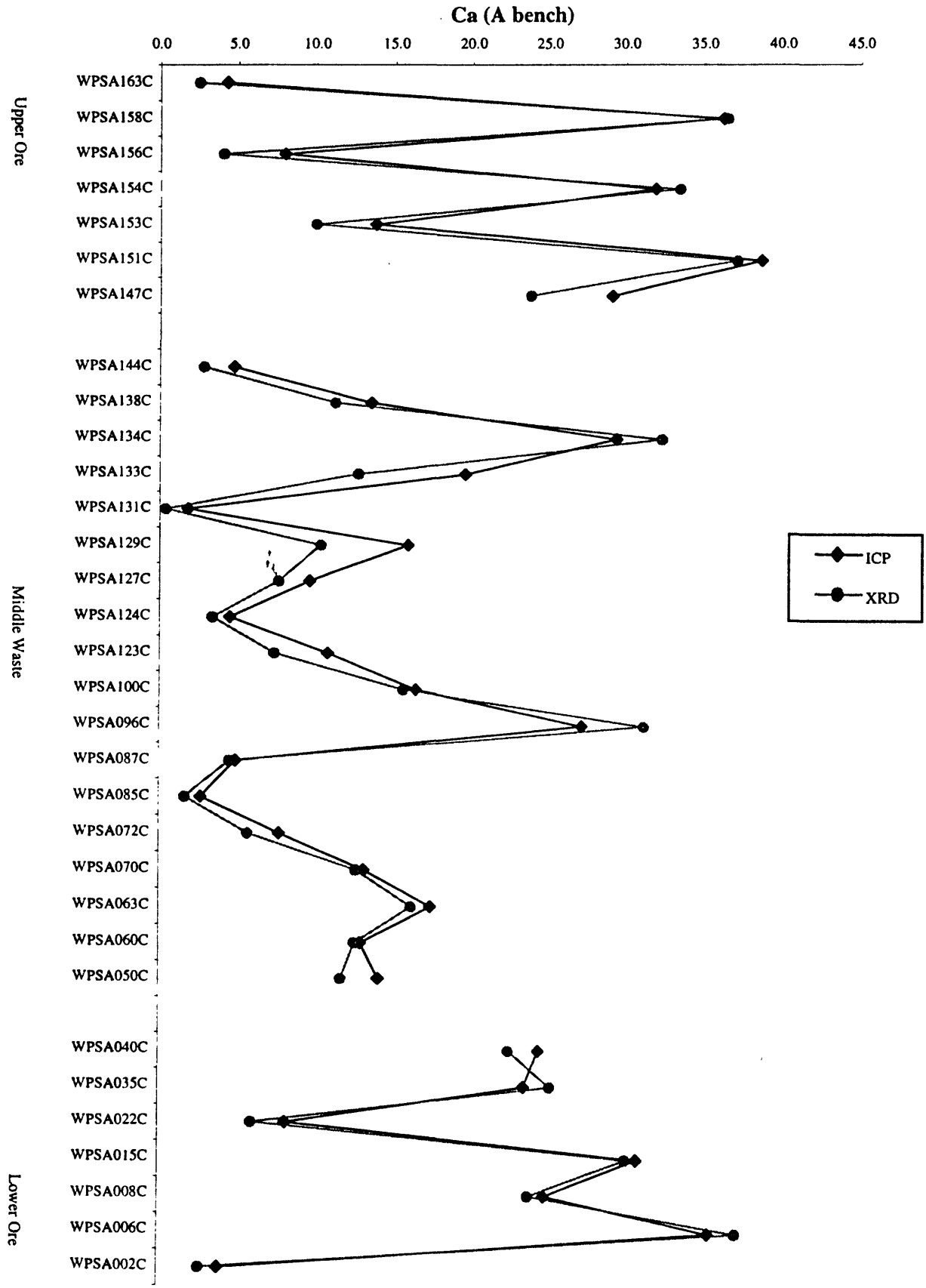

**Table 4:** Comparison of ICP data (Herring and others 1999) and calculated chemistry based on mineral compositions from Rietveld analysis. ICP data are normalized to include the elements that are calculated using the XRD data. The average difference shows whether the XRD data overstate ("-" values) or understate ("+" values) the ICP data. A weighted error is calculated by multiplying the error's absolute value by a weighting factor (measured / measured average). This value shows the comparability of the two data sets.

| Sample # | Measured % (ICP) | Normalized % (ICP) | P Calculated % (XRD) | Difference (Normalized - Calculated) | % Error (Difference / Normalized) | Weighted % error |
|---|---|---|---|---|---|---|
| WPSA002C | 1.6 | 1.8 | 1.2 | 0.6 | 32.6 | 7.2 |
| WPSA006C | 15.4 | 16.2 | 16.6 | -0.4 | -2.5 | 4.9 |
| WPSA008C | 10.5 | 11.3 | 10.5 | 0.8 | 7.1 | 9.9 |
| WPSA015C | 13.2 | 14.0 | 13.5 | 0.5 | 3.9 | 6.7 |
| WPSA022C | 3.6 | 3.9 | 2.7 | 1.2 | 30.9 | 14.7 |
| WPSA024C | 12.3 | 13.1 | 11.1 | 2.0 | 15.0 | 23.9 |
| WPSA026C | 4.1 | 4.6 | 3.3 | 1.2 | 27.1 | 15.1 |
| WPSA030C | 13.2 | 14.1 | 14.1 | 0.0 | 0.3 | 0.5 |
| WPSA035C | 10.2 | 10.8 | 11.2 | -0.4 | -3.9 | 5.1 |
| WPSA040C | 10.7 | 11.6 | 10.1 | 1.5 | 13.1 | 18.6 |
| WPSA050C | 6.2 | 7.2 | 5.4 | 1.8 | 24.9 | 21.8 |
| WPSA057C | 6.5 | 7.4 | 7.4 | 0.0 | 0.3 | 0.2 |
| WPSA060C | 5.2 | 6.9 | 5.7 | 1.3 | 18.2 | 15.4 |
| WPSA062C | 1.9 | 6.5 | 7.1 | -0.6 | -9.1 | 7.2 |
| WPSA063C | 6.8 | 8.7 | 7.2 | 1.5 | 17.0 | 18.1 |
| WPSA070C | 5.3 | 6.3 | 5.7 | 0.6 | 9.2 | 7.0 |
| WPSA072C | 3.3 | 3.8 | 2.5 | 1.3 | 33.7 | 15.6 |
| WPSA080C | 2.9 | 3.7 | 2.3 | 1.4 | 37.1 | 16.9 |
| WPSA085C | 1.3 | 1.6 | 0.8 | 0.8 | 51.5 | 10.0 |
| WPSA087C | 2.5 | 2.9 | 2.0 | 0.9 | 31.1 | 11.0 |
| WPSA096C* | 12.8 | 14.3 | 14.2 | 0.0 | 0.1 | 0.2 |
| WPSA100C* | 7.4 | 8.4 | 7.1 | 1.4 | 16.1 | 16.6 |
| WPSA123C* | 4.9 | 5.6 | 3.3 | 2.3 | 40.2 | 27.4 |
| WPSA124C* | 3.1 | 3.4 | 1.6 | 1.8 | 53.3 | 21.8 |
| WPSA127C* | 4.4 | 4.9 | 3.5 | 1.4 | 29.2 | 17.6 |
| WPSA129C | 7.0 | 7.6 | 4.8 | 2.8 | 37.3 | 34.6 |
| WPSA131C | 1.4 | 1.6 | 0.2 | 1.4 | 89.5 | 17.5 |
| WPSA133C* | 8.7 | 9.5 | 5.7 | 3.8 | 39.6 | 45.8 |
| WPSA134C* | 13.1 | 14.0 | 14.5 | -0.5 | -3.5 | 6.0 |
| WPSA138C* | 5.6 | 6.7 | 5.0 | 1.6 | 24.7 | 20.1 |
| WPSA144C | 2.0 | 2.3 | 1.2 | 1.1 | 45.8 | 12.8 |
| WPSA147C | 12.4 | 13.4 | 10.5 | 2.9 | 21.7 | 35.5 |
| WPSA151C | 17.0 | 17.8 | 16.2 | 1.6 | 9.1 | 19.8 |
| WPSA153C | 6.2 | 6.6 | 4.4 | 2.2 | 32.8 | 26.5 |
| WPSA154C | 14.6 | 15.1 | 15.1 | 0.0 | 0.2 | 0.4 |
| WPSA156C | 3.5 | 3.8 | 1.8 | 2.0 | 52.5 | 24.3 |
| WPSA158C | 16.0 | 16.6 | 16.5 | 0.1 | 0.4 | 0.7 |
| WPSA163C | 1.9 | 2.0 | 1.1 | 0.9 | 44.5 | 11.1 |
| average | 7.3 | 8.2 | 7.0 | 1.1 | 22.9 | 15.0 |

**Figure 6:** Graphical view of the data presented in Table 4, showing the comparability of the ICP and XRD data sets over the measured stratigraphic sections. Gaps are inserted in the graph to separate the middle waste from the upper and lower ore producing bodies.

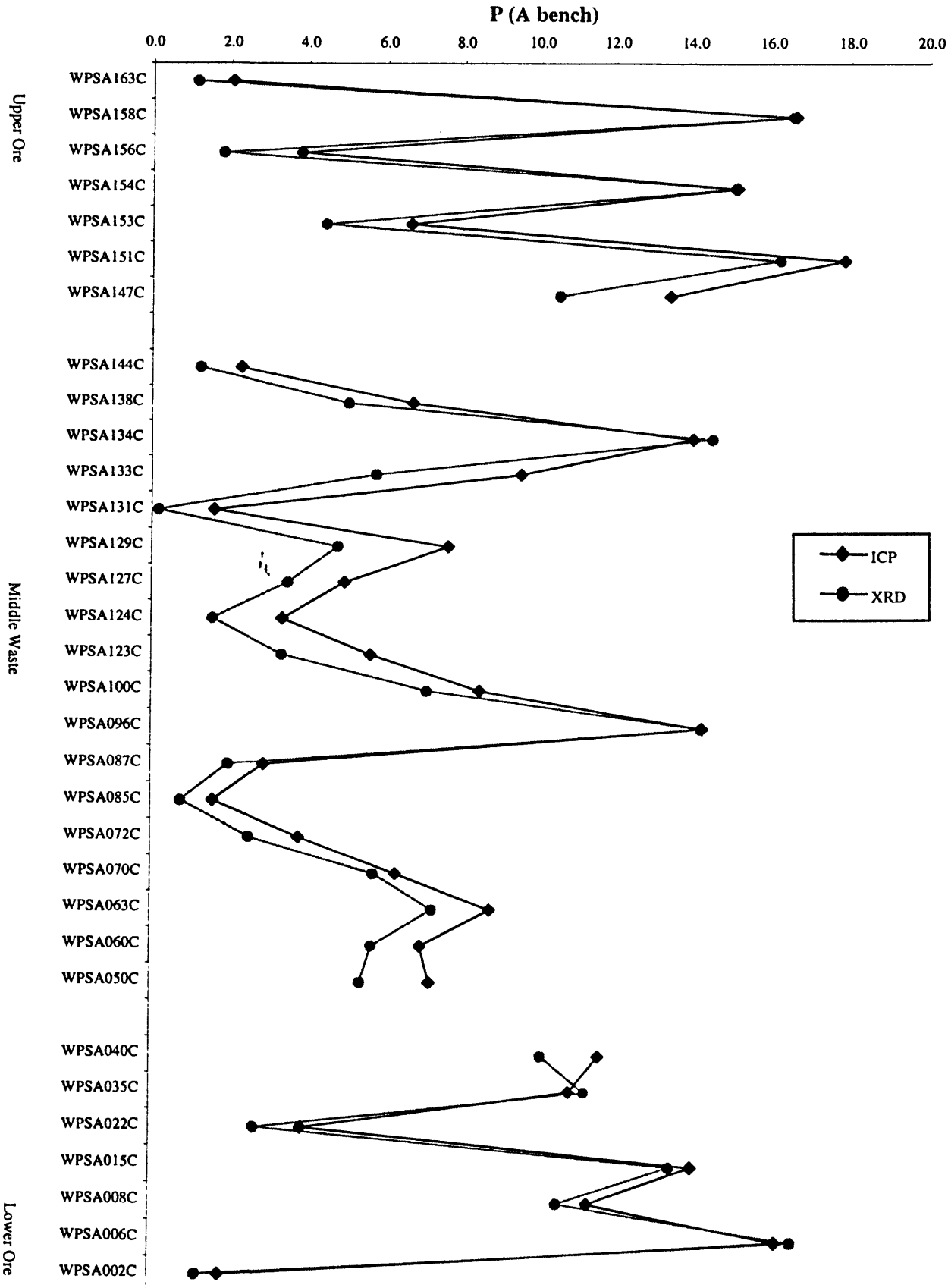

**Table 4:** Comparison of ICP data (Herring and others 1999) and calculated chemistry based on mineral compositions from Rietveld analysis. ICP data are normalized to include the elements that are calculated using the XRD data. The average difference shows whether the XRD data overstate ("-" values) or understate ("+" values) the ICP data. A weighted error is calculated by multiplying the error's absolute value by a weighting factor (measured / measured average). This value shows the comparability of the two data sets.

| Sample # | Measured % (ICP) | Normalized % (ICP) | Si Calculated % (XRD) | Difference (Normalized - Calculated) | % Error (Difference / Normalized) | Weighted % error |
|---|---|---|---|---|---|---|
| WPSA002C | 27.9 | 31.6 | 39.5 | -8.0 | -25.2 | 41.9 |
| WPSA006C | 3.5 | 3.7 | 4.2 | -0.5 | -13.9 | 2.7 |
| WPSA008C | 12.6 | 13.6 | 16.9 | -3.3 | -24.5 | 17.5 |
| WPSA015C | 7.1 | 7.5 | 10.9 | -3.4 | -45.9 | 18.1 |
| WPSA022C | 25.5 | 27.3 | 32.5 | -5.2 | -18.9 | 27.1 |
| WPSA024C | 8.0 | 8.5 | 15.5 | -7.0 | -82.6 | 36.9 |
| WPSA026C | 22.0 | 24.3 | 32.6 | -8.3 | -34.3 | 43.8 |
| WPSA030C | 6.8 | 7.2 | 9.8 | -2.5 | -35.0 | 13.3 |
| WPSA035C | 12.0 | 12.7 | 15.2 | -2.5 | -19.3 | 13.0 |
| WPSA040C | 10.9 | 11.8 | 17.8 | -5.9 | -50.2 | 31.2 |
| WPSA050C | 18.4 | 21.3 | 25.2 | -3.9 | -18.1 | 20.3 |
| WPSA057C | 17.2 | 19.6 | 23.6 | -4.0 | -20.6 | 21.2 |
| WPSA060C | 15.5 | 20.6 | 23.5 | -2.9 | -14.2 | 15.4 |
| WPSA062C | 5.3 | 18.0 | 19.0 | -1.0 | -5.8 | 5.5 |
| WPSA063C | 13.4 | 17.1 | 22.5 | -5.4 | -31.7 | 28.6 |
| WPSA070C | 16.9 | 20.1 | 25.7 | -5.7 | -28.3 | 29.8 |
| WPSA072C | 22.6 | 25.6 | 33.4 | -7.7 | -30.1 | 40.6 |
| WPSA080C | 23.0 | 29.7 | 32.9 | -3.2 | -10.9 | 17.1 |
| WPSA085C | 25.3 | 30.0 | 35.7 | -5.7 | -19.1 | 30.1 |
| WPSA087C | 21.4 | 24.9 | 28.5 | -3.7 | -14.8 | 19.3 |
| WPSA096C* | 7.9 | 8.8 | 9.7 | -1.0 | -11.0 | 5.1 |
| WPSA100C* | 15.3 | 17.5 | 22.5 | -5.0 | -28.7 | 26.4 |
| WPSA123C* | 22.4 | 25.6 | 32.7 | -7.1 | -27.6 | 37.2 |
| WPSA124C* | 25.6 | 27.8 | 38.9 | -11.1 | -40.1 | 58.6 |
| WPSA127C* | 24.6 | 27.9 | 31.3 | -3.4 | -12.2 | 18.0 |
| WPSA129C | 19.9 | 21.6 | 30.9 | -9.3 | -43.2 | 49.0 |
| WPSA131C | 28.7 | 32.0 | 37.5 | -5.5 | -17.2 | 28.9 |
| WPSA133C* | 16.4 | 18.0 | 26.0 | -8.0 | -44.7 | 42.3 |
| WPSA134C* | 8.6 | 9.2 | 9.2 | 0.0 | -0.1 | 0.1 |
| WPSA138C* | 18.4 | 22.1 | 27.3 | -5.2 | -23.7 | 27.5 |
| WPSA144C | 24.9 | 28.0 | 34.2 | -6.2 | -22.2 | 32.7 |
| WPSA147C | 8.9 | 9.6 | 16.4 | -6.8 | -70.9 | 35.9 |
| WPSA151C | 2.8 | 2.9 | 3.8 | -0.9 | -31.4 | 4.8 |
| WPSA153C | 22.9 | 24.6 | 31.2 | -6.6 | -27.0 | 34.8 |
| WPSA154C | 6.9 | 7.1 | 8.4 | -1.2 | -17.2 | 6.4 |
| WPSA156C | 26.7 | 29.1 | 36.0 | -6.8 | -23.5 | 36.1 |
| WPSA158C | 2.3 | 2.4 | 3.5 | -1.1 | -43.6 | 5.6 |
| WPSA163C | 29.7 | 32.0 | 37.4 | -5.4 | -16.8 | 28.3 |
| average | | 19.0 | | | -27.5 | 27.4 |

**Figure 6:** Graphical view of the data presented in Table 4, showing the comparability of the ICP and XRD data sets over the measured stratigraphic sections. Gaps are inserted in the graph to separate the middle waste from the upper and lower ore producing bodies.

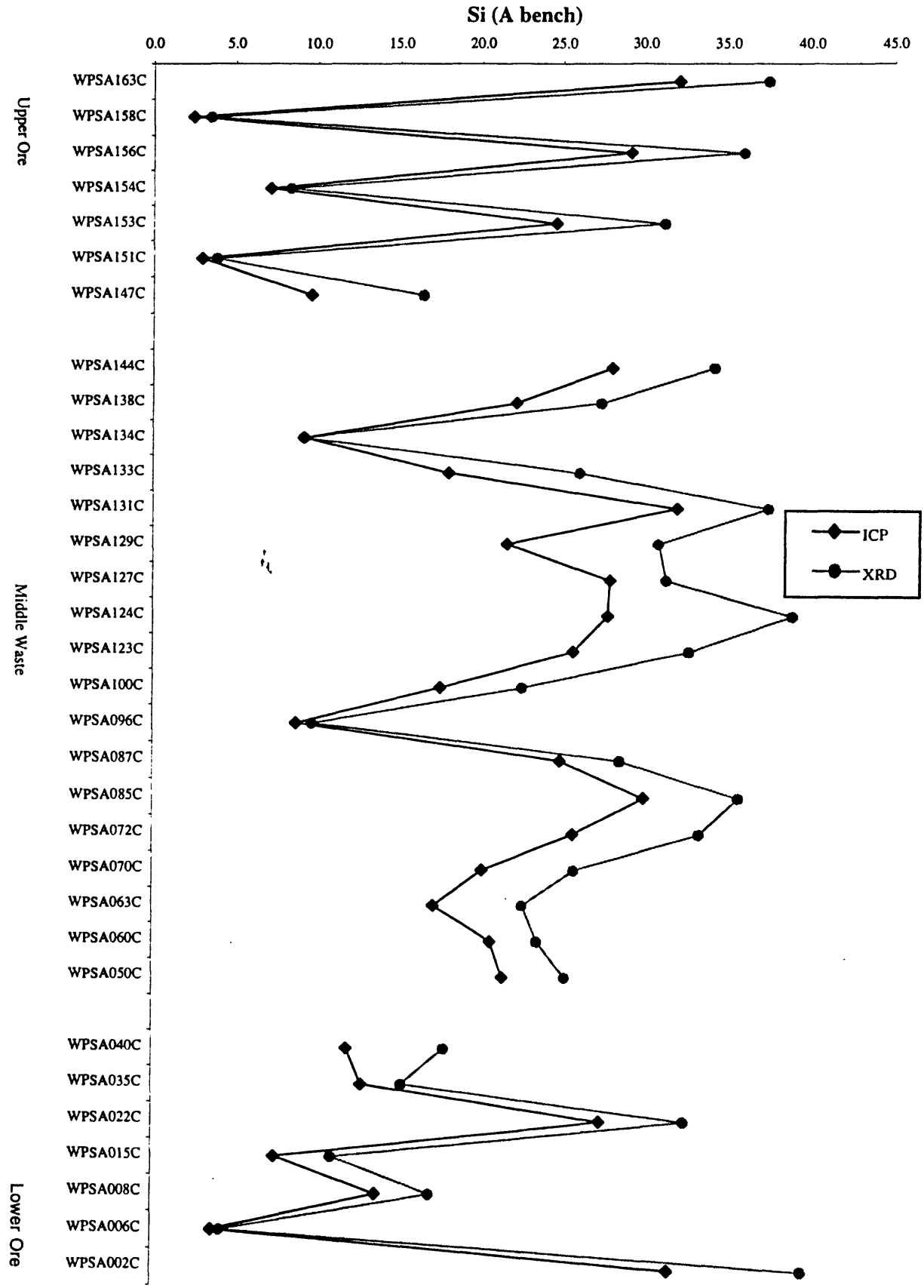

**Table 4:** Comparison of ICP data (Herring and others 1999) and calculated chemistry based on mineral compositions from Rietveld analysis. ICP data are normalized to include the elements that are calculated using the XRD data. The average difference shows whether the XRD data overstate ("-" values) or understate ("+" values) the ICP data. A weighted error is calculated by multiplying the error's absolute value by a weighting factor (measured / measured average). This value shows the comparability of the two data sets.

| Sample # | Measured % (ICP) | Normalized % (ICP) | K Calculated % (XRD) | Difference (Normalized - Calculated) | % Error (Difference / Normalized) | Weighted % error |
|---|---|---|---|---|---|---|
| WPSA002C | 2.4 | 2.7 | 1.1 | 1.7 | 60.9 | 104.7 |
| WPSA006C | 0.3 | 0.4 | 0.1 | 0.2 | 65.8 | 14.7 |
| WPSA008C | 1.0 | 1.1 | 1.1 | 0.0 | 3.7 | 2.6 |
| WPSA015C | 0.7 | 0.7 | 0.5 | 0.3 | 34.9 | 15.7 |
| WPSA022C | 2.7 | 2.9 | 2.7 | 0.3 | 8.7 | 15.8 |
| WPSA024C | 1.0 | 1.0 | 0.7 | 0.3 | 33.3 | 21.0 |
| WPSA026C | 2.2 | 2.4 | 2.8 | -0.4 | -15.4 | 23.2 |
| WPSA030C | 0.8 | 0.9 | 0.7 | 0.2 | 22.0 | 12.1 |
| WPSA035C | 1.5 | 1.5 | 0.9 | 0.6 | 40.4 | 38.8 |
| WPSA040C | 1.1 | 1.2 | 1.1 | 0.1 | 6.8 | 5.0 |
| WPSA050C | 2.4 | 2.8 | 2.5 | 0.3 | 10.7 | 18.6 |
| WPSA057C | 2.1 | 2.3 | 0.6 | 1.7 | 72.8 | 106.2 |
| WPSA060C | 2.1 | 2.8 | 2.3 | 0.5 | 17.7 | 31.3 |
| WPSA062C | 0.7 | 2.3 | 3.7 | -1.4 | -59.2 | 85.3 |
| WPSA063C | 1.5 | 1.9 | 1.4 | 0.6 | 29.5 | 35.8 |
| WPSA070C | 1.8 | 2.1 | 1.1 | 1.1 | 49.9 | 66.3 |
| WPSA072C | 1.6 | 1.8 | 1.3 | 0.5 | 29.1 | 32.7 |
| WPSA080C | 1.9 | 2.4 | 1.9 | 0.5 | 19.7 | 29.7 |
| WPSA085C | 2.6 | 3.1 | 2.3 | 0.8 | 24.8 | 47.3 |
| WPSA087C | 2.4 | 2.8 | 2.7 | 0.1 | 4.0 | 6.9 |
| WPSA096C* | 0.5 | 0.6 | 0.3 | 0.3 | 50.8 | 18.0 |
| WPSA100C* | 1.3 | 1.5 | 2.4 | -0.9 | -59.1 | 55.3 |
| WPSA123C* | 1.7 | 2.0 | 1.3 | 0.6 | 32.5 | 39.7 |
| WPSA124C* | 1.7 | 1.8 | 0.6 | 1.2 | 64.4 | 72.9 |
| WPSA127C* | 1.4 | 1.6 | 2.0 | -0.4 | -21.7 | 22.2 |
| WPSA129C | 1.2 | 1.3 | 2.9 | -1.6 | -122.8 | 99.7 |
| WPSA131C | 1.7 | 1.8 | 2.0 | -0.2 | -10.8 | 12.5 |
| WPSA133C* | 1.1 | 1.2 | 2.4 | -1.2 | -93.0 | 72.0 |
| WPSA134C* | 0.5 | 0.6 | 0.4 | 0.2 | 33.7 | 11.9 |
| WPSA138C* | 1.7 | 2.1 | 1.9 | 0.2 | 9.9 | 13.0 |
| WPSA144C | 2.0 | 2.2 | 2.0 | 0.2 | 10.7 | 14.8 |
| WPSA147C | 0.8 | 0.8 | 2.2 | -1.4 | -163.6 | 86.3 |
| WPSA151C | 0.2 | 0.2 | 0.4 | -0.3 | -151.9 | 15.9 |
| WPSA153C | 1.1 | 1.2 | 1.4 | -0.2 | -20.4 | 14.7 |
| WPSA154C | 0.4 | 0.4 | 0.2 | 0.2 | 56.5 | 14.6 |
| WPSA156C | 1.3 | 1.4 | 2.5 | -1.1 | -77.7 | 69.3 |
| WPSA158C | 0.2 | 0.2 | 0.8 | -0.6 | -353.1 | 38.9 |
| WPSA163C | 1.5 | 1.6 | 2.3 | -0.7 | -43.9 | 42.9 |
| average | | 1.6 | | | -10.5 | 37.6 |

**Figure 6:** Graphical view of the data presented in Table 4, showing the comparability of the ICP and XRD data sets over the measured stratigraphic sections. Gaps are inserted in the graph to separate the middle waste from the upper and lower ore producing bodies.

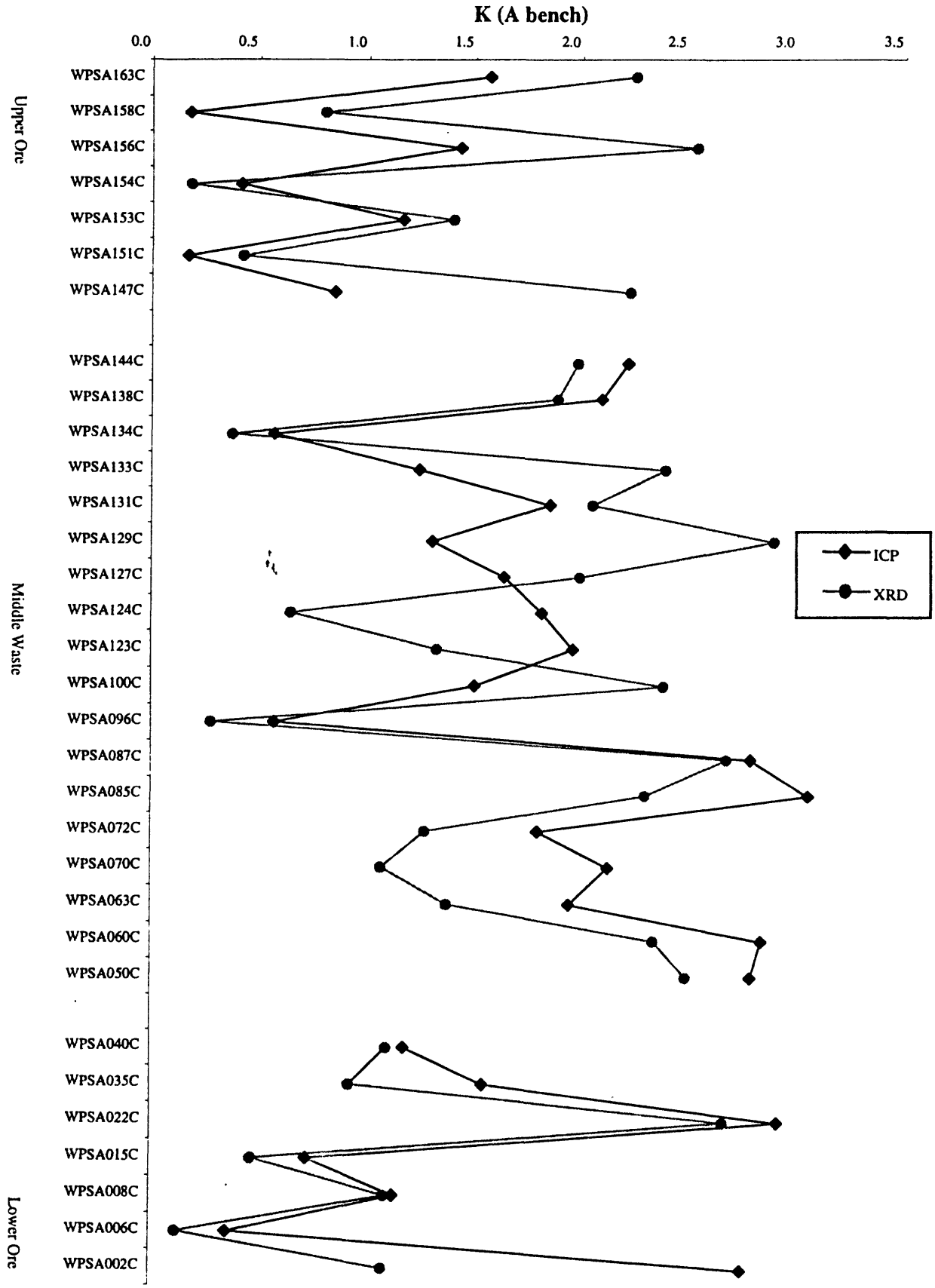

**Table 4:** Comparison of ICP data (Herring and others 1999) and calculated chemistry based on mineral compositions from Rietveld analysis. ICP data are normalized to include the elements that are calculated using the XRD data. The average difference shows whether the XRD data overstate ("-" values) or understate ("+" values) the ICP data. A weighted error is calculated by multiplying the error's absolute value by a weighting factor (measured / measured average). This value shows the comparability of the two data sets.

| Sample # | Measured % (ICP) | Normalized % (ICP) | Al Calculated % (XRD) | Difference (Normalized - Calculated) | % Error (Difference / Normalized) | Weighted % error |
|---|---|---|---|---|---|---|
| WPSA002C | 5.4 | 6.1 | 3.4 | 2.6 | 43.5 | 58.8 |
| WPSA006C | 0.8 | 0.8 | 0.5 | 0.3 | 40.8 | 7.5 |
| WPSA008C | 2.4 | 2.5 | 2.3 | 0.2 | 9.7 | 5.5 |
| WPSA015C | 1.4 | 1.5 | 1.5 | 0.1 | 3.5 | 1.2 |
| WPSA022C | 6.1 | 6.6 | 5.5 | 1.1 | 16.7 | 24.4 |
| WPSA024C | 1.7 | 1.8 | 2.7 | -0.9 | -48.3 | 19.6 |
| WPSA026C | 4.5 | 5.0 | 4.3 | 0.6 | 12.3 | 13.5 |
| WPSA030C | 1.4 | 1.5 | 1.3 | 0.3 | 16.8 | 5.7 |
| WPSA035C | 3.5 | 3.7 | 2.4 | 1.3 | 34.3 | 27.9 |
| WPSA040C | 2.2 | 2.4 | 2.9 | -0.5 | -20.8 | 11.1 |
| WPSA050C | 5.5 | 6.4 | 6.7 | -0.3 | -5.5 | 7.8 |
| WPSA057C | 5.0 | 5.7 | 3.5 | 2.2 | 38.3 | 48.1 |
| WPSA060C | 5.5 | 7.3 | 7.5 | -0.2 | -2.4 | 3.9 |
| WPSA062C | 2.8 | 9.3 | 7.9 | 1.4 | 14.8 | 30.6 |
| WPSA063C | 4.5 | 5.8 | 4.9 | 0.9 | 15.7 | 20.2 |
| WPSA070C | 5.1 | 6.0 | 5.7 | 0.3 | 5.7 | 7.7 |
| WPSA072C | 5.0 | 5.7 | 5.5 | 0.1 | 2.1 | 2.6 |
| WPSA080C | 4.8 | 6.2 | 6.3 | -0.1 | -1.0 | 1.3 |
| WPSA085C | 6.4 | 7.6 | 7.4 | 0.2 | 2.2 | 3.7 |
| WPSA087C | 7.8 | 9.0 | 10.8 | -1.7 | -19.2 | 38.6 |
| WPSA096C* | 1.5 | 1.6 | 1.5 | 0.2 | 10.6 | 3.9 |
| WPSA100C* | 3.9 | 4.4 | 5.2 | -0.8 | -18.3 | 18.1 |
| WPSA123C* | 4.4 | 5.0 | 4.6 | 0.4 | 8.8 | 9.8 |
| WPSA124C* | 6.5 | 7.0 | 3.0 | 4.0 | 57.0 | 88.9 |
| WPSA127C* | 3.8 | 4.3 | 5.3 | -1.0 | -23.5 | 22.2 |
| WPSA129C | 3.2 | 3.4 | 2.7 | 0.7 | 20.5 | 15.6 |
| WPSA131C | 5.9 | 6.5 | 6.4 | 0.1 | 1.4 | 2.1 |
| WPSA133C* | 2.9 | 3.2 | 4.6 | -1.4 | -44.8 | 31.9 |
| WPSA134C* | 1.4 | 1.5 | 0.8 | 0.7 | 46.6 | 15.8 |
| WPSA138C* | 4.2 | 5.1 | 5.3 | -0.2 | -4.0 | 4.5 |
| WPSA144C | 7.0 | 7.8 | 7.1 | 0.7 | 9.5 | 16.5 |
| WPSA147C | 2.2 | 2.4 | 2.3 | 0.0 | 0.4 | 0.2 |
| WPSA151C | 0.6 | 0.6 | 0.9 | -0.2 | -39.3 | 5.5 |
| WPSA153C | 3.9 | 4.2 | 3.3 | 0.8 | 20.0 | 18.5 |
| WPSA154C | 1.4 | 1.4 | 0.5 | 0.9 | 66.1 | 20.5 |
| WPSA156C | 5.3 | 5.7 | 4.6 | 1.2 | 20.2 | 25.8 |
| WPSA158C | 0.6 | 0.6 | 1.7 | -1.1 | -185.0 | 23.9 |
| WPSA163C | 4.7 | 5.1 | 4.9 | 0.1 | 2.6 | 3.0 |
| average | | 4.5 | | | 2.8 | 17.5 |

**Figure 6:** Graphical view of the data presented in Table 4, showing the comparability of the ICP and XRD data sets over the measured stratigraphic sections. Gaps are inserted in the graph to separate the middle waste from the upper and lower ore producing bodies.

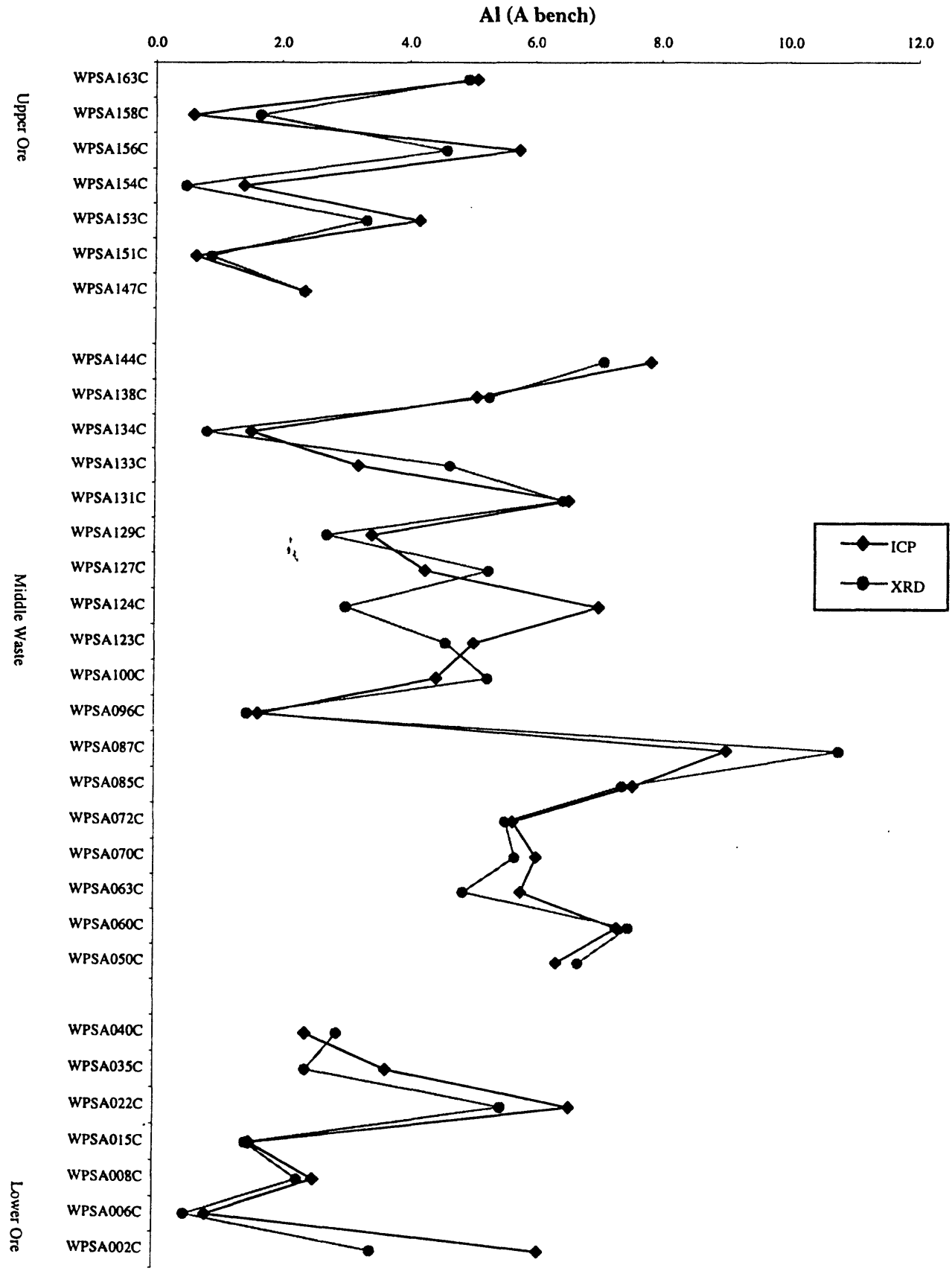

**Table 4:** Comparison of ICP data (Herring and others 1999) and calculated chemistry based on mineral compositions from Rietveld analysis. ICP data are normalized to include the elements that are calculated using the XRD data. The average difference shows whether the XRD data overstate ("-" values) or understate ("+" values) the ICP data. A weighted error is calculated by multiplying the error's absolute value by a weighting factor (measured / measured average). This value shows the comparability of the two data sets.

| Sample # | Measured % (ICP) | Normalized % (ICP) | Na Calculated % (XRD) | Difference (Normalized - Calculated) | % Error (Difference / Normalized) | Weighted % error |
|---|---|---|---|---|---|---|
| WPSA002C | 0.1 | 0.1 | 0.0 | 0.1 | 96.7 | 20.1 |
| WPSA006C | 0.3 | 0.1 | 0.1 | 0.0 | -25.4 | 4.7 |
| WPSA008C | 0.2 | 0.2 | 0.2 | 0.0 | 21.0 | 6.7 |
| WPSA015C | 0.2 | 0.1 | 0.1 | 0.0 | 17.9 | 4.1 |
| WPSA022C | 0.7 | 1.9 | 1.0 | 0.9 | 48.3 | 154.8 |
| WPSA024C | 0.2 | 0.2 | 0.5 | -0.2 | -100.4 | 38.9 |
| WPSA026C | 0.3 | 0.6 | 0.2 | 0.5 | 69.7 | 75.4 |
| WPSA030C | 0.2 | 0.1 | 0.1 | 0.0 | 32.7 | 7.6 |
| WPSA035C | 0.1 | 0.2 | 0.1 | 0.1 | 36.0 | 11.1 |
| WPSA040C | 0.2 | 0.2 | 0.1 | 0.2 | 66.8 | 26.1 |
| WPSA050C | 0.3 | 0.8 | 0.1 | 0.7 | 83.5 | 108.7 |
| WPSA057C | 0.3 | 0.7 | 0.4 | 0.2 | 33.1 | 36.1 |
| WPSA060C | 0.1 | 0.4 | 0.0 | 0.3 | 90.4 | 55.6 |
| WPSA062C | 0.0 | 0.1 | 0.1 | 0.0 | 41.6 | 6.4 |
| WPSA063C | 0.1 | 0.2 | 0.1 | 0.2 | 74.3 | 28.9 |
| WPSA070C | 0.2 | 0.4 | 0.0 | 0.3 | 89.9 | 57.3 |
| WPSA072C | 0.6 | 1.0 | 0.8 | 0.3 | 24.5 | 41.7 |
| WPSA080C | 0.6 | 1.5 | 0.6 | 0.9 | 57.0 | 142.1 |
| WPSA085C | 0.3 | 0.9 | 0.2 | 0.7 | 75.6 | 115.5 |
| WPSA087C | 0.1 | 0.3 | 0.0 | 0.2 | 86.9 | 36.3 |
| WPSA096C* | 0.3 | 0.2 | 0.1 | 0.1 | 67.1 | 18.4 |
| WPSA100C* | 0.3 | 0.4 | 0.0 | 0.4 | 91.4 | 66.2 |
| WPSA123C* | 0.5 | 0.9 | 0.3 | 0.5 | 60.3 | 88.6 |
| WPSA124C* | 0.7 | 1.2 | 1.0 | 0.2 | 16.4 | 32.2 |
| WPSA127C* | 0.5 | 0.8 | 0.8 | 0.0 | 2.2 | 2.9 |
| WPSA129C | 0.4 | 0.5 | 0.1 | 0.5 | 89.5 | 79.5 |
| WPSA131C | 1.0 | 1.9 | 2.3 | -0.5 | -25.0 | 77.7 |
| WPSA133C* | 0.5 | 0.6 | 1.1 | -0.6 | -93.2 | 92.3 |
| WPSA134C* | 0.3 | 0.2 | 0.2 | 0.0 | -3.6 | 1.1 |
| WPSA138C* | 0.4 | 0.8 | 0.8 | 0.1 | 6.1 | 8.5 |
| WPSA144C | 0.7 | 1.5 | 2.4 | -0.9 | -59.9 | 148.3 |
| WPSA147C | 0.2 | 0.1 | 0.1 | 0.0 | 3.8 | 0.8 |
| WPSA151C | 0.1 | 0.0 | 0.2 | -0.2 | -1004.2 | 33.7 |
| WPSA153C | 0.5 | 0.5 | 0.5 | 0.1 | 11.5 | 10.2 |
| WPSA154C | 0.2 | 0.1 | 0.2 | -0.2 | -249.5 | 25.8 |
| WPSA156C | 0.5 | 0.6 | 0.5 | 0.1 | 19.8 | 21.3 |
| WPSA158C | 0.1 | 0.0 | 0.1 | -0.1 | -306.3 | 10.8 |
| WPSA163C | 0.5 | 0.7 | 0.7 | 0.0 | -1.0 | 1.3 |
| average | | 0.6 | | | -12.0 | 44.7 |

**Figure 6:** Graphical view of the data presented in Table 4, showing the comparability of the ICP and XRD data sets over the measured stratigraphic sections. Gaps are inserted in the graph to separate the middle waste from the upper and lower ore producing bodies.

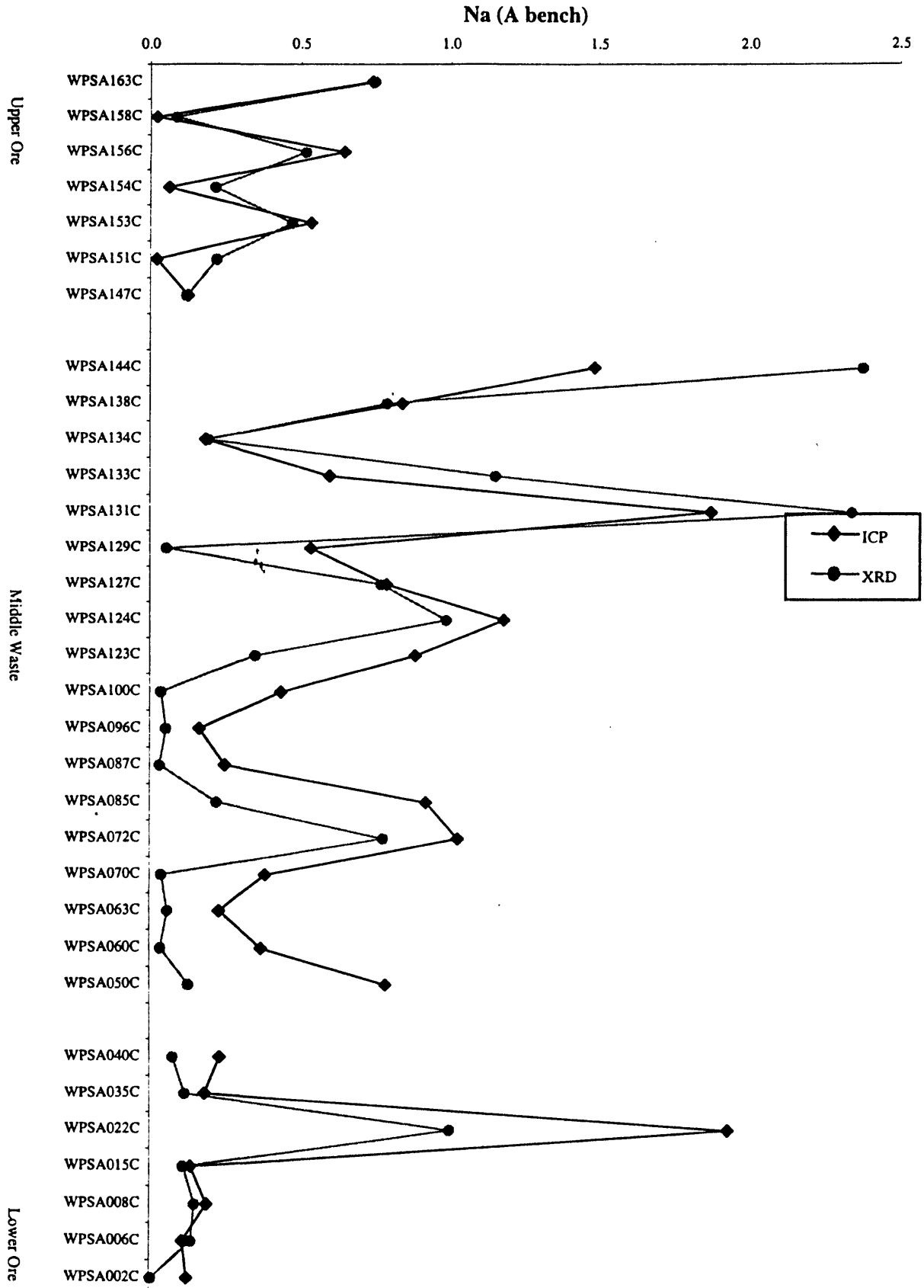

**Table 4:** Comparison of ICP data (Herring and others 1999) and calculated chemistry based on mineral compositions from Rietveld analysis. ICP data are normalized to include the elements that are calculated using the XRD data. The average difference shows whether the XRD data overstate ("-" values) or understate ("+" values) the ICP data. A weighted error is calculated by multiplying the error's absolute value by a weighting factor (measured / measured average). This value shows the comparability of the two data sets.

| Sample # | Measured % (ICP) | Normalized % (ICP) | Mg Calculated % (XRD) | Difference (Normalized - Calculated) | % Error (Difference / Normalized) | Weighted % error |
|---|---|---|---|---|---|---|
| WPSA002C | 0.4 | 0.4 | 0.0 | 0.4 | 99.6 | 208.5 |
| WPSA006C | 0.1 | 0.1 | 0.1 | 0.1 | 50.7 | 29.3 |
| WPSA008C | 0.1 | 0.2 | 0.0 | 0.1 | 71.3 | 53.9 |
| WPSA015C | 0.1 | 0.1 | 0.0 | 0.1 | 69.2 | 47.8 |
| WPSA022C | 0.1 | 0.1 | 0.0 | 0.1 | 95.1 | 66.2 |
| WPSA024C | 0.1 | 0.1 | 0.0 | 0.1 | 76.4 | 44.6 |
| WPSA026C | 0.1 | 0.1 | 0.0 | 0.1 | 99.5 | 71.3 |
| WPSA030C | 0.1 | 0.1 | 0.0 | 0.1 | 74.8 | 52.0 |
| WPSA035C | 0.2 | 0.2 | 0.0 | 0.2 | 81.5 | 82.2 |
| WPSA040C | 0.2 | 0.2 | 0.0 | 0.1 | 82.6 | 67.2 |
| WPSA050C | 0.2 | 0.3 | 0.0 | 0.3 | 99.5 | 126.8 |
| WPSA057C | 0.2 | 0.2 | 0.0 | 0.2 | 86.7 | 88.8 |
| WPSA060C | 0.3 | 0.5 | 0.0 | 0.4 | 97.6 | 220.1 |
| WPSA062C | 0.4 | 1.2 | 0.0 | 1.2 | 98.5 | 601.1 |
| WPSA063C | 0.3 | 0.3 | 0.0 | 0.3 | 93.5 | 149.3 |
| WPSA070C | 0.3 | 0.3 | 0.0 | 0.3 | 96.2 | 154.1 |
| WPSA072C | 0.1 | 0.1 | 0.0 | 0.1 | 91.0 | 56.8 |
| WPSA080C | 0.1 | 0.2 | 0.0 | 0.2 | 96.5 | 80.8 |
| WPSA085C | 0.3 | 0.3 | 0.0 | 0.3 | 100.0 | 153.9 |
| WPSA087C | 0.2 | 0.2 | 0.0 | 0.2 | 95.6 | 105.5 |
| WPSA096C* | 0.1 | 0.1 | 0.0 | 0.1 | 79.2 | 35.3 |
| WPSA100C* | 0.2 | 0.3 | 0.0 | 0.3 | 95.6 | 125.7 |
| WPSA123C* | 0.2 | 0.2 | 0.0 | 0.2 | 92.3 | 105.7 |
| WPSA124C* | 0.1 | 0.1 | 0.0 | 0.1 | 100.0 | 65.1 |
| WPSA127C* | 0.1 | 0.2 | 0.0 | 0.2 | 97.6 | 77.4 |
| WPSA129C | 0.1 | 0.1 | 0.0 | 0.1 | 98.9 | 48.2 |
| WPSA131C | 0.1 | 0.1 | 0.0 | 0.1 | 100.0 | 27.8 |
| WPSA133C* | 0.1 | 0.1 | 0.0 | 0.1 | 91.0 | 59.9 |
| WPSA134C* | 0.1 | 0.1 | 0.0 | 0.1 | 56.0 | 26.9 |
| WPSA138C* | 0.3 | 0.3 | 0.0 | 0.3 | 95.6 | 155.1 |
| WPSA144C | 0.4 | 0.4 | 0.0 | 0.4 | 98.7 | 199.8 |
| WPSA147C | 0.2 | 0.2 | 0.0 | 0.2 | 81.4 | 101.2 |
| WPSA151C | 0.1 | 0.1 | 0.1 | 0.0 | 7.3 | 3.4 |
| WPSA153C | 0.2 | 0.2 | 0.0 | 0.2 | 93.2 | 105.0 |
| WPSA154C | 0.1 | 0.1 | 0.0 | 0.1 | 70.3 | 43.6 |
| WPSA156C | 0.2 | 0.3 | 0.0 | 0.3 | 98.0 | 128.1 |
| WPSA158C | 0.1 | 0.1 | 0.0 | 0.1 | 66.2 | 30.9 |
| WPSA163C | 0.3 | 0.3 | 0.0 | 0.3 | 99.3 | 166.2 |
| average | | 0.2 | | | 86.2 | 104.4 |

**Figure 6:** Graphical view of the data presented in Table 4, showing the comparability of the ICP and XRD data sets over the measured stratigraphic sections. Gaps are inserted in the graph to separate the middle waste from the upper and lower ore producing bodies.

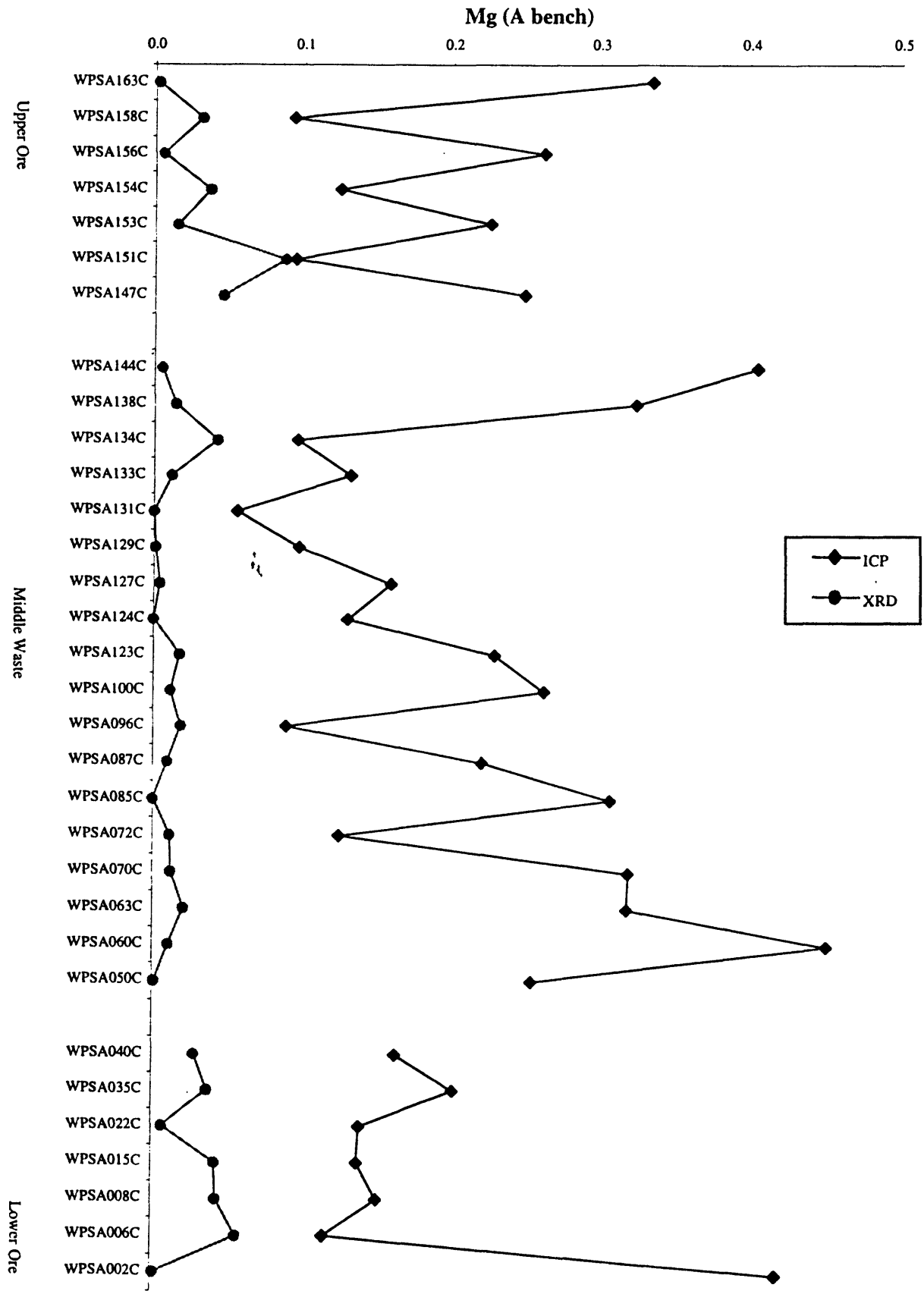

**Table 4:** Comparison of ICP data (Herring and others 1999) and calculated chemistry based on mineral compositions from Rietveld analysis. ICP data are normalized to include the elements that are calculated using the XRD data. The average difference shows whether the XRD data overstate ("-" values) or understate ("+" values) the ICP data. A weighted error is calculated by multiplying the error's absolute value by a weighting factor (measured / measured average). This value shows the comparability of the two data sets.

| Sample # | Measured % (ICP) | Normalized % (ICP) | $CO_3$ Calculated % (XRD) | Difference (Normalized - Calculated) | % Error (Difference / Normalized) | Weighted % error |
|---|---|---|---|---|---|---|
| WPSA002C | 0.1 | 0.1 | 0.0 | 0.1 | 86.1 | 29.2 |
| WPSA006C | 0.4 | 0.4 | 0.3 | 0.1 | 25.6 | 53.7 |
| WPSA008C | 0.2 | 0.2 | 0.2 | 0.0 | -9.3 | 10.1 |
| WPSA015C | 0.3 | 0.3 | 0.2 | 0.0 | 15.1 | 20.9 |
| WPSA022C | 0.1 | 0.1 | 0.0 | 0.0 | 49.7 | 18.6 |
| WPSA024C | 0.2 | 0.3 | 0.2 | 0.1 | 39.7 | 50.7 |
| WPSA026C | 0.1 | 0.1 | 0.0 | 0.1 | 95.3 | 42.0 |
| WPSA030C | 0.3 | 0.3 | 0.2 | 0.1 | 32.6 | 47.0 |
| WPSA035C | 0.2 | 0.2 | 0.2 | 0.0 | -1.7 | 1.7 |
| WPSA040C | 0.2 | 0.2 | 0.2 | 0.1 | 31.3 | 35.7 |
| WPSA050C | 0.1 | 0.1 | 0.0 | 0.1 | 92.7 | 42.9 |
| WPSA057C | 0.1 | 0.1 | 0.1 | 0.0 | -9.2 | 6.3 |
| WPSA060C | 0.1 | 0.1 | 0.1 | 0.0 | 34.8 | 16.2 |
| WPSA062C | 0.0 | 0.1 | 0.1 | 0.0 | -47.1 | 16.0 |
| WPSA063C | 0.1 | 0.2 | 0.1 | 0.0 | 24.9 | 19.1 |
| WPSA070C | 0.1 | 0.1 | 0.1 | 0.0 | 36.3 | 19.4 |
| WPSA072C | 0.1 | 0.1 | 0.1 | 0.0 | 11.0 | 3.7 |
| WPSA080C | 0.0 | 0.1 | 0.0 | 0.0 | 36.2 | 9.3 |
| WPSA085C | 0.0 | 0.0 | 0.0 | 0.0 | 100.0 | 5.9 |
| WPSA087C | 0.1 | 0.1 | 0.1 | 0.0 | 25.1 | 8.7 |
| WPSA096C* | 0.2 | 0.2 | 0.1 | 0.1 | 47.9 | 48.0 |
| WPSA100C* | 0.1 | 0.1 | 0.1 | 0.1 | 48.2 | 30.3 |
| WPSA123C* | 0.1 | 0.1 | 0.0 | 0.0 | 45.9 | 15.8 |
| WPSA124C* | 0.0 | 0.0 | 0.0 | 0.0 | 100.0 | 16.3 |
| WPSA127C* | 0.1 | 0.1 | 0.0 | 0.0 | 61.3 | 17.4 |
| WPSA129C | 0.1 | 0.1 | 0.0 | 0.1 | 94.5 | 51.2 |
| WPSA131C | 0.0 | 0.0 | 0.0 | 0.0 | 100.0 | 11.1 |
| WPSA133C* | 0.1 | 0.1 | 0.1 | 0.1 | 53.6 | 38.2 |
| WPSA134C* | 0.2 | 0.2 | 0.2 | 0.0 | 4.8 | 5.9 |
| WPSA138C* | 0.1 | 0.1 | 0.1 | 0.0 | 34.3 | 20.6 |
| WPSA144C | 0.0 | 0.0 | 0.0 | 0.0 | 37.5 | 8.4 |
| WPSA147C | 0.3 | 0.3 | 0.3 | 0.1 | 17.1 | 25.9 |
| WPSA151C | 0.4 | 0.4 | 0.5 | -0.1 | -17.6 | 35.2 |
| WPSA153C | 0.1 | 0.1 | 0.1 | 0.0 | 28.9 | 17.1 |
| WPSA154C | 0.3 | 0.3 | 0.2 | 0.1 | 33.8 | 52.5 |
| WPSA156C | 0.1 | 0.1 | 0.0 | 0.0 | 61.3 | 23.4 |
| WPSA158C | 0.4 | 0.4 | 0.2 | 0.2 | 55.2 | 108.6 |
| WPSA163C | 0.0 | 0.0 | 0.0 | 0.0 | 71.4 | 15.4 |
| average | | 0.2 | | | 40.7 | 26.3 |

**Figure 6:** Graphical view of the data presented in Table 4, showing the comparability of the ICP and XRD data sets over the measured stratigraphic sections. Gaps are inserted in the graph to separate the middle waste from the upper and lower ore producing bodies.

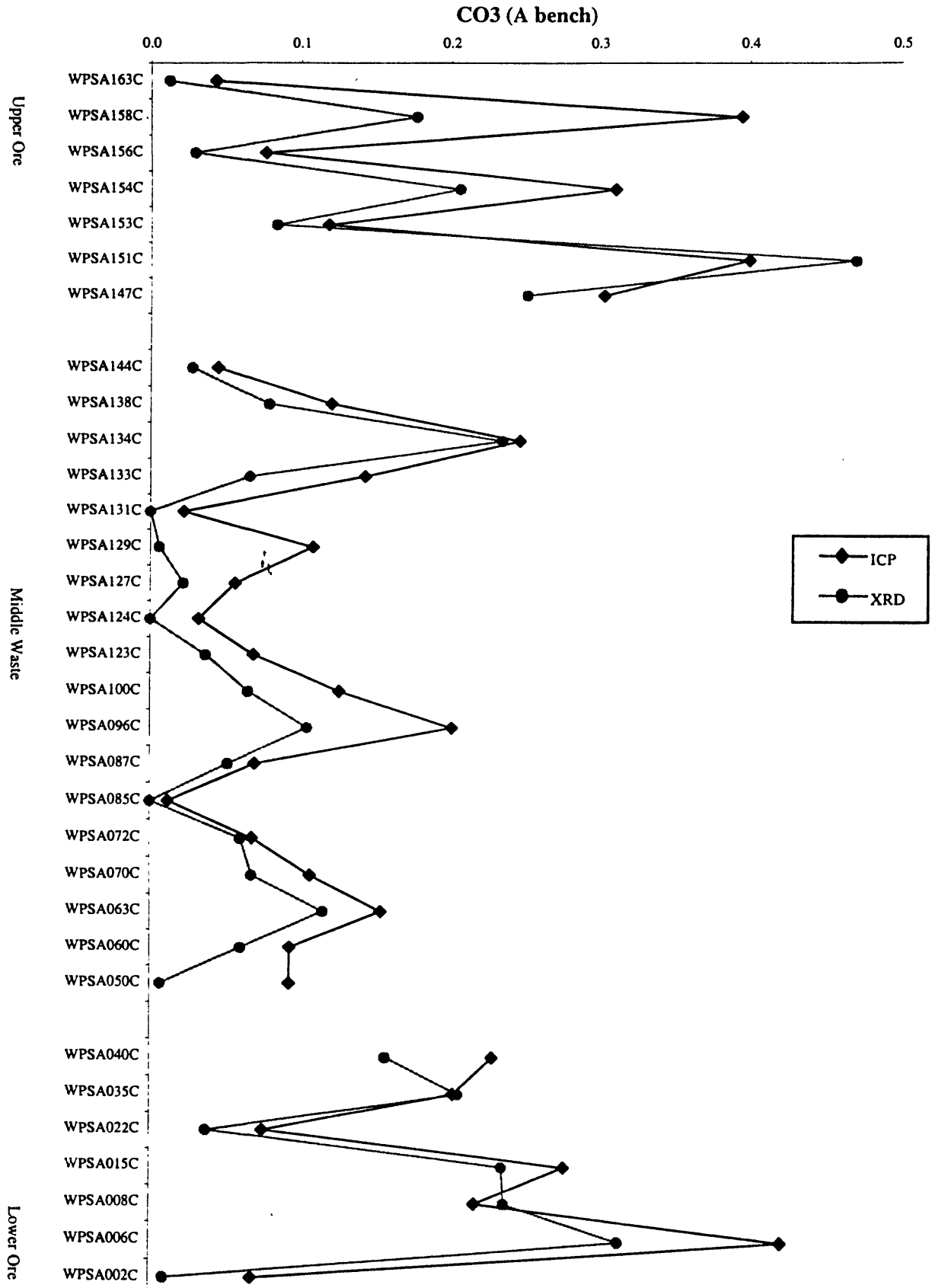

**Table 4:** Comparison of ICP data (Herring and others 1999) and calculated chemistry based on mineral compositions from Rietveld analysis. ICP data are normalized to include the elements that are calculated using the XRD data. The average difference shows whether the XRD data overstate ("-" values) or understate ("+" values) the ICP data. A weighted error is calculated by multiplying the error's absolute value by a weighting factor (measured / measured average). This value shows the comparability of the two data sets.

| Sample # | Measured % (ICP) | Normalized % (ICP) | Ca Calculated % (XRD) | Difference (Normalized - Calculated) | % Error (Difference / Normalized) | Weighted % error |
|---|---|---|---|---|---|---|
| WPSB003C | 7.0 | 7.7 | 7.8 | -0.1 | -1.1 | 0.4 |
| WPSB008C | 32.1 | 34.4 | 36.6 | -2.3 | -6.6 | 10.5 |
| WPSB018C* | 33.6 | 35.8 | 37.9 | -2.1 | -5.9 | 9.9 |
| WPSB025C* | 26.2 | 27.0 | 19.2 | 7.8 | 28.8 | 36.1 |
| WPSB026C | 29.7 | 31.7 | 30.7 | 1.0 | 3.2 | 4.8 |
| WPSB027C | 18.9 | 19.4 | 20.4 | -1.0 | -5.3 | 4.8 |
| WPSB033C | 31.4 | 33.4 | 33.9 | -0.5 | -1.6 | 2.5 |
| WPSB038C | 17.2 | 18.0 | 19.0 | -0.9 | -5.2 | 4.4 |
| WPSB047C | 23.7 | 27.1 | 24.5 | 2.6 | 9.5 | 11.9 |
| WPSB059C | 22.2 | 26.2 | 25.9 | 0.4 | 1.5 | 1.8 |
| WPSB065C | 19.5 | 20.3 | 18.4 | 1.9 | 9.3 | 8.8 |
| WPSB070C | 12.1 | 16.0 | 16.3 | -0.4 | -2.3 | 1.7 |
| WPSB080C | 6.2 | 7.8 | 6.1 | 1.8 | 22.4 | 8.2 |
| WPSB084C | 15.9 | 18.4 | 15.3 | 3.1 | 16.7 | 14.3 |
| WPSB087C* | 15.9 | 21.5 | 18.0 | 3.5 | 16.5 | 16.5 |
| WPSB091C* | 20.4 | 26.3 | 23.8 | 2.4 | 9.3 | 11.4 |
| WPSB095C | 7.7 | 9.1 | 6.7 | 2.5 | 27.1 | 11.5 |
| WPSB097C | 27.4 | 31.2 | 30.6 | 0.6 | 1.8 | 2.6 |
| WPSB100C | 8.2 | 9.9 | 8.9 | 1.0 | 9.8 | 4.5 |
| WPSB107C | 3.1 | 3.4 | 2.4 | 1.0 | 29.0 | 4.6 |
| WPSB117C | 10.4 | 14.2 | 10.9 | 3.3 | 23.4 | 15.5 |
| WPSB131C | 28.3 | 36.5 | 32.9 | 3.6 | 9.8 | 16.6 |
| WPSB133C | 34.2 | 36.4 | 34.1 | 2.4 | 6.5 | 10.9 |
| WPSB134C | 11.6 | 12.7 | 8.2 | 4.5 | 35.7 | 21.1 |
| WPSB136C | 33.0 | 34.3 | 36.4 | -2.2 | -6.3 | 10.0 |
| WPSB137C** | 2.7 | 2.9 | 0.0 | 2.9 | 100.0 | 13.7 |
| WPSB139C | 37.0 | 38.5 | 38.6 | -0.1 | -0.2 | 0.3 |
| WPSB145C | 2.2 | 2.4 | 1.9 | 0.5 | 20.5 | 2.3 |
| average | | 21.5 | | | 12.4 | 9.3 |

* * Samples with a poor match between Rietveld calculated feldspars and XRD measured feldspars.

**Figure 6:** Graphical view of the data presented in Table 4, showing the comparability of the ICP and XRD data sets over the measured stratigraphic sections. Gaps are inserted in the graph to separate the middle waste from the upper and lower ore producing bodies.

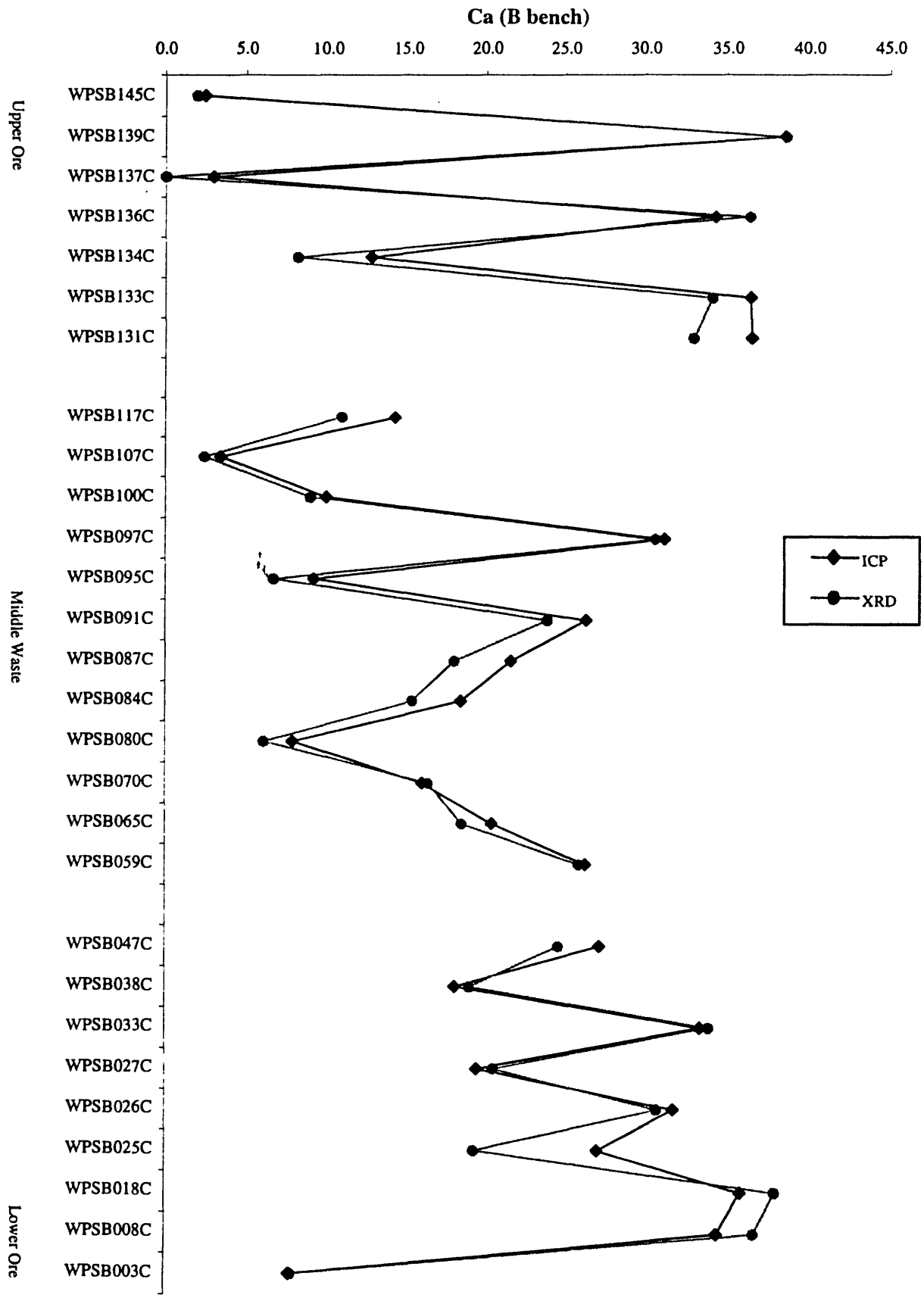

**Table 4:** Comparison of ICP data (Herring and others 1999) and calculated chemistry based on mineral compositions from Rietveld analysis. ICP data are normalized to include the elements that are calculated using the XRD data. The average difference shows whether the XRD data overstate ("-" values) or understate ("+" values) the ICP data. A weighted error is calculated by multiplying the error's absolute value by a weighting factor (measured / measured average). This value shows the comparability of the two data sets.

| Sample # | Measured % (ICP) | Normalized % (ICP) | P Calculated % (XRD) | Difference (Normalized - Calculated) | % Error (Difference / Normalized) | Weighted % error |
|---|---|---|---|---|---|---|
| WPSB003C | 0.2 | 0.2 | 0.1 | 0.0 | 15.2 | 0.3 |
| WPSB008C | 14.5 | 15.5 | 16.2 | -0.7 | -4.5 | 8.3 |
| WPSB018C* | 15.1 | 16.1 | 16.7 | -0.6 | -3.5 | 6.7 |
| WPSB025C* | 6.3 | 6.5 | 2.1 | 4.4 | 68.3 | 52.9 |
| WPSB026C | 13.3 | 14.2 | 13.0 | 1.2 | 8.6 | 14.6 |
| WPSB027C | 2.1 | 2.1 | 1.7 | 0.4 | 19.7 | 5.0 |
| WPSB033C | 14.5 | 15.4 | 15.4 | 0.0 | 0.2 | 0.4 |
| WPSB038C | 0.9 | 0.9 | 0.8 | 0.1 | 13.9 | 1.5 |
| WPSB047C | 10.1 | 11.6 | 10.2 | 1.4 | 11.8 | 16.3 |
| WPSB059C | 8.1 | 9.6 | 9.2 | 0.4 | 3.7 | 4.3 |
| WPSB065C | 0.4 | 0.4 | 0.2 | 0.2 | 42.3 | 1.9 |
| WPSB070C | 5.0 | 6.6 | 6.9 | -0.3 | -4.4 | 3.5 |
| WPSB080C | 3.0 | 3.8 | 2.7 | 1.1 | 28.8 | 13.2 |
| WPSB084C | 6.6 | 7.6 | 6.2 | 1.5 | 19.3 | 17.5 |
| WPSB087C* | 7.6 | 10.2 | 8.0 | 2.3 | 22.3 | 27.2 |
| WPSB091C* | 9.8 | 12.6 | 10.7 | 1.9 | 15.2 | 22.9 |
| WPSB095C | 2.7 | 3.3 | 1.9 | 1.3 | 40.9 | 15.8 |
| WPSB097C | 12.6 | 14.3 | 13.9 | 0.4 | 3.1 | 5.3 |
| WPSB100C | 3.8 | 4.5 | 4.0 | 0.5 | 12.0 | 6.4 |
| WPSB107C | 1.4 | 1.6 | 1.1 | 0.5 | 30.7 | 5.8 |
| WPSB117C | 4.0 | 5.5 | 4.1 | 1.4 | 25.1 | 16.5 |
| WPSB131C | 12.7 | 16.4 | 14.5 | 1.8 | 11.2 | 21.8 |
| WPSB133C | 15.2 | 16.2 | 15.0 | 1.2 | 7.3 | 14.0 |
| WPSB134C | 5.2 | 5.7 | 3.7 | 2.1 | 35.9 | 24.5 |
| WPSB136C | 15.1 | 15.7 | 16.2 | -0.6 | -3.6 | 6.7 |
| WPSB137C** | 1.3 | 1.4 | 0.0 | 1.4 | 100.0 | 16.5 |
| WPSB139C | 16.4 | 17.1 | 16.9 | 0.2 | 1.1 | 2.2 |
| WPSB145C | 1.0 | 1.1 | 0.9 | 0.2 | 18.3 | 2.3 |
| average | | 8.4 | | | 19.2 | 11.9 |

**Figure 6:** Graphical view of the data presented in Table 4, showing the comparability of the ICP and XRD data sets over the measured stratigraphic sections. Gaps are inserted in the graph to separate the middle waste from the upper and lower ore producing bodies.

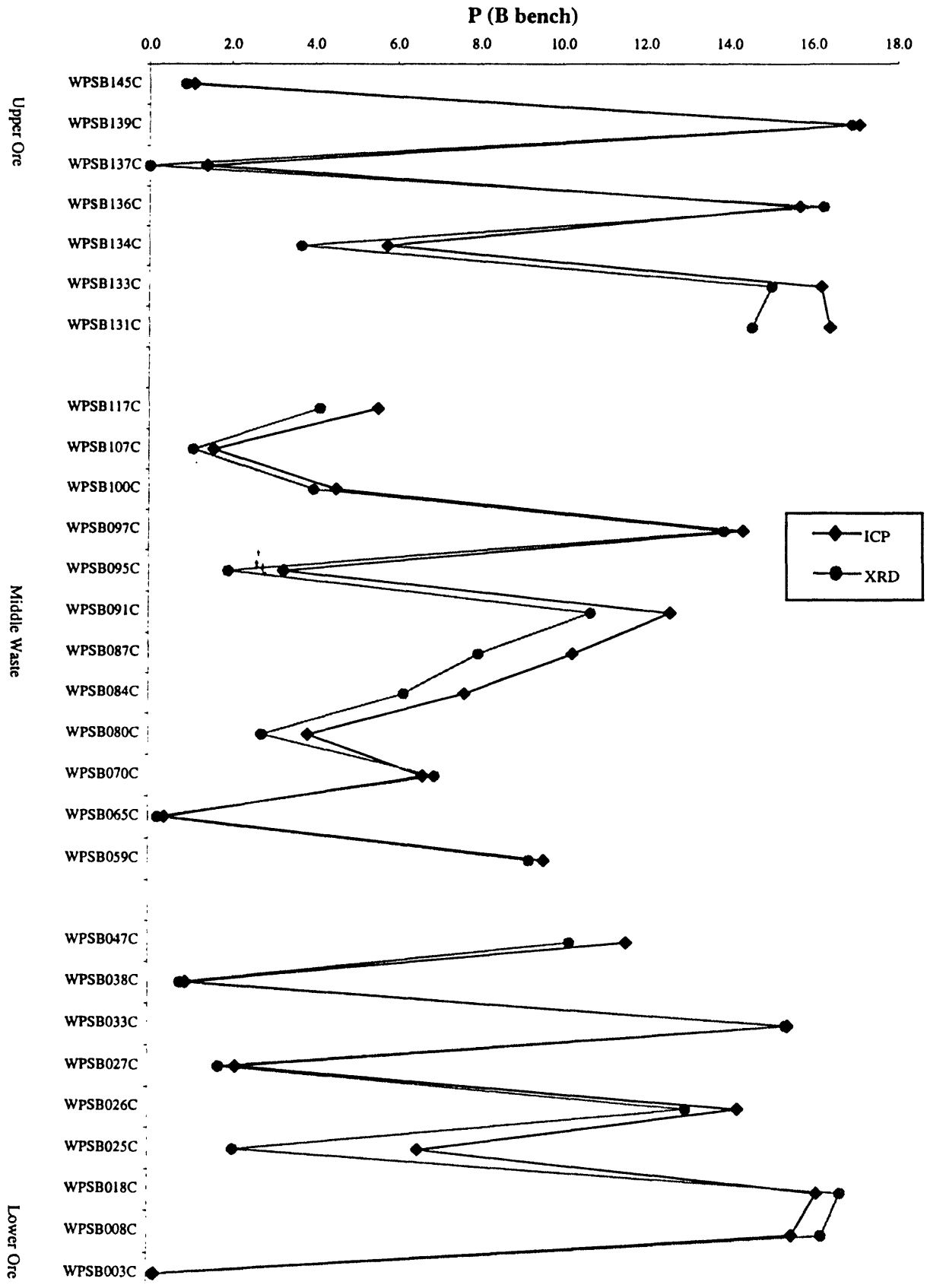

**Table 4:** Comparison of ICP data (Herring and others 1999) and calculated chemistry based on mineral compositions from Rietveld analysis. ICP data are normalized to include the elements that are calculated using the XRD data. The average difference shows whether the XRD data overstate ("-" values) or understate ("+" values) the ICP data. A weighted error is calculated by multiplying the error's absolute value by a weighting factor (measured / measured average). This value shows the comparability of the two data sets.

| Sample # | Measured % (ICP) | Normalized % (ICP) | Si Calculated % (XRD) | Difference (Normalized - Calculated) | % Error (Difference / Normalized) | Weighted % error |
|---|---|---|---|---|---|---|
| WPSB003C | 22.4 | 24.5 | 27.2 | -2.8 | -11.4 | 18.4 |
| WPSB008C | 2.8 | 3.0 | 4.5 | -1.5 | -49.3 | 9.7 |
| WPSB018C* | 3.0 | 3.2 | 3.2 | 0.0 | 0.1 | 0.0 |
| WPSB025C* | 5.3 | 5.4 | 7.8 | -2.3 | -42.4 | 15.2 |
| WPSB026C | 5.8 | 6.2 | 9.8 | -3.6 | -58.3 | 23.8 |
| WPSB027C | 6.8 | 6.9 | 4.9 | 2.1 | 29.9 | 13.6 |
| WPSB033C | 5.0 | 5.3 | 6.7 | -1.4 | -25.5 | 8.9 |
| WPSB038C | 8.2 | 8.6 | 6.8 | 1.8 | 21.4 | 12.1 |
| WPSB047C | 9.4 | 10.7 | 14.6 | -3.8 | -35.8 | 25.2 |
| WPSB059C | 9.1 | 10.7 | 9.8 | 1.0 | 9.1 | 6.4 |
| WPSB065C | 7.9 | 8.2 | 7.8 | 0.4 | 4.6 | 2.5 |
| WPSB070C | 15.9 | 21.0 | 21.8 | -0.9 | -4.2 | 5.8 |
| WPSB080C | 23.6 | 29.8 | 31.8 | -2.0 | -6.7 | 13.1 |
| WPSB084C | 14.6 | 16.9 | 21.7 | -4.8 | -28.6 | 31.8 |
| WPSB087C* | 13.1 | 17.7 | 20.1 | -2.3 | -13.2 | 15.4 |
| WPSB091C* | 10.6 | 13.7 | 15.2 | -1.5 | -11.0 | 9.9 |
| WPSB095C | 23.0 | 27.4 | 30.6 | -3.2 | -11.6 | 21.0 |
| WPSB097C | 7.3 | 8.3 | 10.1 | -1.8 | -22.2 | 12.1 |
| WPSB100C | 24.0 | 28.9 | 32.8 | -3.9 | -13.7 | 26.0 |
| WPSB107C | 26.1 | 28.6 | 35.9 | -7.4 | -25.7 | 48.4 |
| WPSB117C | 18.9 | 25.8 | 26.7 | -0.9 | -3.5 | 6.0 |
| WPSB131C | 4.1 | 5.2 | 6.6 | -1.3 | -25.6 | 8.8 |
| WPSB133C | 5.4 | 5.8 | 6.3 | -0.6 | -9.5 | 3.6 |
| WPSB134C | 24.0 | 26.3 | 31.6 | -5.3 | -20.3 | 35.0 |
| WPSB136C | 4.5 | 4.7 | 4.7 | 0.0 | 0.3 | 0.1 |
| WPSB137C** | 31.9 | 34.8 | 37.8 | -2.9 | -8.5 | 19.4 |
| WPSB139C | 1.9 | 2.0 | 2.5 | -0.5 | -24.2 | 3.2 |
| WPSB145C | 31.1 | 34.9 | 38.1 | -3.2 | -9.3 | 21.3 |
| average | | 15.2 | | | -14.1 | 14.9 |

**Figure 6:** Graphical view of the data presented in Table 4, showing the comparability of the ICP and XRD data sets over the measured stratigraphic sections. Gaps are inserted in the graph to separate the middle waste from the upper and lower ore producing bodies.

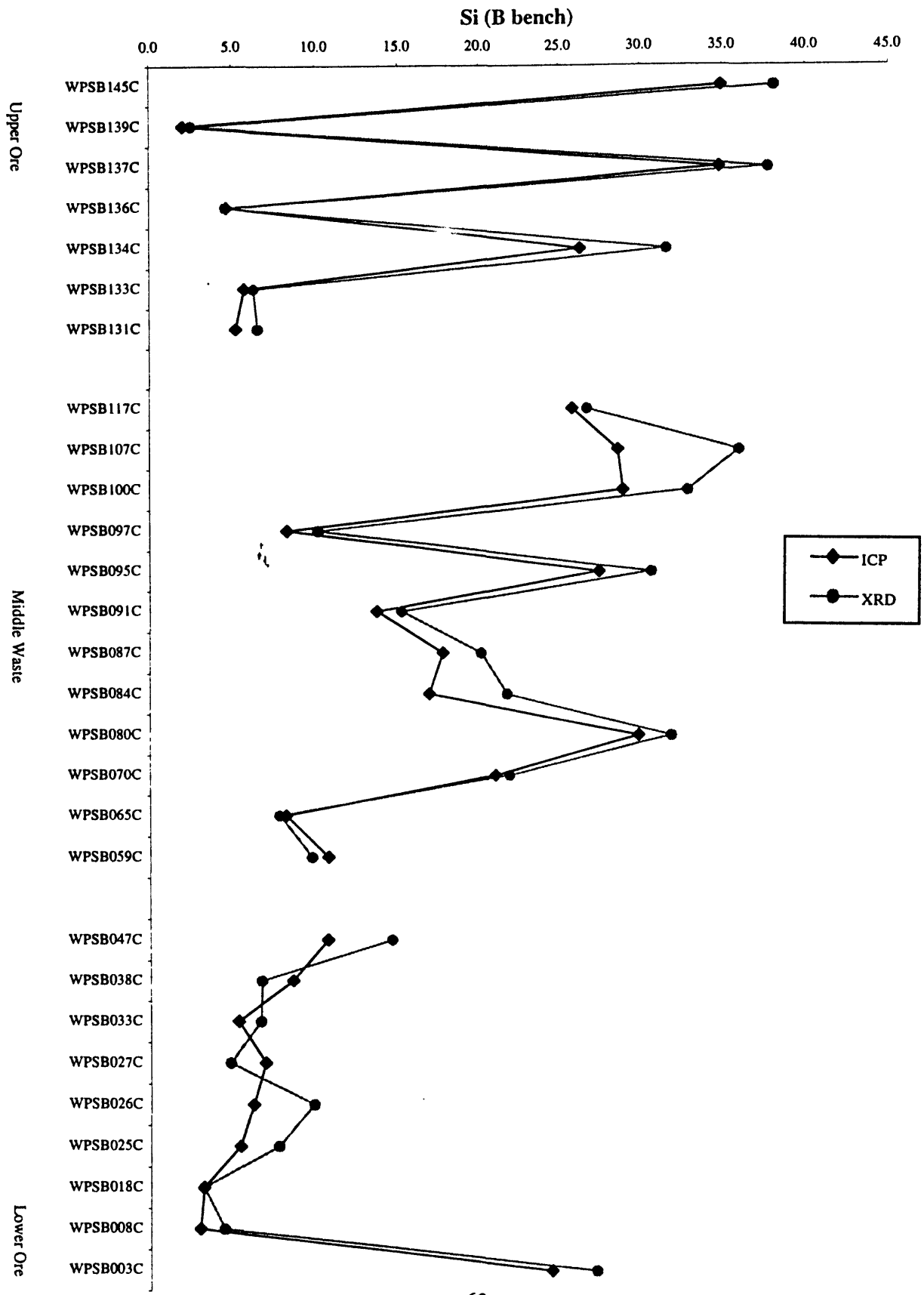

**Table 4:** Comparison of ICP data (Herring and others 1999) and calculated chemistry based on mineral compositions from Rietveld analysis. ICP data are normalized to include the elements that are calculated using the XRD data. The average difference shows whether the XRD data overstate ("-" values) or understate ("+" values) the ICP data. A weighted error is calculated by multiplying the error's absolute value by a weighting factor (measured / measured average). This value shows the comparability of the two data sets.

| Sample # | Measured % (ICP) | Normalized % (ICP) | K Calculated % (XRD) | Difference (Normalized - Calculated) | % Error (Difference / Normalized) | Weighted % error |
|---|---|---|---|---|---|---|
| WPSB003C | 1.4 | 1.6 | 1.3 | 0.3 | 17.0 | 24.3 |
| WPSB008C | 0.3 | 0.3 | 0.3 | 0.0 | -8.2 | 2.0 |
| WPSB018C* | 0.3 | 0.3 | 0.3 | 0.0 | -8.2 | 2.2 |
| WPSB025C* | 0.3 | 0.3 | 0.9 | -0.7 | -253.9 | 61.8 |
| WPSB026C | 0.6 | 0.6 | 0.6 | 0.0 | 4.5 | 2.6 |
| WPSB027C | 1.3 | 1.3 | 0.9 | 0.4 | 31.9 | 37.5 |
| WPSB033C | 0.5 | 0.6 | 0.6 | -0.1 | -11.2 | 5.7 |
| WPSB038C | 0.8 | 0.9 | 0.3 | 0.6 | 67.0 | 53.0 |
| WPSB047C | 0.9 | 1.0 | 0.7 | 0.3 | 26.4 | 23.6 |
| WPSB059C | 1.0 | 1.2 | 0.6 | 0.6 | 53.6 | 58.8 |
| WPSB065C | 0.5 | 0.5 | 0.3 | 0.3 | 50.6 | 24.5 |
| WPSB070C | 1.7 | 2.3 | 1.0 | 1.3 | 57.6 | 120.2 |
| WPSB080C | 2.0 | 2.5 | 1.6 | 0.9 | 37.5 | 85.3 |
| WPSB084C | 1.4 | 1.6 | 1.3 | 0.3 | 18.0 | 26.4 |
| WPSB087C* | 1.3 | 1.7 | 1.7 | 0.1 | 3.6 | 5.7 |
| WPSB091C* | 0.9 | 1.2 | 1.3 | -0.1 | -7.0 | 7.6 |
| WPSB095C | 1.6 | 1.9 | 1.5 | 0.4 | 19.9 | 34.9 |
| WPSB097C | 0.5 | 0.5 | 0.6 | 0.0 | -7.0 | 3.5 |
| WPSB100C | 1.2 | 1.5 | 1.1 | 0.4 | 29.2 | 39.6 |
| WPSB107C | 1.5 | 1.6 | 1.5 | 0.1 | 4.9 | 7.3 |
| WPSB117C | 1.7 | 2.3 | 1.5 | 0.8 | 35.9 | 74.0 |
| WPSB131C | 0.4 | 0.5 | 1.2 | -0.7 | -157.1 | 64.5 |
| WPSB133C | 0.4 | 0.4 | 0.6 | -0.2 | -52.9 | 20.0 |
| WPSB134C | 1.3 | 1.4 | 1.8 | -0.4 | -28.0 | 36.0 |
| WPSB136C | 0.2 | 0.2 | 0.4 | -0.1 | -51.0 | 11.1 |
| WPSB137C** | 1.4 | 1.5 | 1.0 | 0.4 | 29.9 | 40.3 |
| WPSB139C | 0.1 | 0.1 | 0.3 | -0.1 | -99.4 | 12.2 |
| WPSB145C | 1.5 | 1.7 | 2.6 | -0.8 | -48.7 | 76.5 |
| average | | 1.1 | | | -8.8 | 34.3 |

**Figure 6:** Graphical view of the data presented in Table 4, showing the comparability of the ICP and XRD data sets over the measured stratigraphic sections. Gaps are inserted in the graph to separate the middle waste from the upper and lower ore producing bodies.

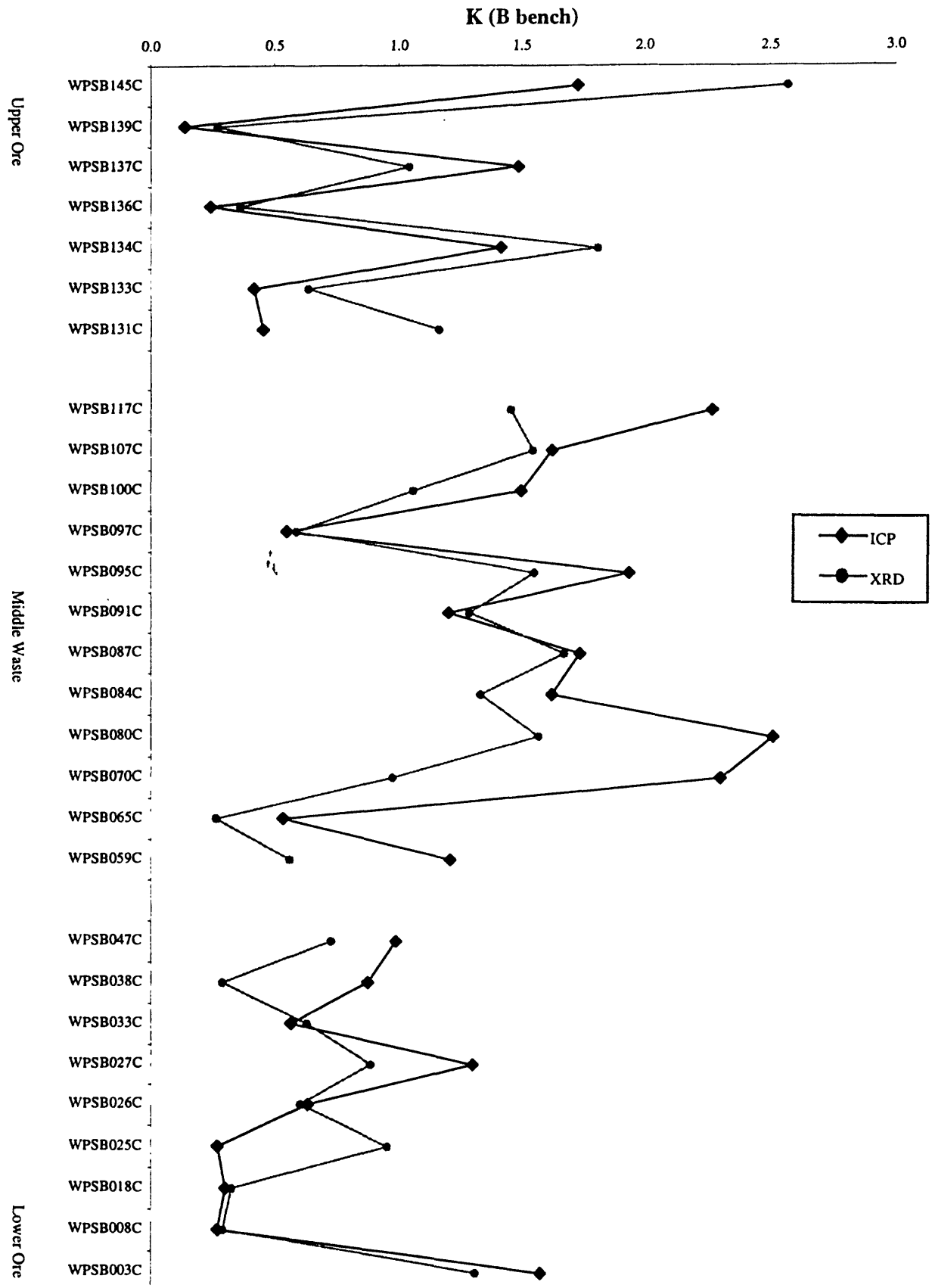

**Table 4:** Comparison of ICP data (Herring and others 1999) and calculated chemistry based on mineral compositions from Rietveld analysis. ICP data are normalized to include the elements that are calculated using the XRD data. The average difference shows whether the XRD data overstate ("-" values) or understate ("+" values) the ICP data. A weighted error is calculated by multiplying the error's absolute value by a weighting factor (measured / measured average). This value shows the comparability of the two data sets.

| Sample # | Measured % (ICP) | Normalized % (ICP) | Al Calculated % (XRD) | Difference (Normalized - Calculated) | % Error (Difference / Normalized) | Weighted % error |
|---|---|---|---|---|---|---|
| WPSB003C | 3.7 | 4.0 | 2.5 | 1.5 | 36.9 | 47.6 |
| WPSB008C | 0.5 | 0.6 | 0.7 | -0.1 | -18.8 | 3.4 |
| WPSB018C* | 0.6 | 0.6 | 0.6 | 0.1 | 11.1 | 2.3 |
| WPSB025C* | 0.7 | 0.8 | 1.8 | -1.0 | -136.1 | 33.5 |
| WPSB026C | 1.2 | 1.3 | 1.1 | 0.2 | 17.2 | 7.3 |
| WPSB027C | 2.6 | 2.6 | 1.5 | 1.1 | 42.0 | 35.6 |
| WPSB033C | 1.0 | 1.1 | 1.1 | -0.1 | -7.2 | 2.4 |
| WPSB038C | 1.7 | 1.7 | 0.7 | 1.1 | 61.0 | 34.3 |
| WPSB047C | 1.7 | 2.0 | 2.0 | 0.0 | -1.7 | 1.1 |
| WPSB059C | 2.3 | 2.7 | 2.3 | 0.5 | 16.5 | 14.6 |
| WPSB065C | 1.7 | 1.8 | 1.6 | 0.2 | 9.4 | 5.4 |
| WPSB070C | 4.4 | 5.7 | 5.1 | 0.7 | 11.4 | 21.2 |
| WPSB080C | 5.1 | 6.5 | 6.2 | 0.3 | 4.6 | 9.6 |
| WPSB084C | 3.6 | 4.1 | 5.7 | -1.5 | -37.3 | 49.7 |
| WPSB087C* | 3.5 | 4.7 | 4.8 | -0.1 | -1.6 | 2.5 |
| WPSB091C* | 2.3 | 3.0 | 3.8 | -0.8 | -27.4 | 26.2 |
| WPSB095C | 4.3 | 5.1 | 5.2 | -0.1 | -1.6 | 2.7 |
| WPSB097C | 1.4 | 1.5 | 1.6 | -0.1 | -5.2 | 2.6 |
| WPSB100C | 3.5 | 4.2 | 2.9 | 1.3 | 31.4 | 42.1 |
| WPSB107C | 4.9 | 5.3 | 6.2 | -0.8 | -15.4 | 26.4 |
| WPSB117C | 4.3 | 5.8 | 4.9 | 1.0 | 16.6 | 31.2 |
| WPSB131C | 1.0 | 1.2 | 2.4 | -1.2 | -94.2 | 37.6 |
| WPSB133C | 1.2 | 1.3 | 1.6 | -0.3 | -23.9 | 9.8 |
| WPSB134C | 4.2 | 4.6 | 4.5 | 0.1 | 3.0 | 4.5 |
| WPSB136C | 0.8 | 0.8 | 0.8 | 0.1 | 6.4 | 1.7 |
| WPSB137C** | 6.1 | 6.7 | 6.5 | 0.1 | 1.9 | 4.0 |
| WPSB139C | 0.4 | 0.4 | 0.6 | -0.1 | -25.0 | 3.6 |
| WPSB145C | 4.7 | 5.2 | 4.7 | 0.5 | 10.0 | 16.9 |
| average | | 3.1 | | | -4.1 | 17.1 |

**Figure 6:** Graphical view of the data presented in Table 4, showing the comparability of the ICP and XRD data sets over the measured stratigraphic sections. Gaps are inserted in the graph to separate the middle waste from the upper and lower ore producing bodies.

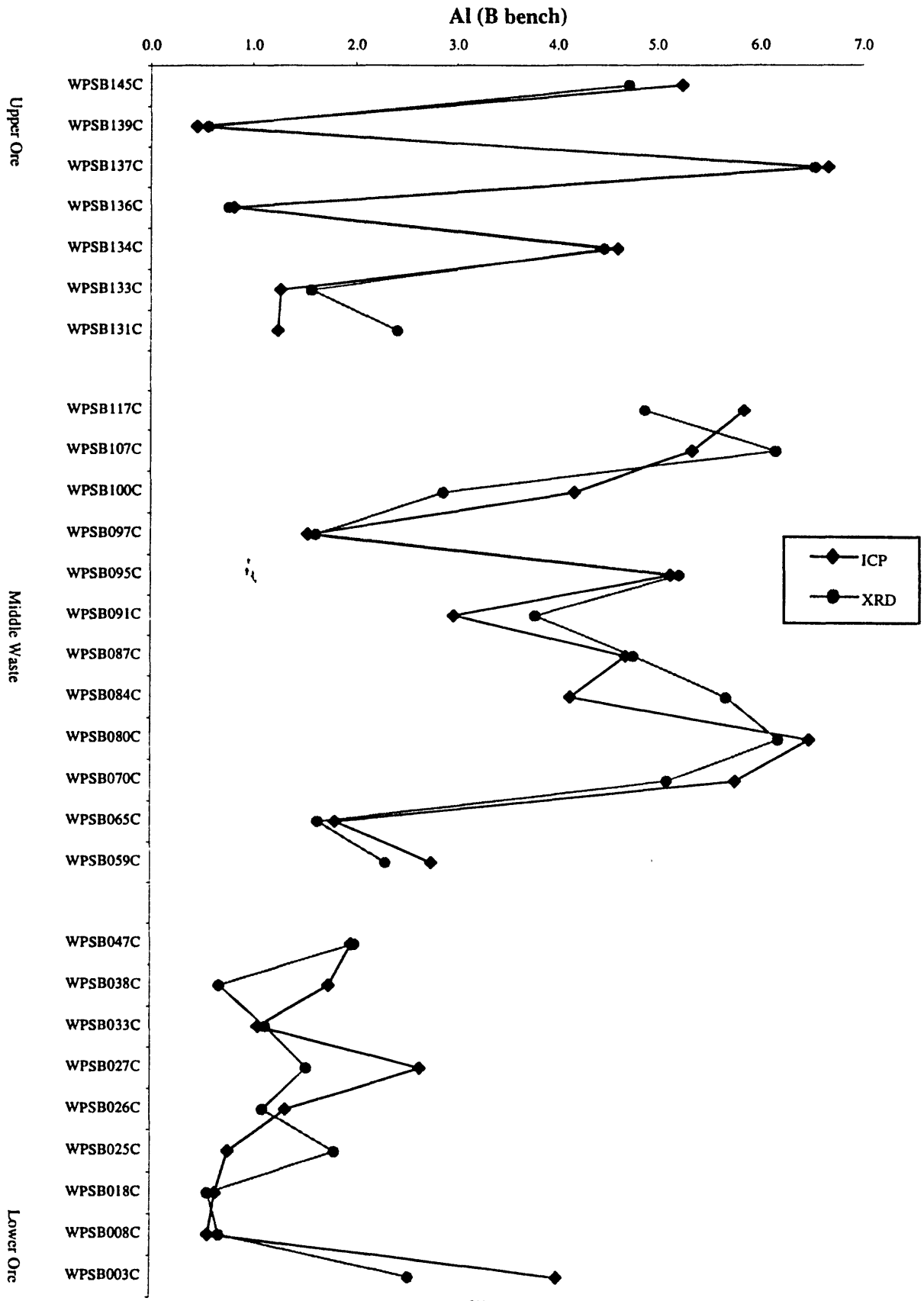

**Table 4:** Comparison of ICP data (Herring and others 1999) and calculated chemistry based on mineral compositions from Rietveld analysis. ICP data are normalized to include the elements that are calculated using the XRD data. The average difference shows whether the XRD data overstate ("-" values) or understate ("+" values) the ICP data. A weighted error is calculated by multiplying the error's absolute value by a weighting factor (measured / measured average). This value shows the comparability of the two data sets.

| Sample # | Measured % (ICP) | Normalized % (ICP) | Na Calculated % (XRD) | Difference (Normalized - Calculated) | % Error (Difference / Normalized) | Weighted % error |
|---|---|---|---|---|---|---|
| WPSB003C | 0.1 | 0.2 | 0.0 | 0.2 | 100.0 | 29.2 |
| WPSB008C | 0.4 | 0.1 | 0.2 | -0.1 | -57.1 | 8.5 |
| WPSB018C* | 0.4 | 0.1 | 0.2 | -0.1 | -74.1 | 13.0 |
| WPSB025C* | 0.2 | 0.0 | 0.0 | 0.0 | 36.7 | 2.2 |
| WPSB026C | 0.4 | 0.2 | 0.2 | 0.0 | 8.2 | 2.6 |
| WPSB027C | 0.1 | 0.1 | 0.0 | 0.1 | 78.4 | 14.5 |
| WPSB033C | 0.2 | 0.1 | 0.1 | 0.1 | 47.2 | 8.4 |
| WPSB038C | 0.4 | 0.4 | 0.3 | 0.1 | 18.6 | 9.9 |
| WPSB047C | 0.3 | 0.3 | 0.3 | 0.0 | 3.1 | 1.3 |
| WPSB059C | 0.4 | 0.5 | 0.1 | 0.4 | 79.8 | 57.8 |
| WPSB065C | 0.6 | 0.3 | 0.4 | -0.1 | -29.0 | 13.9 |
| WPSB070C | 0.5 | 1.1 | 0.1 | 1.0 | 93.0 | 143.3 |
| WPSB080C | 0.9 | 2.3 | 1.4 | 0.9 | 38.8 | 129.0 |
| WPSB084C | 0.5 | 0.7 | 0.6 | 0.1 | 14.3 | 15.2 |
| WPSB087C* | 0.4 | 0.6 | 0.3 | 0.4 | 54.9 | 50.3 |
| WPSB091C* | 0.4 | 0.5 | 0.2 | 0.3 | 58.9 | 40.3 |
| WPSB095C | 0.8 | 1.5 | 0.9 | 0.6 | 40.7 | 88.7 |
| WPSB097C | 0.4 | 0.2 | 0.2 | 0.0 | 4.9 | 1.3 |
| WPSB100C | 0.7 | 1.0 | 0.5 | 0.5 | 47.2 | 67.5 |
| WPSB107C | 1.4 | 2.3 | 1.5 | 0.8 | 33.6 | 108.2 |
| WPSB117C | 0.7 | 1.5 | 0.8 | 0.7 | 45.8 | 99.2 |
| WPSB131C | 0.1 | 0.1 | 0.2 | -0.1 | -161.5 | 14.6 |
| WPSB133C | 0.2 | 0.1 | 0.2 | -0.1 | -167.5 | 15.9 |
| WPSB134C | 0.7 | 1.0 | 0.9 | 0.0 | 4.6 | 6.4 |
| WPSB136C | 0.2 | 0.0 | 0.2 | -0.1 | -311.7 | 17.0 |
| WPSB137C** | 2.0 | 3.0 | 3.9 | -0.9 | -30.2 | 128.1 |
| WPSB139C | 0.1 | 0.0 | 0.2 | -0.2 | -1313.9 | 30.5 |
| WPSB145C | 0.7 | 1.1 | 0.7 | 0.4 | 34.9 | 56.9 |
| average | | 0.7 | | | -46.5 | 41.9 |

**Figure 6:** Graphical view of the data presented in Table 4, showing the comparability of the ICP and XRD data sets over the measured stratigraphic sections. Gaps are inserted in the graph to separate the middle waste from the upper and lower ore producing bodies.

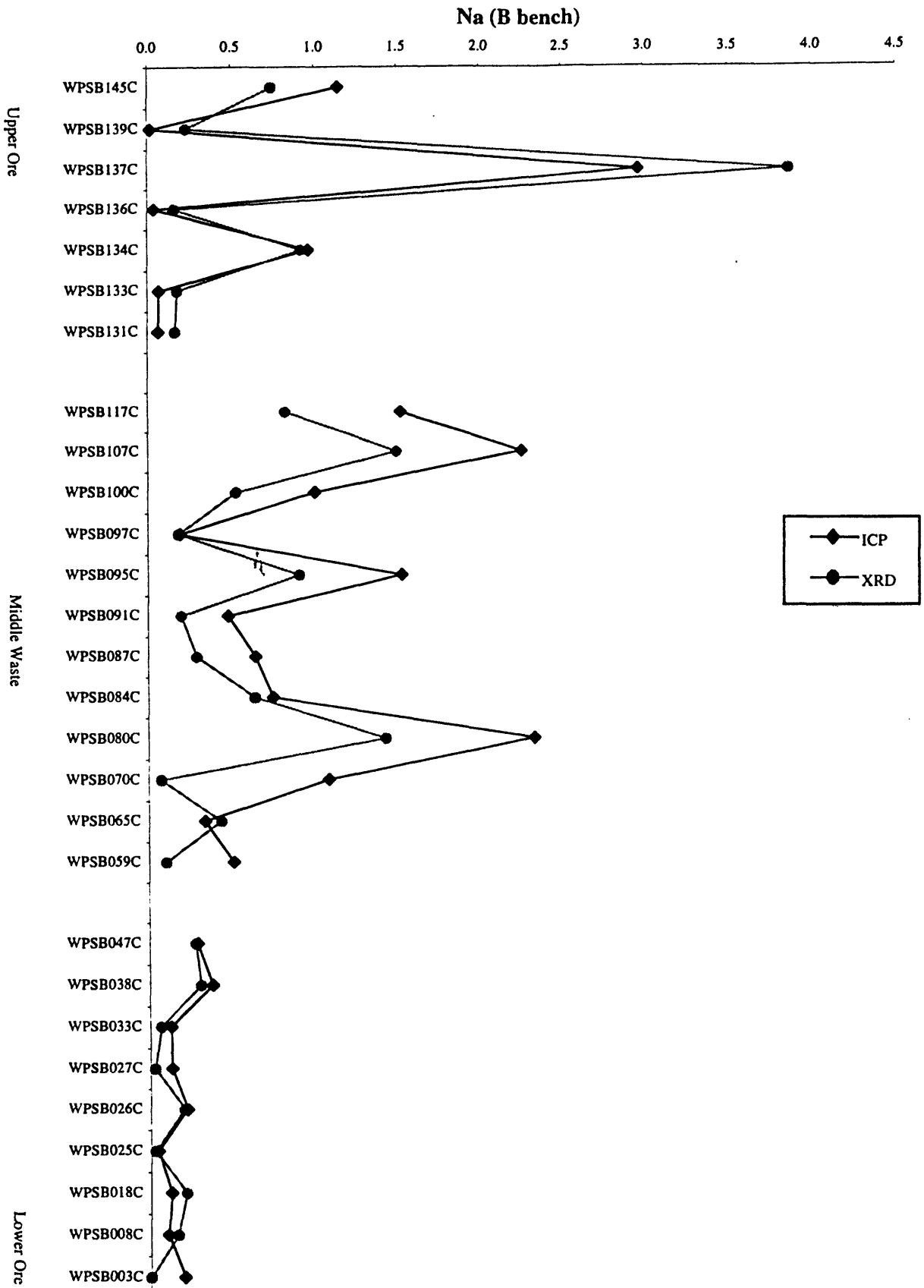

**Table 4:** Comparison of ICP data (Herring and others 1999) and calculated chemistry based on mineral compositions from Rietveld analysis. ICP data are normalized to include the elements that are calculated using the XRD data. The average difference shows whether the XRD data overstate ("-" values) or understate ("+" values) the ICP data. A weighted error is calculated by multiplying the error's absolute value by a weighting factor (measured / measured average). This value shows the comparability of the two data sets.

| Sample # | Measured % (ICP) | Normalized % (ICP) | Mg Calculated % (XRD) | Difference (Normalized - Calculated) | % Error (Difference / Normalized) | Weighted % error |
|---|---|---|---|---|---|---|
| WPSB003C | 3.6 | 4.0 | 4.4 | -0.5 | -12.1 | 28.2 |
| WPSB008C | 0.2 | 0.2 | 0.1 | 0.1 | 35.0 | 3.7 |
| WPSB018C* | 0.2 | 0.2 | 0.1 | 0.1 | 47.6 | 4.5 |
| WPSB025C* | 6.3 | 6.5 | 8.9 | -2.4 | -37.1 | 140.8 |
| WPSB026C | 0.6 | 0.6 | 0.6 | 0.0 | 0.9 | 0.3 |
| WPSB027C | 8.0 | 8.2 | 10.0 | -1.8 | -21.4 | 103.6 |
| WPSB033C | 0.2 | 0.2 | 0.2 | 0.1 | 30.7 | 4.4 |
| WPSB038C | 8.8 | 9.2 | 10.4 | -1.2 | -13.2 | 71.7 |
| WPSB047C | 0.9 | 1.1 | 1.2 | -0.1 | -10.7 | 6.6 |
| WPSB059C | 2.1 | 2.4 | 3.0 | -0.5 | -22.2 | 31.6 |
| WPSB065C | 8.5 | 8.9 | 9.4 | -0.5 | -5.9 | 30.9 |
| WPSB070C | 0.3 | 0.4 | 0.2 | 0.2 | 52.3 | 13.4 |
| WPSB080C | 0.2 | 0.2 | 0.0 | 0.2 | 90.2 | 10.7 |
| WPSB084C | 0.7 | 0.8 | 0.5 | 0.3 | 36.1 | 16.0 |
| WPSB087C* | 0.4 | 0.6 | 0.3 | 0.3 | 53.2 | 18.2 |
| WPSB091C* | 0.2 | 0.2 | 0.0 | 0.2 | 83.2 | 9.5 |
| WPSB095C | 1.0 | 1.2 | 1.1 | 0.1 | 4.6 | 3.2 |
| WPSB097C | 0.1 | 0.1 | 0.0 | 0.1 | 81.0 | 6.5 |
| WPSB100C | 0.2 | 0.2 | 0.0 | 0.2 | 91.6 | 9.7 |
| WPSB107C | 0.1 | 0.1 | 0.0 | 0.0 | 73.0 | 2.4 |
| WPSB117C | 1.0 | 1.3 | 0.9 | 0.4 | 28.5 | 22.2 |
| WPSB131C | 0.2 | 0.2 | 0.1 | 0.1 | 68.9 | 8.4 |
| WPSB133C | 0.2 | 0.2 | 0.1 | 0.1 | 51.4 | 5.2 |
| WPSB134C | 0.3 | 0.3 | 0.0 | 0.3 | 97.2 | 16.9 |
| WPSB136C | 0.1 | 0.1 | 0.1 | 0.0 | 45.0 | 2.7 |
| WPSB137C** | 0.3 | 0.3 | 0.0 | 0.3 | 100.0 | 16.0 |
| WPSB139C | 0.1 | 0.1 | 0.1 | 0.0 | 13.1 | 0.8 |
| WPSB145C | 0.3 | 0.4 | 0.0 | 0.4 | 99.8 | 22.4 |
| average | | 1.7 | | | 37.9 | 21.8 |

**Figure 6:** Graphical view of the data presented in Table 4, showing the comparability of the ICP and XRD data sets over the measured stratigraphic sections. Gaps are inserted in the graph to separate the middle waste from the upper and lower ore producing bodies.

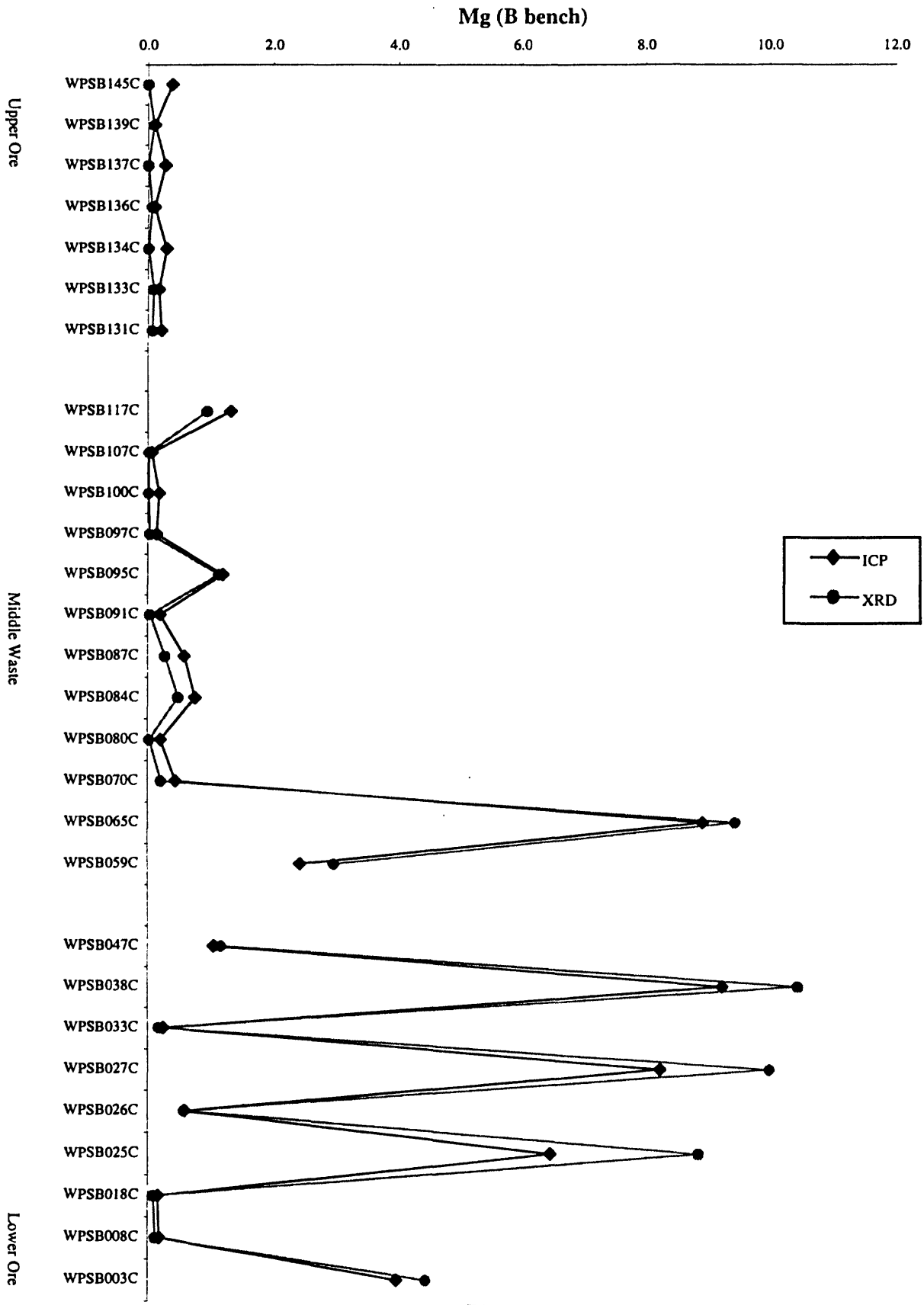

**Table 4:** Comparison of ICP data (Herring and others 1999) and calculated chemistry based on mineral compositions from Rietveld analysis. ICP data are normalized to include the elements that are calculated using the XRD data. The average difference shows whether the XRD data overstate ("-" values) or understate ("+" values) the ICP data. A weighted error is calculated by multiplying the error's absolute value by a weighting factor (measured / measured average). This value shows the comparability of the two data sets.

| Sample # | Measured % (ICP) | Normalized % (ICP) | $CO_3$ Calculated % (XRD) | Difference (Normalized - Calculated) | % Error (Difference / Normalized) | Weighted % error |
|---|---|---|---|---|---|---|
| WPSB003C | 3.7 | 4.1 | 4.4 | -0.4 | -9.3 | 21.0 |
| WPSB008C | 0.5 | 0.5 | 0.4 | 0.1 | 25.1 | 7.5 |
| WPSB018C* | 0.5 | 0.5 | 0.5 | 0.0 | 8.1 | 2.2 |
| WPSB025C* | 6.6 | 6.8 | 8.8 | -2.0 | -28.6 | 108.5 |
| WPSB026C | 0.8 | 0.8 | 0.9 | -0.1 | -11.7 | 5.4 |
| WPSB027C | 8.4 | 8.6 | 9.9 | -1.4 | -15.8 | 75.3 |
| WPSB033C | 0.5 | 0.5 | 0.3 | 0.2 | 48.4 | 13.4 |
| WPSB038C | 9.1 | 9.5 | 10.3 | -0.8 | -8.4 | 44.7 |
| WPSB047C | 1.1 | 1.2 | 1.3 | -0.1 | -6.6 | 4.4 |
| WPSB059C | 2.3 | 2.7 | 3.2 | -0.5 | -19.2 | 28.8 |
| WPSB065C | 9.5 | 9.9 | 10.0 | -0.2 | -1.7 | 9.5 |
| WPSB070C | 0.3 | 0.4 | 0.5 | 0.0 | -9.2 | 2.3 |
| WPSB080C | 0.1 | 0.1 | 0.0 | 0.0 | 22.6 | 0.8 |
| WPSB084C | 0.9 | 1.0 | 0.8 | 0.3 | 25.5 | 14.7 |
| WPSB087C* | 0.3 | 0.4 | 0.3 | 0.0 | 7.5 | 1.5 |
| WPSB091C* | 0.2 | 0.2 | 0.2 | 0.0 | 7.3 | 0.8 |
| WPSB095C | 0.9 | 1.1 | 1.3 | -0.2 | -16.2 | 10.1 |
| WPSB097C | 0.2 | 0.3 | 0.1 | 0.1 | 41.9 | 5.8 |
| WPSB100C | 0.1 | 0.1 | 0.1 | 0.0 | 14.4 | 0.8 |
| WPSB107C | 0.0 | 0.0 | 0.0 | 0.0 | 52.4 | 1.3 |
| WPSB117C | 0.9 | 1.2 | 1.0 | 0.2 | 15.7 | 10.6 |
| WPSB131C | 0.3 | 0.4 | 0.3 | 0.1 | 20.7 | 5.1 |
| WPSB133C | 0.4 | 0.4 | 0.4 | 0.0 | -1.2 | 0.3 |
| WPSB134C | 0.1 | 0.1 | 0.1 | 0.1 | 51.6 | 3.5 |
| WPSB136C | 0.4 | 0.4 | 0.3 | 0.1 | 16.2 | 3.4 |
| WPSB137C** | 0.0 | 0.0 | 0.0 | 0.0 | 100.0 | 1.8 |
| WPSB139C | 0.4 | 0.4 | 0.5 | -0.1 | -16.5 | 3.8 |
| WPSB145C | 0.1 | 0.1 | 0.0 | 0.1 | 92.4 | 2.9 |
| average | | 1.8 | | | 14.5 | 13.9 |

**Figure 6:** Graphical view of the data presented in Table 4, showing the comparability of the ICP and XRD data sets over the measured stratigraphic sections. Gaps are inserted in the graph to separate the middle waste from the upper and lower ore producing bodies.

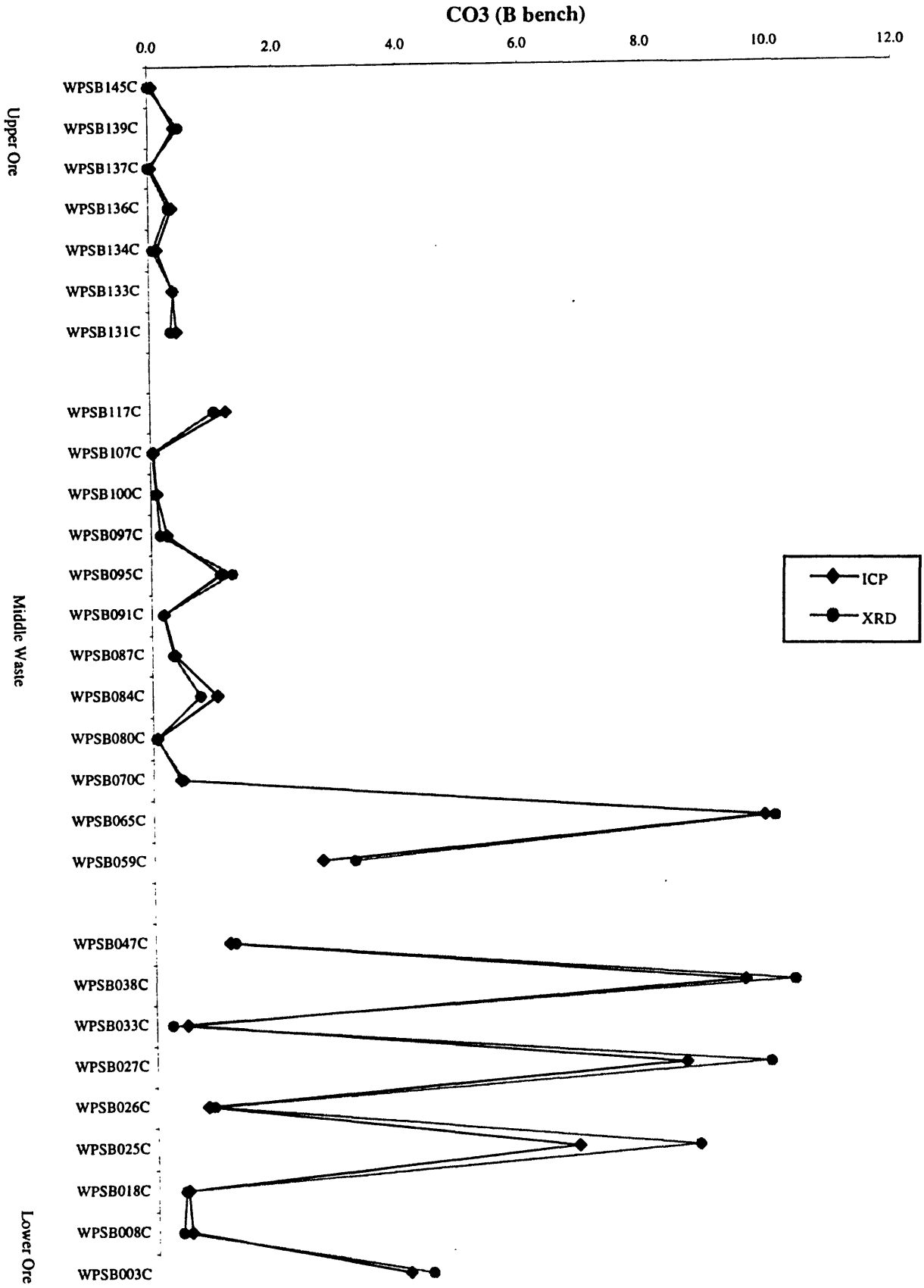

**Table 5:** Errors for Herring and others (1999) ICP data, with the observed (obs) and standard (std) values given (unpublished data, 1999).

| | Ca | | P | | Si | | K | |
|---|---|---|---|---|---|---|---|---|
| | value | % | value | % | value | % | value | % |
| obs | 1.03 | -2.8 | 0.07 | -22.2 | 31.2 | -7.1 | 2.81 | -5.7 |
| std | 1.06 | | 0.09 | | 33.6 | | 2.98 | |
| obs | 0.54 | -6.9 | 0.07 | -12.5 | 31.3 | -6.6 | 2.80 | -4.1 |
| std | 0.58 | | 0.08 | | 33.5 | | 2.92 | |
| obs | 34.3 | 4.3 | 15.3 | 4.8 | 2.3 | -4.2 | 0.11 | -8.3 |
| std | 32.9 | | 14.6 | | 2.4 | | 0.12 | |

| | Al | | Na | | Mg | | $CO_3$ | |
|---|---|---|---|---|---|---|---|---|
| | value | % | value | % | value | % | value | % |
| obs | 5.74 | -0.9 | 1.42 | -7.2 | 0.51 | -7.3 | 0.11 | 0.0 |
| std | 5.79 | | 1.53 | | 0.55 | | 0.11 | |
| obs | 6.11 | -0.3 | 1.12 | -5.9 | 0.46 | -8.0 | 0.02 | 0.0 |
| std | 6.09 | | 1.19 | | 0.50 | | 0.02 | |
| obs | 0.71 | 6.0 | 0.37 | -5.1 | 0.21 | -10.5 | 0.92 | 1.1 |
| std | 0.67 | | 0.39 | | 0.19 | | 0.91 | |